T2R2 東京科学大学 リサーチリポジトリ
Science Tokyo Research Repository

# 論文 / 著書情報
# Article / Book Information

| | |
|---|---|
| 題目(和文) | 広域交通ネットワークにおける異常な交通パターンの解析 |
| Title(English) | Analysis of Abnormal Traffic Patterns in Large Transportation Networks |
| 著者(和文) | Lykov Stanislav Sergeevich |
| Author(English) | Lykov Stanislav Sergeevich |
| 出典(和文) | 学位:博士(学術),<br>学位授与機関:東京工業大学,<br>報告番号:甲第11209号,<br>授与年月日:2019年3月26日,<br>学位の種別:課程博士,<br>審査員:朝倉 康夫,屋井 鉄雄,室町 泰徳,福田 大輔,花岡 伸也 |
| Citation(English) | Degree:Doctor (Academic),<br>Conferring organization: Tokyo Institute of Technology,<br>Report number:甲第11209号,<br>Conferred date:2019/3/26,<br>Degree Type:Course doctor,<br>Examiner:,,,, |
| 学位種別(和文) | 博士論文 |
| Type(English) | Doctoral Thesis |

Powered by T2R2 (Science Tokyo Research Repository)

# Analysis of Abnormal Traffic Patterns in Large Transportation Networks

by

Lykov Stanislav

Submitted to the

Department of Civil and Environmental Engineering

in partial fulfillment of the requirements for the degree of

Doctor of Philosophy

at the

Tokyo Institute of Technology

2019

## Abstract

Transportation systems have become an integral part of our society. These systems are constantly evolving and becoming more and more advanced. However, despite all the advances, due to internal or external factors the failures in these systems could occur, resulting in great social and economic losses. Therefore, the analysis of behavior of transportation systems not only under the normal, but also under abnormal conditions is essential in order to keep an efficient and stable operations of these systems.

However, due to complexity of modern transportation systems this analysis is very challenging procedure. For instance, in our modern society automobiles play a significant role in transportation and one could hardly talk about urban transportation while avoiding talking about vehicle traffic. Meanwhile, the rapid increase in travel demand and growing motorization rate in urban areas all over the World making the analysis of traffic dynamics more and more complicated. This situation is becoming even more challenging, taking into account the existence and negative impact of unexpected disruptions, such as natural or manmade disasters. These disasters have a disruptive effect on traffic conditions and typically result in formation of unexpected or abnormal traffic patterns. As a result, normal operations could be severely degraded or even completely stopped. These situations have to be timely noticed and avoided as much as possible.

In current dissertation the aforementioned problem of abnormal traffic patterns detection and description in large urban transportation networks is addressed. More precisely, the primary objective of this study is to develop and approach capable not only to detect aforementioned anomalous patterns, yet capable to clarify what actually was the reason, since not all of these patterns are necessarily caused by the external disruptions. Moreover, since modeling of traffic dynamics in large urban transportation networks is a complicated procedure it is also desirable to investigate how these systems could be accessed and how the information from them could be retrieved. Additionally, in this study it is investigated what type of traffic data is more suitable for traffic dynamics description in those networks and how this data could be actually used in combination with abnormal traffic pattern detection approach in order to be useful for practitioners.

In this dissertation the following research framework is considered. The first chapter is devoted to the problem introduction and clarification of research objectives. In second chapter the review of previous studies related to the dissertation is provided. More precisely, the discussion starts with the description of most commonly used traffic data collection methods. Advantages and disadvantages of each particular method in application to the traffic dynamics analysis are described. The discussion continues with the description of abnormal traffic patterns discovery techniques. Most commonly used approaches are described and explained, and the discussion on the utilization of traffic data in the process of anomalous traffic patterns detection is provided. Further, in following chapter three, tensor-based traffic data representation is put forward in order to keep complex spatiotemporal nature of traffic dynamics in large urban transportation networks, and the novel tensor-based technique for anomalous traffic patterns detection in complex urban transportation networks is proposed, explained in details and theoretically proved. In chapter four, the comprehensive examination of performance and properties of proposed abnormal traffic patterns detection approach with the help of synthetic data is provided. Chapter five starts with the description of real large-scale traffic data and the discussion on how this data could be utilized for traffic dynamics monitoring. Further, the proposed abnormal traffic patterns detection approach is applied to this real large-scale traffic data in order to mine abnormal traffic patterns formed due to the severe weather conditions. The final chapter of this dissertation is devoted to the conclusions, where key research findings are summarized and the future research directions are described.

At this point it is worth to mention that the aforementioned research findings of this dissertation include the novel tensor-based approach capable not only to detect abnormal traffic patterns, yet also capable to clarify if those patterns have been caused by the external disruptions and distinguish these pattern from the expected ones. Additionally, with the help of continuum modeling approach it was demonstrated how the overall behavioral characteristics of traffic dynamics in large urban areas could be captured and how this information could be utilized together with proposed tensor-based approach. Finally, in this dissertation it was demonstrated how the actual large-scale probe vehicle data could be used for the purposes of traffic dynamics description in large urban areas and how this data could be utilized along with aforementioned abnormal traffic patterns detection approach. Therefore, the results of this study have not only the academic interest, but also the

practical implications, since besides theoretical description of proposed approach, the whole process of real traffic data processing and utilization for the purpose of anomalous traffic patterns discovery has been demonstrated.

## Acknowledgements

I would like to express my sincere gratitude to my academic advisors Professor Yasuo Asakura and Professor Shinya Hanaoka for their continuous support and guidance from my very first day at Tokyo Institute of Technology. I could hardly imagine that this dissertation could be completed without their insightful comments, immense knowledge and encouragement. My sincere thanks also goes to all current and former Asakura laboratory members for their constant cooperation and fruitful discussions. Without their support it would not be possible to overcome numerous obstacles I have been facing through my research. Last but not the least, I would like to thank my family members for supporting me spiritually throughout writing this dissertation and my life in general.

## Contents

# List of Figures

# List of Tables

# 1. Introduction

## 1.1. Research background

Transportation systems have become an integral part of the modern society and our lives. Without exaggeration it could be said that almost all of our activities are related to these systems in some extend. People all over the World rely on transportation systems on the everyday basis when they commute to work or perform the leisure activities. These systems have indeed changed the way how we live and how our society is organized, therefore have a great impact on the development of our civilization.

However, no matter how advanced modern transportation systems are, due to internal or external factors, these systems can fail and their behavior could become abnormal. And the failure in these systems could result in great social and economic losses. Therefore, the understanding of behavior of transportation systems not only under the normal conditions, but also under abnormal conditions is essential in order to keep an efficient and stable operations of these systems.

Despite the necessity of understanding how transportation systems perform under various conditions, the actual analysis of their behavior is extremely challenging procedure. For instance, in our modern society automobiles play a significant role in transportation and one could hardly talk about urban transportation while avoiding talking about vehicle traffic. Meanwhile, the rapid increase in travel demand and growing motorization rate in urban areas all over the World making the analysis of traffic dynamics more and more complicated. This situation is becoming even more challenging, taking into account the existence and negative impact of unexpected disruptions, such as natural or manmade disasters. These disasters have a disruptive effect on traffic conditions and typically result in formation of unexpected or abnormal traffic patterns. As a result, normal operations could be severely degraded or even completely stopped. These situations have to be timely noticed and avoided as much as possible. And once again, due to the complexity of these systems, there is no uniform approach capable to accurately and precisely accomplish this task.

This problem is indeed very difficult to solve, yet fortunately there is a bright side. The constantly growing amount of traffic data available nowadays make it possible for civil engineers to develop new and more efficient solutions based on the insights mined from this data. Speaking

of the traffic data, in general, two different data collection approaches exist, more precisely Lagrangian and Eulerian approaches. According to the Eulerian approach, traffic is monitored using fixed sensors, such as loop detectors or cameras. On the other hand, under the Lagrangian approach, the traffic is typically monitored using moving or mobile observers, in particular using vehicles with Global Positioning System (GPS) onboard devices. Utilization of these methods together or separately allow to gather a considerable amount of traffic data. Notably that while being different conceptually, these techniques have an important underlying aspect in common, namely they allow to capture the spatiotemporal information regarding traffic flows. Indeed, it has been highlighted in several studies (Rempe et al., 2016; Li et al., 2013) that traffic dynamics in urban transportation networks, and as a results abnormal traffic patterns, typically exhibit complex spatiotemporal structure, therefore spatiotemporal correlations are an essential components of analysis and have to be modelled appropriately.

But how one could capture and model this complex spatiotemporal nature of traffic dynamics? Looking a little bit ahead, it is worth to mention that modeling complex spatiotemporal dependencies, as well as traffic data itself, is closely related to mathematical objects used for traffic data representation. For instance, methods relying on matrix-based traffic data representation are not capable of handling dependencies along more than two modes of traffic data simultaneously, since matrices are the two-dimensional objects and allow to jointly exploit correlations between two properties of an object or phenomena. As a result, the dependencies, for example, only along one spatial and one temporal mode (Goulart et al., 2017) could be simultaneously taken into account. However, the real-life situations are usually more complicated and assume existence of dependencies along more than two modes. Regarding traffic dynamics, this could be spatial correlations, temporal correlations within a particular day, as well as day-to-day correlations inside the urban region. In order to take into account all of them simultaneously, other mathematical objects than matrices have to be used. This matter is one of the key issues comprehensively investigated in current study.

To summarize the discussion above, in order to analyze and understand the behavior of traffic dynamics in large transportation systems, more precisely the systems where analysis of traffic dynamics on each particular link is not possible or feasible due to the enormous amount of variables

and parameters, under the abnormal conditions, there are several questions one have to answer. More precisely, how one could model traffic dynamics in large urban transportation networks, while preserving its complex spatiotemporal nature? How one could utilize traffic data in order to detect and describe abnormal traffic patterns caused by various disruptions?

## 1.2. Research objectives

The ultimate goal of this study is to develop a methodology for abnormal traffic patterns discovery in large urban transportation networks, considering complex spatiotemporal structure of traffic dynamics. Need to mention that an important point, which distinguish this study from the previous ones, is that in current study the objective is to develop an approach which is capable not only to detect anomalous traffic patterns, but also to clarify what actually was the reason behind them. So that this approach should help to clarify if an external unexpected event such as natural or manmade disaster caused anomalous patterns, or these patterns occur due to expected reasons, such as morning or evening rush hour, or due to the specific urban topology design. The motivation behind this objective is the following. Being able to accurately detect and describe abnormal traffic patterns caused by various disruptions will allow to provide vital information for improving existing transportation systems, enhancing management of urban transportation and mitigation the impact of similar disruptions in future.

Moreover, taking into account the fact that modeling of traffic dynamics in large urban transportation networks is a complicated procedure due to the enormous amount of variables and parameters, in this dissertation it is also investigated how these systems could be accessed and how the information regarding the traffic dynamics from those networks could be retrieved.

Additionally, another aspect of this study which is put forward, is the investigation of traffic data collection methods and examination of advantages and disadvantages of different traffic data types in application to analysis of traffic dynamics in large urban networks, and how the real traffic data could be actually used for the purpose of anomalous traffic patterns mining.

In order to meet these objectives, in current dissertation the following procedure is considered. First of all, the explanation of background and clarification of research objectives are provided in

the first chapter. The second chapter is dealing with the literature reviews on traffic modeling approaches in large transportation networks, traffic data collection techniques and methods for abnormal traffic patterns detection. In following chapter three, the novel tensor-based technique for anomalous traffic patterns detection in large complex urban transportation networks is proposed, explained in details and theoretically proved. In chapter four, the comprehensive examination of performance and properties of proposed abnormal traffic patterns detection approach with the help of synthetic data is provided. Chapter five starts with the description of real large scale traffic data and how this data could be used for traffic dynamics monitoring. Further, the proposed abnormal traffic patterns detection approach is applied to this real large-scale traffic data in order to mine abnormal traffic patterns. The final chapter of this dissertation is devoted to the conclusions, where key research findings are summarized and the future research directions are described. The structure of the dissertation is depicted on the Figure 1.1.

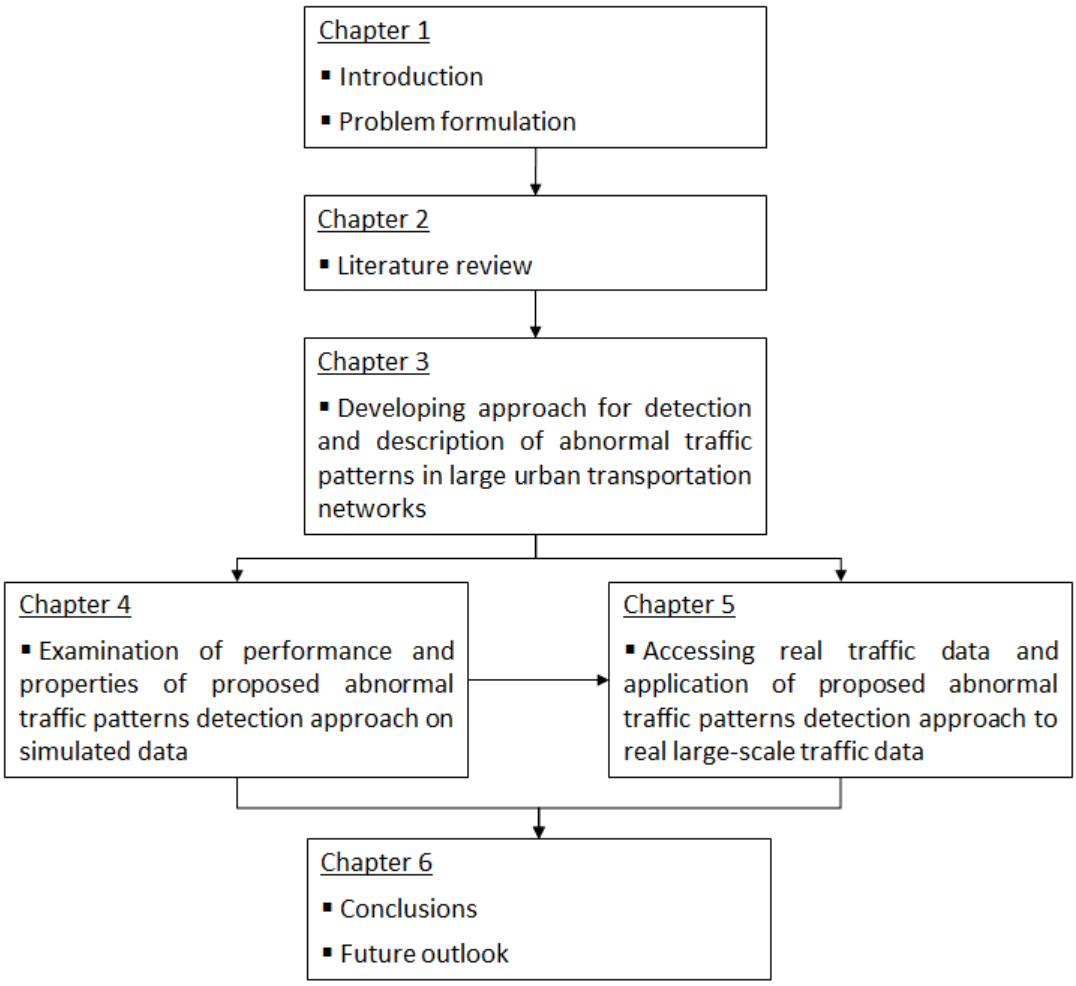


**Figure 1.1** Dissertation structure

# 2. Literature review

This chapter is devoted to the review of previous studies related to this dissertation. The discussion starts with the description of most commonly used traffic data collection methods. Advantages and disadvantages of each particular method in application to the traffic dynamics analysis are described. The discussion continues with the description of abnormal traffic patterns discovery techniques. Most commonly used approaches are described and explained, and the discussion on the utilization of traffic data in the process of anomalous traffic patterns detection is provided.

## 2.1. Traffic data collection approaches

Before switching to the discussion of abnormal traffic patterns discovery, it is important to make a review of commonly used traffic data collection techniques and methods. Indeed, it's important to clarify how and what type of traffic data could be acquired, since different methods have different limitations and scope of use. Until recent, a great variety of traffic data collection techniques has been developed. However, conceptually all these methods could be roughly divided into two big groups, depending on the type of the observer. These groups are referred as Eulerian and Lagrangian approaches. In current subsection the detailed description of these two approaches, as well as their advantages and disadvantages is provided.

### 2.1.1. Eulerian approach

The Eulerian approach assumes that traffic data is collected at a fixed locations, and the information regarding the vehicles is obtained as they pass over time. There are different types of sensors used to collect such type of data.

One of the most commonly used sensors of this type nowadays is inductive loop detectors (Koonce et al., 2008). These detectors typically have a wire loop and embedded into the pavement. The loop creates an electromagnetic field, which is disrupted as the metal object, such as a vehicle passes the field. This type of detectors directly measures such parameters as the presence or absence of vehicles, and the occupancy of passing vehicles. Other parameters of traffic flow, including speed,

density and headway are derived from the collected data (Meta and Cinsdikici, 2010). Need to mention that this is a mature, well-understood technology, which can provide basic information on traffic parameters, and demonstrate the insensitive to inclement weather such as rain, fog, and snow. However, the installation usually requires pavement cut. In addition, the detection accuracy may decrease when design requires detection of a large variety of vehicle classes (Gordon et al., 2005).

Another commonly used type of fixed location sensors is the magnetic sensor. The operation of magnetic sensor is based on the perturbation of the magnetic field as the vehicle passes the sensing zone. The magnetic sensors could be used where the loop detectors are not feasible to be installed, for example inside the bridge decks (Gordon et al., 2005). As for the disadvantages of this type of sensors, the biggest one is inability to detect a stopped vehicle, since there is a need in change of the vehicle's positions in order to be recognized.

Ultrasonic sensors have also found their application for the purpose of traffic flow monitoring. This type of sensors operates with high-frequency sound waves that are beyond of the range which people could hear. The mechanism behind the ultrasonic sensing is the following. Sound waves are emitted and the reflected from the vehicle waves are received. The distance between the sensor and the vehicle is calculated from the wave travel time. This type of sensors can detect vehicles in multiple zones and measure their speeds (Jeon et al., 2014). Moreover, during the experiment conducted by (Seo et al., 2015) on the ring-shaped urban expressway located in central Tokyo (Inner Circular Route), it was demonstrated that in case of a large number of sensors installed they enable to obtain highly detailed and accurate data on the traffic flow variables, such as the flow, spot speed, and spot occupancy directly. As for the disadvantages of this type of sensors, their performance could be affected by the temperature or air turbulence.

Passive and active infrared sensors (Ahmed et al., 1994) are also used for traffic flow monitoring. The passive devices use the energy emitted or reflected from the vehicles and roadways, while the active ones, also called laser radar sensors, generate energy through laser diodes. When a vehicle is passing in vicinity of the system antenna or laser diodes, a portion of the transmitted energy is sent back to the system receiver, so that the detection is made. Radars and infrared sensors operating by transmitting electromagnetic signals and receiving the reflections from the vehicles within the sensing radius. The major difference between radars and infrared sensors is the

wavelength of transmitted energy. For instance, microwave radars usually operates with the microwave wavelengths, while the infrared sensors emit energy in the infrared spectrum. The traffic parameters could be obtained via the analysis of the frequencies of transmitted and the received signals. This type of sensors could determine such parameters as presence of vehicles, traffic volume, occupancy, speed and even classify the vehicles (Oudat et al., 2015). Regarding the advantages and disadvantages of this type of sensors, utilization of active infrared sensors allow to transmits multiple beams for accurate measurement of vehicle position, speed, and class (Gordon et al., 2005). Moreover, operation on multiple lines is possible. However, the operation of both active and passive infrared sensors could be affected by weather conditions, such as existence of fog or snow.

Besides aforementioned sensing techniques, the traffic data could also be collected with the help of video cameras installed near or above the roadways. A single camera is capable to monitor multiple traffic lanes, even without professional installation or calibration (Setcheil et al., 2001). Moreover, contemporary video traffic monitoring systems are capable not only to detect vehicles, but also classify them and accurately track their trajectories (Tseng et al., 2002). Additionally, it is worth to mention that with the help of recent advances in the areas of machine learning and data mining, the detection performance increased dramatically (Zhang et al., 2017). Regarding the advantages of video-based approaches, in general they allow to monitor several lanes and multiple zones, and the rich amount of information could be obtained. On the other hand, the performance of this type of sensors could be affected by weather conditions, such as fog or snow. Moreover utilization of video devices is relatively more expensive, comparing to other approaches.

More detailed description of advantages and disadvantages, as well as the comparison of commonly used commercially available sensor technologies is provided in the Appendix A.

### 2.1.2. Lagrangian approach

In contrast to the Eulerian traffic data collection approach described in previous subsection, the Lagrangian approach assumes that the traffic could be sensed by using the moving observers. This conceptually different approach allow to address one of the major disadvantages of fixed-location

sensors, namely the inability to obtain enough spatial traffic information. Indeed, fixed-location sensors could mainly provide the temporal information in a particular location or a small area where the sensor is installed (Gordon et al., 2005).

Speaking of the moving observers, it is usually assumed that the traffic is monitored with the help of so-called probe vehicles, namely, the vehicles equipped with the Global Positioning System (GPS) tracking devices. The primary information, available from these probe vehicles is a collection of geo-referenced coordinates, obtained via GPS receivers and a corresponding time stamps (Treiber and Kesting, 2013).

It has been demonstrated in several studies that probe vehicle data has many different applications in transportation domain. For instance, in (Asakura et al., 2017; Kerner et al., 2005) the probe vehicle data has been used for the purpose of the traffic incident detection. Moreover, this type of data appeared beneficial for short-term speed and travel time predictions (De Fabritiis et al., 2008), as well as for the analysis of route travel times (Rahmani et al., 2015). Additionally, it was demonstrated in (Seo et al., 2015) that it is possible to perform traffic state estimation using only probe vehicle data, when probe vehicles can observe their spacing and position. The analysis of traffic congestions is also possible to perform with the help of this type of data (Tabibiazar et al., 2011). Besides aforementioned applications, probe vehicle data has been also used for dynamic routing and navigation (Guhnemann et al., 2004), and for the analysis of spatiotemporal dependencies in large-scale urban areas (Lykov et al., 2017).

Need to mention that using the information obtained from the probe vehicles one could directly derive the trajectories of probe vehicles. Further, this trajectory information, coupled with map matching techniques, is usually used in order to analyze the network flow. For instance, the matching process in context of fusion of data from Bluetooth media access control address (MAC) scanners and loops has been discussed in (Bhaskar et al., 2014) for the purpose of seamless, accurate and reliable traffic speed and density estimation. Another example of utilization probe vehicle data, coupled with map matching technique is described in (Zhao et al., 2012), where map matching model based on the gradual-removal of candidate roads was proposed. According to the authors, this model has a high degree of accuracy and can be suitable for traffic dynamics analysis in a highway networks.

### 2.1.3. Remarks on traffic data collection approaches

To summarize the discussion above, the widely used Eulerian approach has been proved to be beneficial in order to grasp the information regarding the traffic dynamics. However, by utilization of this approach, the traffic data could be captured from the relatively small area near the sensor. In order to increase the covering radius, large number of sensors have to be placed in the network. In reality mainly the highways are covered by dedicated sensing infrastructure, and there is a luck of this coverage in arterial roads. Indeed, it has been shown in (Herring, 2010) that even in case of the cheapest sensors, it is very expensive to provide coverage of the whole network. Due to this reason, sufficient amount of spatially detailed information could not be obtained. As a result, during the analysis of traffic dynamics in large transportation networks, the large portion of arterials remains uncovered. On the other hand, Lagrangian approach allow to monitor wider area, since moving sensors are distributed in larger area. And according to (Hofleitner et al., 2012), probe vehicle data is the only significant data source available today for the description of traffic dynamics on arterial roads. Moreover, probe vehicle data could be collected under the abnormal conditions, such as natural disasters, when fixed-location sensors could not operate due to blackouts (Hara and Kuwahara, 2015). In this dissertation the problem of abnormal traffic patterns detection and analysis in large transportation networks is put forward. Based on the discussion above, probe vehicle data seems to be the reasonable choice of traffic data type, which could be utilized for this purpose. In previous subsection it was mentioned that the probe vehicle data is often used together with map matching techniques. This combination is proved to be beneficial, however several limitations exist. For example, map matching itself is a computationally difficult procedure, and the complexity is increasing with increasing size of the network. Secondly, map matching cannot be performed if precise digital map information is not available, which can be a significant limitation in developing countries. Therefore, the way how the probe vehicle data is represented and actually used for the analysis of traffic dynamics in large transportation networks have to be carefully considered. The discussion of this issue is provided in the following subsection.

## 2.2. Traffic data modelling and representation

Based on the discussion in previous subsection it could be concluded that the Lagrangian approach have an advantage comparing to the Eulerian approach in application to the traffic dynamics analysis in large transportation networks, and the probe vehicle data is the reasonable choice for this purpose, mainly due to the ability to provide more spatiotemporal information regarding the traffic flow, unlike the data obtained from the fixed-location sensors. However, here comes one very important question: how one could handle and model this spatiotemporal information?

Indeed, a great variety of methods, ranging from parametric to non-parametric approaches were proposed in order to describe and analyze traffic dynamics in large transportation networks. Despite being different conceptually, these techniques have an important underlying aspect in common: spatiotemporal information regarding the traffic flows. And it has been highlighted in several studies (Rempe et al., 2016; Li et al., 2013) that the traffic dynamics in urban transportation networks, and as a result abnormal traffic patterns, typically exhibit complex spatiotemporal structure, therefore spatiotemporal correlations are an essential components of analysis and have to be handled and modeled appropriately.

This appropriate modeling of complex spatiotemporal structure is closely related to the mathematical objects used for traffic data representation. For instance, methods relying on matrix-based traffic data representation, where one dimension, for example, corresponds to the spatial location and the second dimension corresponds to the temporal dimension, are not capable of handling dependencies along more than two modes of traffic data simultaneously. As a result, the dependencies, only along aforementioned one spatial and one temporal mode (Goulart et al., 2017) could be simultaneously taken into account. However, the real-life situations are usually more complicated and assume existence of the dependencies along more than two modes. Regarding traffic dynamics, this could be spatial correlations, temporal correlations within a day, as well as day-to-day correlations inside urban region. In order to take into account all of them simultaneously, other mathematical objects than matrices have to be used.

In order to address this issue, in current dissertation the utilization of tensor-based techniques for traffic data representation and analysis is put forward. Tensors, being a generalization of such

mathematical objects as scalars, vectors and matrices were recently introduced to transportation domain. Tensor-based methods operate with multi-way matrices in order to capture underlying multi-mode structure of traffic dynamics (Ran et al., 2016). This key feature of tensors, namely the ability to capture and preserve multi-mode correlations appeared to be crucial for such applications as missing traffic data imputation obtained from sensors (Goulart et al., 2017; Ran et al., 2016; Chen et al., 2018), spatiotemporal traffic speed patterns discovery (Chen et al., 2018) and analysis of large-scale traffic dynamics in urban areas (Han et al., 2016).

However, need to mention that despite the promising results, there are still very limited number of studies which utilize tensor-based techniques for traffic data analysis. Moreover, the majority of studies devoted to tensor-based methods in transportation domain rely only on different tensor decomposition techniques, such as Tucker, CANDECOMP/PARAFAC (CP) or Non-negative tensor decompositions (Chi et al., 2011). Despite advantages, there are several issues connected with application of aforementioned tensor decomposition techniques. In particular, the sensitivity to outliers and gross corruptions in data. For instance, it was demonstrated in (Chi et al., 2011) that CP tensor factorization is sensitive to violations in the Gaussian assumption. Therefore additional steps to robustify tensor decompositions against such corruptions have to be made. Additionally, even lesser amount of studies (Wang et al., 2014; Fanaee-T and Gama, 2016) utilize tensor techniques for the purposes of spatiotemporal traffic structure mining. In contrast, this study is devoted to anomalous traffic patterns discovery, therefore the existence of grossly corrupted observations could not be neglected. Additionally, unlike the previous studies, in this dissertation the problem of anomalous traffic patterns discovery is treated from the point of view of low-rank modeling problem, which seems more suitable to model expected and unexpected traffic patterns. This low-rank modeling, its application to traffic data, as well as the formal introduction to tensors and tensor-based traffic data representation are described in details in the following chapter three.

Besides preserving complex spatiotemporal nature of traffic dynamics in large transportation networks, another important issue has to be discussed. More precisely, the issue which has been mentioned before and has to be discussed in current subsection is connected with aforementioned utilization of probe vehicle data in order to describe traffic dynamics in large transportation networks. As it had been highlighted in previous subsection, the typical combination of probe

vehicle data and the map matching techniques might not be suitable for analysis of large urban transportation networks, since the map matching itself is computationally difficult procedure, and the complexity is increasing with increasing size of the network, and also since the map matching in general cannot be performed if precise digital map information is not available. In this dissertation, instead of considering the traffic at each road link in transportation network, the generalized definition of traffic state proposed in (Edie, 1963) is adapted. According to this generalized definition, the traffic state variables, more precisely the traffic flow $q$ (veh/h), traffic density $k$ (veh/km) and traffic speed $v$ (km/h) in a time-space region Ω can be defined as follows

$$q(\Omega) = \frac{l(\Omega)}{|\Omega|} \tag{2.1}$$

$$k(\Omega) = \frac{t(\Omega)}{|\Omega|} \tag{2.2}$$

$$v(\Omega) = \frac{l(\Omega)}{t(\Omega)} \tag{2.3}$$

where $l(\Omega)$ is a total travel distance traveled by all the vehicles in a region Ω, and $t(\Omega)$ is a total time spend by all the vehicles in the region Ω. Following this definition, if it is further assumed that the targeted region for analysis inside urban area could be divided into the uniform mesh with square mesh cells, whose latitudinal and longitudinal mesh cell indexes are $i$ ($i \in \overline{1,I}$) and $j$($j \in \overline{1,J}$) respectively, the aforementioned speed, for example, could be written as follows

$$v_{i,j} = \frac{l_{i,j}}{t_{i,j}} \tag{2.4}$$

where $v_{i,j}$ is the average speed in a mesh cell $(i,j)$; $l_{i,j}$ stands for the total travel distance and $t_{i,j}$ stands for the total travel time spend in the corresponding mesh cell. This representation allow to focus on macroscopic behavior of motorists and avoid analyzing each road link separately. However, the practical utilization of aforementioned generalized traffic state variables is not straightforward. For instance, such matters as how to choose an appropriate spatial resolution (mesh cell size) or temporal resolution, and how this choice is related to the number of vehicles have to

be considered. These problems have a great practical implications, and therefore will be investigated in current dissertation.

## 2.3. Abnormal traffic pattern detection techniques

The discussion in this subsection starts with the general overview of data anomaly detection approaches, and continues with the examples related to traffic dynamics analysis.

To start with, the problem of anomaly detection could be formulated as the problem of finding the patterns in data that do not conform to expected behavior. These nonconforming patterns are usually referred as anomalies or outliers depending on the context. Till now, a great variety of different anomaly detection techniques had been developed. Some of these methods are used for a specific application domains, while others are more generic. As for some examples of applications of anomaly detection, one could consider a credit card fraud detection (Ghosh and Reilly, 1994), intrusion detection in cyber-security (Chandola et al., 2006), military surveillance (Brotherton and Johnson, 2001) or health conditions monitoring (Lin et al., 2005). According to the formulation of anomaly detection problem, a straightforward anomaly detection approach could be considered as a two-step process. First, a region representing normal behavior is identified, and then all the observations which do not belong to this region are labeled as anomalous. Unfortunately, usually it is very difficult to identify this normal region, and the boundary between normal and abnormal states is vague. Therefore, in many real-life situations, more specific formulation is necessary, and such factors as the nature of data, its availability and desired types of anomaly are important.

In general, the majority of anomaly detection techniques could be roughly divided into several classes. The first one contains classification based anomaly detection techniques. The underlying idea of this types of methods is that the classification is used in order to learn a model from a collection of labeled data points, and then the new data entry is classified using the learned model. Examples of techniques in this category are the neural networks-based methods (Stefano et al., 2000; Williams et al., 2002; Odin and Addison, 2000), where the artificial neural network is trained to perform a classification task; Support Vector Machines-based methods (Ratsch et al., 2002; Ma and Perkins, 2003), which can be used for both classification or regression challenges; and Bayesian

networks-based methods (Wong et al., 2003; Bronstein et al., 2001), widely used for multivariate data sets. Another big class of anomaly detection techniques is related to the nearest neighbor-based anomaly detection techniques. One of the most prominent methods of this class is the k-nearest neighbor algorithm (Eskin et al., 2002; Bolton and Hand, 1999), which judge the anomaly scores of the data points based on the distances to their k nearest neighbors in a data set. Besides aforementioned classes of anomaly detection techniques, an important one and the one of the most commonly used contains the statistical anomaly detection techniques. The key idea behind algorithms of this class is that normal data instances occur in high probability regions of a stochastic model, while anomalies occur in the low probability regions of the stochastic model (Chandola et al., 2009). This class could be further subdivided into two subclasses, namely parametric and nonparametric technique. The parametric techniques usually assume an a priori knowledge of the distribution and estimate the parameters from observed data (Eskin, 2000), while nonparametric techniques do not have this assumption (Desforges et al., 1998). As an example of parametric techniques, Gaussian model-based techniques, which assume that the data is generated from a Gaussian distribution, could be considered. In contract, the histogram-based methods, which are the simplest nonparametric statistical techniques, are an example of nonparametric techniques. The comprehensive review of anomaly detection techniques, their comparison and evaluation could be found in (Chandola et al., 2009).

The choice of particular anomaly detection technique in application to the traffic data analysis is generally connected with the type of traffic data which is subject to be utilized and the type of anomaly desired to be detected. For instance, when dealing with the microscopic traffic variables, describing individual vehicles and interactions between them, such information as the relative speed, spacing between vehicles and the lane changing behavior could be used in order to detect abnormal traffic patterns (Thajchayapong and Barria, 2010; Sheu, 2004; Abuelela et al., 2008). However, the majority of studies which utilizes these microscopic traffic variables are focusing only on local anomalies in particular intersections or road segments. For instance, in (Zameni et al., 2018) the authors proposed robust unsupervised anomaly detection system, which is focusing on microscopic behavior, and emphasized the difference between the anomalous local event and the global traffic changes. Therefore it seems more reasonable to focus on macroscopic rather than microscopic

traffic variable when analyzing the traffic dynamics in large transportation networks, which consists of many road links, intersections and other topological objects, and investigating the impact of external disruptions such as natural or manmade disasters. By utilization macroscopic traffic variables it is possible to focus on overall behavior of motorists and analyze larger areas. However, the number of studies which utilizes aforementioned macroscopic traffic variables for the purpose of abnormal traffic patterns detection in large transportation networks is limited. More precisely, while dealing with large urban transportation networks, in several studies (Liu et al., 2011; Chawla et al., 2012) the targeted urban area has been divided into a several sub regions by major roads, and the anomalous patterns has been identified by observing unexpected traffic between any of those sub regions. In the study by (Pang et al., 2011), the researchers divided the city into the uniform grid and report anomalies if neighboring grid cells have a very different total traffic volumes, considering the data collected from the taxis with GPS onboard devices. However, as it has been highlighted by the researchers, these methods are sensitive to how the regions are defined, and therefore an additional examination of this aspect is necessary.

Advanced technologies, such as vehicle-to-vehicle (V2V) communications also found their application to the problem of anomalies detection. For instance, in (Bauza and Gozalvez, 2013) the researchers proposed a distributed technique using vehicle-to-vehicle (V2V) communications to detect and characterize traffic anomalies, which has been evaluated in a large scale highway scenario. However, the authors paid limited attention to the arterial roads despite the fact that in reality the large urban transportation networks consists of a mixture of freeways and arterials. Indeed, according to the (Parkany, 2005), historically many abnormal event detection systems, for example considering traffic incidents, were developed for the use in freeways, and the less effort had been made to develop a systems for arterials. Speaking of arterials, due to the different reasons, such as signal control, and other disturbances as pedestrian crossings, parking and others, the traffic varies more frequently and has more complex profile, comparing to freeways. In (Chen and Chang, 1993) the researchers proposed a dynamic arterial incident detection algorithm, based on the Kalman filtering technique. Khan and Ritchie (1998) proposed utilization of multiple neural networks in a modular architecture to detect arterial operational problems, including special on-street events and detector malfunctioning. In time series algorithms it is assumed that the traffic

normally follows a predictable pattern over time, and therefore when the measurements deviate significantly from the values calculated with the help of time series models, the anomaly is reported. A well-known example is the autoregressive integrated moving average (ARIMA) model (Ahmed and Cook, 1977). Anomalies detection by traffic modeling approaches apply traffic flow theory to describe and predict traffic behavior under unusual conditions, and the comparison between observed values and the values estimated by traffic models is made. As an example, one could consider the dynamics model (Willsky et al., 1980), where the fundamental speed-density and flow-density relationships are used as the basis for abnormality detection.

Another important point related to the anomalous traffic patterns detection is connected with the understanding of the reasons of anomaly. The lesser amount of studies are trying not only to detect the anomaly, but to figure out the actual reason of this anomaly. For instance, in (Chawla et al., 2012) the authors proposed a two-step framework for inferring the root cause of anomalies that appear in road traffic data. In the first step the link anomalies has been identified based on their deviation from the historical traffic profile. Further, in order to investigate the cause of anomalies, researchers incorporate modeling traffic flow in the network in terms of origin-destination matrix which physically relates the latent flow between origin and destination and observable flow on the link. In their study an experiment with a very large GPS data set consisting on nearly eight hundred million data points has been conducted, and the validity of proposed approach was demonstrated, yet the focus had been made only on links anomalies. Worth to mention that the authors mentioned that their study is closely related to the studies in network community. In particular, the proposed approach is close to the work by (Lakhina et al., 2004), where the principal component analysis (PCA) is used to detect the network anomalies. In the study the PCA was used to exploit the correlation between link traffic.

Speaking of the PCA for anomalies detection, the researchers (Fanaee-T and Gama, 2016) claimed that this powerful and popular method (PCA) has been applied in wide range of areas and domains, however if data includes tensor (multiway) structure (e.g. space-time-measurements), some meaningful anomalies may remain hidden unless tensor-based representation is used. They also claimed that even if tensor-based anomaly detection methods has been applied across various disciplines, they are still not recognized as a formal category in anomaly detection. In their review

on application of tensors to the problem of anomaly detection related to traffic analysis, they mentioned that the tensor decomposition has been used on the tensor origin-destination-time for discovery of spatiotemporal traffic structure (Wang et al., 2014; Fanaee-T and Gama, 2016); the problem which is known as outlier recovery is addressed in (Tan et al., 2013) with tensors; and tensors also has been used for prediction of missing values in traffic data (Tan et al., 2013). Nevertheless, there could hardly be found any studies which try to use the synergy of such powerful anomaly detection techniques as PCA with the tensor-based techniques in order to assure more accurate traffic data representation, as well as to robustify the anomaly detection process, taking into account the existence of grossly corrupted observations. This issue is one of the key points in current dissertation and the comprehensive examination is provided in chapter three.

## 2.4. Chapter summary

Summarizing the discussion in current chapter, the following key aspects have to be considered while analyzing traffic patterns in large urban transportation networks. First of all, it is important to appropriately model complex spatiotemporal structure of traffic dynamics in order to achieve an adequate representation of real-life scenarios. Indeed, it was demonstrated that the traffic dynamics in urban transportation networks, and as a result abnormal traffic patterns, typically exhibit complex spatiotemporal structure, therefore spatiotemporal correlations are an essential components of analysis and have to be handled and modeled appropriately. This appropriate modeling of complex spatiotemporal structure is closely related to the mathematical objects used for traffic data representation. To meet this objective, in current dissertation tensor-based traffic data representation is put forward. This tensor-based representation allow to take into account and preserve complex spatiotemporal nature of traffic dynamics. Secondly, while mining abnormal traffic patterns it is desirable not only to detect them, but also to understand the reasons behind these anomalous conditions. This issue was not covered in the majority of studies, where only the detection problem has been considered. Therefore, in this study it is investigated how one could use the synergy of anomaly detection techniques, for instance the widely used PCA with the tensor-based techniques in order to assure more accurate traffic data representation, as well as to robustify

the anomaly detection process, taking into account the existence of grossly corrupted observations. In particular, in current study the novel approach based on tensor robust principal component analysis is proposed. Finally, considering the real traffic data used for analyzing traffic patterns in large urban transportation networks, it has been demonstrated that the Lagrangian approach has many advantages comparing to the Eulerian approach. More precisely, according to several studies, probe vehicle data is the only significant data source available today for the description of traffic dynamics on arterial roads. And since large urban transportation networks usually consists of a mixture of freeways and arterials, this type of data is considered in this dissertation as a primary source of information regarding the traffic dynamics. Moreover, probe vehicle data could be collected under the abnormal conditions, such as natural disasters, when fixed-location sensors could not operate due to blackouts, which is important under the scope of this study.

# 3. Tensor-based abnormal traffic pattern discovery

## 3.1. Mathematical notations and tensor basics

### 3.1.1. Definitions and operations on tensors

Current subsection is devoted to the formal introduction to tensors, as well as to the description of mathematical notations on tensors used throughout the dissertation. Conventions typically found in the literature are introduced and adopted from the (Kolda and Bader, 2009) review on tensors.

Mathematically, $N^{th}$-order tensor is an element of the tensor product of $N$ vector spaces, each of which has its own coordinate system. Tensor is a multidimensional array, generalization of such mathematical objects as scalars ($0^{th}$-order tensor), vectors ($1^{st}$-order tensor) and matrices ($2^{nd}$-order tensor). In this study, following (Kolda and Bader, 2009) we denote scalars by lowercase letters, e.g. $x$. On the other hand, vectors are denoted by boldface lowercase letters, e.g. $\boldsymbol{x}$. Matrices and tensors are denoted by boldface capital letters, e.g. $\boldsymbol{X}$, and boldface Euler script letters, e.g. $\boldsymbol{\mathcal{X}}$, respectively. An element of $N^{th}$-order tensor $\boldsymbol{\mathcal{X}} \in \mathbb{R}^{I_1 \times I_2 \times \ldots \times I_N}$ is a scalar and denoted as $X_{i_1 i_2 \ldots i_N}$.

Mathematical operations of addition and subtraction for tensors are defined elementwise, in similar manner as for vectors and matrices. The inner product of two tensors $\boldsymbol{\mathcal{X}}, \boldsymbol{\mathcal{Y}} \in \mathbb{R}^{I_1 \times I_2 \times \ldots \times I_N}$ is given by

$$\langle \boldsymbol{\mathcal{X}}, \boldsymbol{\mathcal{Y}} \rangle = \sum_{i_1=1}^{I_1} \sum_{i_2=1}^{I_2} \ldots \sum_{i_N=1}^{I_N} X_{i_1 i_2 \ldots i_N} Y_{i_1 i_2 \ldots i_N} \tag{3.1}$$

The *n*-mode product of a $N^{th}$-order tensor $\boldsymbol{\mathcal{X}} \in \mathbb{R}^{I_1 \times I_2 \times \ldots \times I_N}$ and a matrix $\boldsymbol{A} \in \mathbb{R}^{J \times I_n}$ is denoted as a $\boldsymbol{\mathcal{X}} \times_n \boldsymbol{A}$ with entries calculated as follows

$$(\boldsymbol{\mathcal{X}} \times_n \boldsymbol{A})_{i_1 \ldots i_{n-1} j i_{n+1} \ldots i_N} = \sum_{i_n=1}^{I_n} X_{i_1 i_2 \ldots i_N} A_{j i_n} \tag{3.2}$$

While working with tensors, it is often convenient to transform them into vectors or matrices. These processes are called vectorization and matricization and described below consequently. The

vectorized tensor is a vector denoted as $vec(\boldsymbol{\mathcal{X}})$ formed by the tensor entries, such that tensor entry $(i_1, i_2, \dots, i_N)$ is mapped to the vector entry $j$ as follows

$$j = 1 + \sum_{k=1}^{N} (i_k - 1) J_k \quad and \quad J_k = \prod_{m=1}^{k-1} I_m \tag{3.3}$$

In case of $n$-mode matricization with $n \in \{1,2, \dots, N\}$ the result is a matrix $X_{[n]}$ formed by the tensor entries, such that tensor entry $(i_1, i_2, \dots, i_N)$ is mapped to the matrix entry $(i_n, j)$ as follows

$$j = 1 + \sum_{\substack{k=1 \\ k \neq n}}^{N} (i_k - 1) J_k \quad and \quad J_k = \prod_{\substack{m=1 \\ m \neq n}}^{k-1} I_m \tag{3.4}$$

Besides operations on tensors it is necessary to define tensor norms. In current study, in similar manner as for matrices, the $l_p$-norm of a $N^{th}$-order tensor $\boldsymbol{\mathcal{X}}$ is introduced and defined as follows

$$\| \boldsymbol{\mathcal{X}} \|_p = \left( \sum_{i_1=1}^{I_1} \sum_{i_2=1}^{I_2} \dots \sum_{i_N=1}^{I_N} \left| X_{i_1 i_2 \dots i_N} \right|^p \right)^{\frac{1}{p}} \tag{3.5}$$

Based on the fact that tensor inner product and the tensor $l_p$-norm are defined in the same elementwise manner as for matrices, they inherit the same properties. More precisely, elementwise $l_2$-norm, which is referred as tensor Frobenius norm $\|\boldsymbol{\mathcal{X}}\|_F$ is equal to $\| \boldsymbol{\mathcal{X}} \|_p$ for $p = 2$ and can be calculated as $\| \boldsymbol{\mathcal{X}} \|_2 = \sqrt{\langle \boldsymbol{\mathcal{X}}, \boldsymbol{\mathcal{X}} \rangle}$. Moreover, similarly to matrices, the number of non-zero elements of a tensor $\boldsymbol{\mathcal{X}}$ is referred to as a $l_0$-norm.

### 3.1.2. Tensor rank

In linear algebra the rank of a matrix is defined as a number of linearly independent column vectors or equivalently as the number of non-zero singular values. This definition could not be directly extended to tensors. Instead, the rank of a $N^{th}$-order tensor $\boldsymbol{\mathcal{X}} \in \mathbb{R}^{I_1 \times I_2 \times \dots \times I_N}$, denoted as $rank(\boldsymbol{\mathcal{X}})$,

is defined as a smallest positive integer $R$ for which given tensor $\boldsymbol{\mathcal{X}}$ could be written as a sum of *rank*-1 tensors (vectors) as follows

$$\boldsymbol{\mathcal{X}} = \sum_{r=1}^{R} r_{r1} \circ r_{r2} \circ \ldots \circ r_{rN} \tag{3.6}$$

Despite simplicity, the above definition of tensor rank is known to be an NP-hard computational problem. Therefore, for many practical applications so-called tensor *n*-rank, which in fact a rank of *n*-mode matricization, is used and calculated as follows

$$rank_n(\boldsymbol{\mathcal{X}}) = rank\left(\boldsymbol{X}_{[n]}\right) \tag{3.7}$$

It is important to mention that for a general case of $N^{th}$ -order tensor $rank_n(\boldsymbol{\mathcal{X}}) \neq rank_m(\boldsymbol{\mathcal{X}})$ when $n \neq m$. This situation is opposite to matrices case, where the column rank is always equal to the row rank.

## 3.2. Tensor robust principal component analysis

### 3.2.1. Low-rank tensor representation

Tensors are usually utilized in order to model a high-dimensional datasets. For example, tensors could be used to model image or video data in computer vision applications, documents in natural language processing or experiment outcomes, considering an observation of a physical process. Despite various types of the data, in many situations observed data is rarely pure, and usually corrupted by the noise. Recovering information from these noisy observations is a fundamental problem in many applications, such as signal processing, data mining and many others. In recent years a collection of promising and powerful approaches, referred as robust low-rank modelling, had appeared. These approaches are based on an observation that in many real-life cases uncorrupted information appears to be similar or correlated to a certain degree. For instance, the image of the same object taken under various lighting conditions is expected to have fewer degrees

of freedom than a generally chosen image. In other words, its common situation when the high-dimensional data lie in a low-dimensional subspace.

In current study we follow aforementioned fundamental idea regarding low-rank structure of many real-life datasets and apply it to the problem of abnormal traffic patterns discovery. More precisely, it is assumed that normal or expected traffic patterns in general exhibit similar periodic structure, for example similar day-to-day dynamics inside a particular urban region, so that have a low-rank structure. This low-rank assumption comes from the fact that day-wise observations of traffic dynamics within particular urban area appear to be similar or correlated to a certain degree. Therefore, these observations are expected to have fewer degree of freedom than observations of traffic dynamics in an arbitrary regions. Further, it is assumed that abnormal or unexpected traffic patterns do not occur very often, and therefore have so-called sparse structure. This separation of traffic dynamics into two distinctive components, namely low-rank and sparse components is similar to the information recovery problem, where the ultimate goal is to reconstruct uncorrupted information from the noisy observations.

### 3.2.2. Formulation of tensor robust principal component analysis

In current subsection the formal mathematical formulation of aforementioned discussion regarding low-rank modeling is provided. The explanation starts with the matrices and then extended to a more general case of higher-order tensors. First of all, we consider that the real-life data or some observations could be represented as a matrix $\boldsymbol{X}$, which is a combination of uncorrupted component $\boldsymbol{Y}$ and a noise $\boldsymbol{Z}$. This could be written as following

$$\boldsymbol{X} = \boldsymbol{Y} + \boldsymbol{Z} \tag{3.8}$$

And the key question is how one could recover the uncorrupted component $\boldsymbol{Y}$ and separate it from the noise component $\boldsymbol{Z}$, given raw data $\boldsymbol{X}$. By brief look at the problem (3.8) it become clear that in current formulation this problem is ill-posed, since by given *nm* values (size of a matrix $\boldsymbol{X}$) one wish to estimate *2nm* values. Overcoming of this ill-posedness is closely related to the assumptions

imposed on the data. More precisely, as it had been shown in previous subsection, the real-life observations of the same phenomena typically are of low-rank, which means that the above decomposition problem (3.8) could be formulated as a low-rank modelling problem. In particular, the given data matrix $\boldsymbol{X}$ is subject to be decomposed into a low-rank component $\boldsymbol{Y}$ and a sparse component $\boldsymbol{Z}$. In other words, among all the possible decompositions, we seek for a lowest-rank $\boldsymbol{Y}$ and the sparsest $\boldsymbol{Z}$. As an optimization problem this could be formulated as follows

$$\min_{\boldsymbol{Y},\boldsymbol{Z}} rank(\boldsymbol{Y}) + \lambda\|\boldsymbol{Z}\|_0 \qquad s.t. \qquad \boldsymbol{X} = \boldsymbol{Y} + \boldsymbol{Z} \tag{3.9}$$

unfortunately, in current formulation the problem (3.9) is intractable due to the discrete nature of the rank and non-convexity of $l_0$-norm. The non-convexity of $l_0$-norm could be shown, for example by choosing two vectors $\boldsymbol{x}, \boldsymbol{y}$ for which Jensen's inequality does not hold. Mathematically it could be expressed as follows

$$\exists \boldsymbol{x}, \boldsymbol{y} \in \mathbb{R}\,,\ \theta \in (0,1)\colon\ f(\theta\boldsymbol{x} + (1-\theta)\boldsymbol{y}) \geq \theta f(\boldsymbol{x}) + (1-\theta) f(\boldsymbol{y}), \quad e.g.$$

$$\|x\|_0 \triangleq \sum_{i=1}^{n} 1_{x_i \neq 0}\colon\ \left\|\frac{1}{2}(1,0) + \frac{1}{2}(0,1)\right\|_0 = 2 > 1 = \frac{1}{2}\|(1,0)\|_0 + \frac{1}{2}\|(0,1)\|_0 \tag{3.10}$$

In order to overcome this issue and make the problem (3.9) tractable, necessary convex relaxation have to be made. The core idea behind this relaxation is the substitution of the rank and $l_0$-norm with their convex envelopes, which are the nuclear and $l_1$-norm respectively. After this relaxation, the initial optimization problem (3.9) could be reformulated as follows

$$\min_{\boldsymbol{Y},\boldsymbol{Z}} \|\boldsymbol{Y}\|_* + \lambda\|\boldsymbol{Z}\|_1 \qquad s.t. \qquad \boldsymbol{X} = \boldsymbol{Y} + \boldsymbol{Z} \tag{3.11}$$

An optimization problem (3.11) is referred as the Robust Principal Component Analysis (RPCA). Being a convex problems implies that it can be globally optimized, and as it had been demonstrated

by several researchers (Candes et al., 2011), the solution of the problem (3.11) is with high probability the same as the solution of the initial problem (3.9).

The extension of aforementioned discussing to more general case of higher-order tensors is straightforward. More precisely, considering raw data tensor $\boldsymbol{\mathcal{X}} \in \mathbb{R}^{I_1 \times I_2 \times \ldots \times I_N}$, which is a subject to be decomposed into the low-rank component $\boldsymbol{\mathcal{Y}}$ and a sparse component $\boldsymbol{\mathcal{Z}}$ as shown below

$$\boldsymbol{\mathcal{X}} = \boldsymbol{\mathcal{Y}} + \boldsymbol{\mathcal{Z}} \tag{3.12}$$

Following the same steps as for matrices, we first formulate this decomposition problem as an optimization problem as follows

$$\min_{\boldsymbol{\mathcal{Y}},\boldsymbol{\mathcal{Z}}} rank(\boldsymbol{\mathcal{Y}}) + \lambda \|\boldsymbol{\mathcal{Z}}\|_0 \qquad s.t. \qquad \boldsymbol{\mathcal{X}} = \boldsymbol{\mathcal{Y}} + \boldsymbol{\mathcal{Z}} \tag{3.13}$$

Once again, in order to make the optimization problem (3.13) tractable, the necessary convex relaxation had to be done. However, since defining the tensor rank is an NP-hard computational problem, tensor *n*-rank is further utilized. More precisely, instead of minimizing the rank of the tensor $rank(\boldsymbol{\mathcal{Y}})$, the focus on minimization of the convex combination of all *n*-ranks shown on the equation below as follows

$$\sum_{i=1}^{\mathrm{N}} \alpha_i rank_i(\boldsymbol{\mathcal{Y}}) \quad where \quad rank_i(\boldsymbol{\mathcal{Y}}) = rank\left(\boldsymbol{Y}_{[i]}\right) \quad \text{and} \quad \alpha_i \geq 0; \sum_{i=1}^{N} \alpha_i = 1 \tag{3.14}$$

The values of a positive coefficients $\alpha_i$ in equation (3.14) are chosen in accordance with the (Signoretto et al., 2010) as following: $\alpha_1 = \alpha_2 = \cdots = \alpha_N = N^{-1}$. Finally, the $l_0$-norm in equation (3.13) and all $rank_i(\boldsymbol{\mathcal{Y}})$ in equation (3.14) are substituted with their convex envelopes, which are $l_1$-norm and the nuclear norm respectively, resulting in following optimization problem, referred as the Tensor Robust Principal Component Analysis (TRPCA)

$$\min_{\boldsymbol{\mathcal{Y}},\boldsymbol{\mathcal{Z}}} \sum_{i=1}^{N} \alpha_i \left\| \boldsymbol{Y}_{[i]} \right\|_* + \lambda \|\boldsymbol{\mathcal{Z}}\|_1 \qquad s.t. \quad \boldsymbol{\mathcal{X}} = \boldsymbol{\mathcal{Y}} + \boldsymbol{\mathcal{Z}} \tag{3.15}$$

Notable that in this formulation the problem connected with local minima issue could be avoided, since the minimization of nuclear norm is a convex optimization problem. Additionally, need to mention that the value of the regularization parameter lambda needs to be tuned to each particular dataset. For a larger $\lambda$ the optimal solution will contain the sparser $\boldsymbol{\mathcal{Z}}$ and a less low-rank $\boldsymbol{\mathcal{Y}}$. On the other hand, smaller $\lambda$ will result into a denser $\boldsymbol{\mathcal{Z}}$ and a lower-rank $\boldsymbol{\mathcal{Y}}$. The cross-validation could help to choose between several possible alternative values of parameter lambda via measurement of out-of-sample accuracy by averaging over several randomly chosen portions of data into training and test samples. In the following subsection the commonly used solution of this optimization problem (3.15) with the help of Augmented Lagrange Multipliers (ALM) is described.

### 3.2.3. Solution based on Augmented Lagrange Multipliers

In current dissertation, following the procedure in (Huachun et al., 2011), the widely-used method of Augmented Lagrange Multipliers (ALM) is applied in order to solve the optimization problem (3.15). Before coming to the description of ALM method, we make a convention that previously introduced in subsection 3.1.1 operation of *n*-mode matricization of a tensor $\boldsymbol{\mathcal{X}}$ will be referred as unfolding. This operation is resulting in matrix $unfold(\boldsymbol{\mathcal{X}}, n) = \boldsymbol{X}_{[n]}$. An inverse operation will be called folding and defined as $fold(\boldsymbol{X}_{[n]}, n) = \boldsymbol{\mathcal{X}}$. Using these operators and following the style in (Huachun et al., 2011), instead of considering optimization problem (3.15) directly, the following problem is tackled first

$$\min_{\boldsymbol{Y}_{[i]},\boldsymbol{Z}_{[i]}} \left\| \boldsymbol{Y}_{[i]} \right\|_* + \lambda_n \left\| \boldsymbol{Z}_{[i]} \right\|_1 \qquad s.t. \quad \boldsymbol{X}_{[i]} = \boldsymbol{Y}_{[i]} + \boldsymbol{Z}_{[i]} \quad \forall i = \overline{1,N} \tag{3.16}$$

Solving the problem above (3.16) for all unfoldings, the final solution is obtained by utilizing the results of each mode with the weighted parameters $\alpha_i$ in equation (3.15). This process will be demonstrated throughout this subsection. To start with, in general the ALM method is designed for

solving constrained optimization problems of the kind

$$minf(X) \qquad s.t. \quad h(X) = 0 \;\; where \;\; f: \mathbb{R}^n \longrightarrow \mathbb{R} \;\; and \;\; h: \mathbb{R}^n \longrightarrow \mathbb{R}^m \tag{3.17}$$

For this type of problems, the Augmented Lagrange Function $L(X, \theta, \mu)$ is introduces and defined as following

$$L(X, \theta, \mu) = f(X) + \langle \theta, h(X) \rangle + \frac{\mu}{2} \|h(X)\|_F^2 \tag{3.18}$$

where $\mu$ is a positive scalar, and the optimization problem can be solved with the help of ALM method. The Augmented Lagrange Function for the problem (3.16) could be written as following

$$\min_{\boldsymbol{Y}_{[i]}, \boldsymbol{Z}_{[i]}} \left\|\boldsymbol{Y}_{[i]}\right\|_* + \lambda_n \left\|\boldsymbol{Z}_{[i]}\right\|_1 + \langle \theta_i, \boldsymbol{X}_{[i]} - \boldsymbol{Y}_{[i]} - \boldsymbol{Z}_{[i]} \rangle + \frac{\mu_i}{2} \left\|\boldsymbol{X}_{[i]} - \boldsymbol{Y}_{[i]} - \boldsymbol{Z}_{[i]}\right\|_F^2 \tag{3.19}$$

The idea behind solving the problem (3.19) is to optimize one group of variables while fixing another. The variables in the optimization are $\boldsymbol{Y}_{[i]}$ and $\boldsymbol{Z}_{[i]}$ are divided into two groups. The optimal $\boldsymbol{Y}_{[i]}$ is solved by the following sub-problem with $\boldsymbol{Z}_{[i]}$ fixed

$$\min_{\boldsymbol{Y}_{[i]}} \left\|\boldsymbol{Y}_{[i]}\right\|_* + \langle \theta_i, \boldsymbol{X}_{[i]} - \boldsymbol{Y}_{[i]} - \boldsymbol{Z}_{[i]} \rangle + \frac{\mu_i}{2} \left\|\boldsymbol{X}_{[i]} - \boldsymbol{Y}_{[i]} - \boldsymbol{Z}_{[i]}\right\|_F^2 \tag{3.20}$$

It has been demonstrated in previous studies (Cai et al., 2008) that the optimal solution of (3.20) is given by the following equation

$$\boldsymbol{Y}_{[i]} = U_i D_{\mu_i^{-1}}(\Lambda) V_i^T \tag{3.21}$$

where $U_i \Lambda V_i^T$ is the singular value decomposition which is defined by the equation below as follows

$$U_i \Lambda V_i^T = \boldsymbol{X}_{[i]} - \boldsymbol{Z}_{[i]} + \mu_i^{-1}\theta_i \tag{3.22}$$

The operator $D_\mu(\delta)$ is extended to tensor case by performing the operations on each tensor element and defined as the following

$$D_\mu(\delta) = \begin{cases} \delta - \mu, & \delta > \mu \\ 0, & |\delta| \le \mu \\ \delta + \mu, & \delta < -\mu \end{cases} \tag{3.23}$$

On the other hand, the optimal $\boldsymbol{Z}_{[i]}$ is solved by considering the following sub-problem with $\boldsymbol{Y}_{[i]}$ fixed

$$\min_{\boldsymbol{Z}_{[i]}} \lambda_n \left\|\boldsymbol{Z}_{[i]}\right\|_1 + \langle \theta_i, \boldsymbol{X}_{[i]} - \boldsymbol{Y}_{[i]} - \boldsymbol{Z}_{[i]} \rangle + \frac{\mu_i}{2} \left\|\boldsymbol{X}_{[i]} - \boldsymbol{Y}_{[i]} - \boldsymbol{Z}_{[i]}\right\|_F^2 \tag{3.24}$$

According to the previous studies (Hale et al., 2008), the optimal solution of the problem (3.24) can be calculated as following

$$\boldsymbol{Z}_{[i]} = D_{\frac{\lambda_i}{\mu_i}}\left(\boldsymbol{X}_{[i]} - \boldsymbol{Y}_{[i]} + \mu_i^{-1}\theta_i\right) \tag{3.25}$$

Further, by utilizing aforementioned operation of folding, the matrices of each mode computed into tensors and weighted with the respect to the weighted parameters $\alpha_i$ as follows

$$\boldsymbol{\mathcal{Y}} = \frac{\sum_{i=1}^{N} \alpha_i fold(\boldsymbol{Y}_{[i]}, i)}{\sum_{i=1}^{N} \alpha_i} \; and \; \boldsymbol{\mathcal{Z}} = \frac{\sum_{i=1}^{N} \alpha_i fold(\boldsymbol{Z}_{[i]}, i)}{\sum_{i=1}^{N} \alpha_i} \tag{3.26}$$

The tensors in equation (3.26) above give the solution to the problem (3.15). In current dissertation aforementioned ALM method was programmatically implemented in order to solve problem (3.15).

### 3.2.4. Applications of tensor robust principal component analysis

Tensor robust principal component analysis is a useful technique, which could be utilized when the

observed data fit the low-rank and sparse assumptions at some degree. For instance, this technique is frequently used for denoising and reconstruction of video and image data. In this case, original (without noise) video sequence is assumed to be of low-rank and the noise is assumed to have a sparse structure. The problem of face recognition, important for many surveillance systems, is also addressed by this tensor robust principal component analysis. In this case, the face features are remain the same, so fit the low-rank assumption, and the corruptions may include different facial expressions, glasses, and shadows and so on. Moreover, this tensor technique is frequently utilized for the problem of object identification and background subtraction. Background subtraction is a fundamental preprocessing step in various computer vision applications. Taking into account that background of a video sequence usually changes only slightly between consecutive video frames, it can be modelled as a low-rank structure, and the moving foreground objects can be thought as a sparse corruptions.

## 3.3. Tensor-based traffic data representation

In order to accurately capture complex spatiotemporal nature of traffic dynamics, in current study tensor-based traffic data representation is put forward. It has been highlighted by several studies (Ran et al., 2016) that tensor-based methods operate with multi-way matrices in order to capture underlying multi-mode structure of traffic dynamics. This feature of tensors, namely the ability to capture and preserve multi-mode correlations appeared to be important for such applications as imputation of missing traffic data obtained from sensors (Ran et al., 2016; Chen et al., 2018) and analysis of traffic dynamics in large-scale urban areas (Han et al., 2016). In current study the average speed of vehicles is considered as an indicator describing traffic dynamics, since anomalous traffic patterns detection is on focus, and vehicles speed has been extensively and frequently used for the abnormalities detection purposes in many studies. However it possibly could be other indicators, such as the density of vehicles. More importantly that constructed in this subsection traffic data tensor contains the information regarding normal and abnormal traffic patterns, which are the subject to be distinguished. Following the discussion in literature review section, in current study the generalized definitions of traffic state variables are used. According to the generalized

definition of traffic state proposed in (Edie, 1963) the average speed in a time-space region Ω could be defined as following

$$V(\Omega) = \frac{TTD(\Omega)}{TTT(\Omega)} \tag{3.27}$$

Where $TTD(\Omega)$ stands for the total distance traveled by all the vehicles in the region Ω; $TTT(\Omega)$ is the total time spent by all the vehicles in the region Ω. Following this definition, in current study it is further assumed that targeted region for analysis inside urban area is divided into uniform mesh with square mesh cells, whose latitudinal and longitudinal mesh cell indexes are $i$ ($i \in \overline{1,I}$) and $j$($j \in \overline{1,J}$) respectively. Additionally, it is assumed that time within a day is divided into equal time intervals indexed by $t$($t \in \overline{1,T}$). Therefore, the average speed for particular mesh cell with indexes $(i,j)$ for a given time interval $t$ during a particular day $d$($d \in \overline{1,D}$) could be written as follows

$$V_{i,j}^{t,d} = \frac{TTD_{i,j}^{t,d}}{TTT_{i,j}^{t,d}} \tag{3.28}$$

In order to convert this mesh-wise average speed into tensor-based representation the following

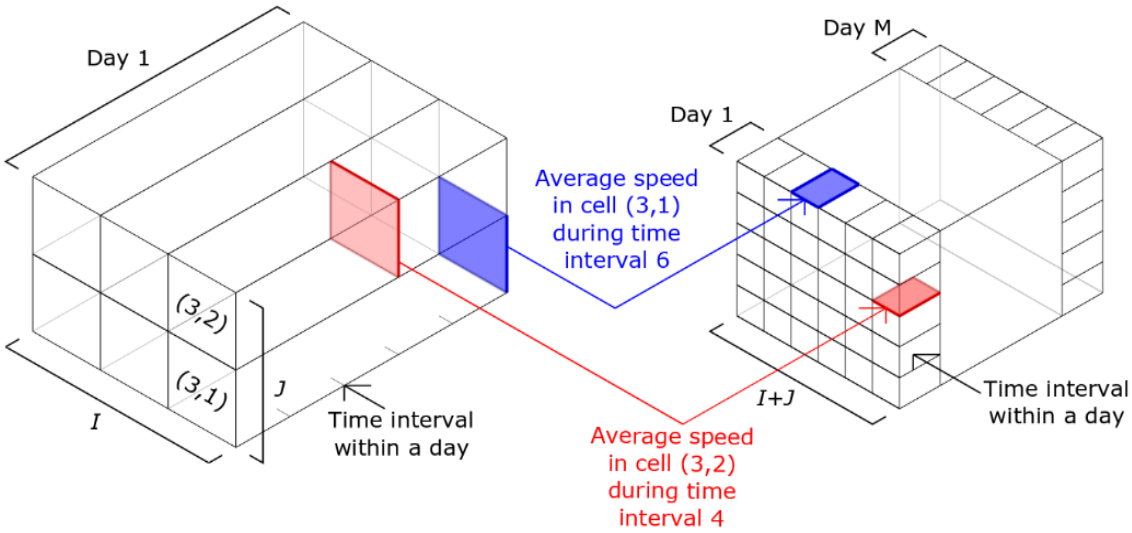


**Figure 3.1** Mesh-wise average speed map during one day (left) and tensor-based data representation (right). For illustrative purposes latitudinal and longitudinal mesh sizes are assumed: $\boldsymbol{I = 3}$; $\boldsymbol{J = 2}$ respectively. Number of time intervals within one day is assumed: $\boldsymbol{N = 6}$. Colored arrows depict transformation process.

procedure is considered. We construct a 3rd order tensor $\boldsymbol{\mathcal{X}} \in \mathbb{R}^{I_1 \times I_2 \times I_3}$ with one spatial dimension ($I_1$) and two temporal dimensions ($I_2$ and $I_3$). The spatial dimension ($I_1$) is of size ($I * J$) and corresponds to mesh cells. Two temporal dimensions ($I_2$ and $I_3$) are of size (T and D) and correspond to time interval within a day and the day itself respectively. This data transformation procedure is shown on the Figure 3.1. The constructed tensor is of size $\boldsymbol{\mathcal{X}} \in \mathbb{R}^{(\mathrm{I}*\mathrm{J})\times\mathrm{T}\times\mathrm{D}}$, with the values equal to the average speed in particular mesh cell, time interval within a day and the day itself. More precisely, the value of average speed $V_{i,j}^{t,d}$ in a mesh cell with indexes $(i, j)$ during time interval $t$ within a day $d$ is mapped to the tensor element, using the following mapping formula $V_{i,j}^{t,d} \rightarrow X_{(i+(j-1)I),t,d}$. Further, constructed tensor is used for mining anomalous traffic patterns with the help of the tensor robust principal component analysis. The performance of aforementioned tensor-based approach, as well as the examination of its characteristics and properties are discussed in following chapter four.

## 3.4. Chapter summary

This subsection is devoted to the formal introduction to tensors, as well as to the description of mathematical notations on tensors used throughout the dissertation. It has been demonstrated that tensors, being a multidimensional arrays are often used to model high-dimensional datasets, and found applications in such areas as computer vision, natural language processing and many others. An important point which has been discussed in this chapter is that current study follow the fundamental idea regarding low-rank structure of many real-life datasets and apply it to the problem of abnormal traffic patterns discovery. More precisely, it is assumed that normal or expected traffic patterns in general exhibit similar periodic structure, for example similar day-to-day dynamics inside a particular urban region, so that have a low-rank structure. This low-rank assumption comes from the fact that day-wise observations of traffic dynamics within particular urban area appear to be similar or correlated to a certain degree. The aforementioned assumption regarding low-rank structure leads to the formulation of the problem of abnormal traffic patterns discovery as a tensor robust principal component analysis. Mathematical formulation of tensor robust principal component analysis, as well as the solution technique is also provided in this subsection.

Additionally, it's worth to mention once again the advantages of proposed approach in comparison to the previous studies. In previous studies which rely on tensor-based techniques in application to transportation domain, mainly two decomposition methods CANDECOMP/PARAFAC (CP) and Tucker decompositions have been used. However, it is difficult to apply these techniques directly in this study due to the following reason. In general, natural or manmade disasters could be arbitrary in magnitude and size, which means that traffic data is more likely to contain gross corrupted observations, unlike the conventional noise with bounded variance. And it was demonstrated in (Chi and Kolda, 2011) that CP tensor factorization model can be highly sensitive to non-Gaussian noise. In general, CP and Tucker decompositions are prone to local optima because they are solving essentially non-convex optimization problems (Gu et al., 2014). On the other hand, in proposed approach the minimization of nuclear norm is a convex optimization problem, and therefore there is no local minima issues. Additionally, nuclear norm minimization appeared to give almost the exact same result as the original NP-hard rank minimization problem.

# 4. Simulation-based validation

## 4.1. Modelling traffic dynamics in large transportation networks

To examine performance of proposed tensor-based abnormal traffic patterns detection approach and investigate its properties, first of all, it's important to understand how traffic dynamics in large and complex transportation networks could be accessed and modelled. As it has been highlighted in literature review part, traffic dynamics in large and complex urban transportation networks is a complicated phenomenon for analysis. It has been demonstrated by several studies (Sossoe et al., 2015), that one of the major problems with modeling of traffic dynamics in large urban areas is connected with the fact that existing conventional models, such as link-and-node-based traffic flow models could hardly be applicable due to existence of large number of parameters and variables, as well as significant computational efforts. In order to address this issue, conceptually different continuum modeling approach was introduced recently to transportation domain. According to this continuum modeling approach, road network within urban area is assumed to be dense and viewed as a continuum in which travelers can travel in two-dimensional space. This transition allow to focus on the overall behavior of travelers at the macroscopic level, rather than model and analyze each road link separately. Therefore, less amount of data is required for the model and the problem size could be reduced even in case of large and dense transportation networks (Long et al., 2017), which become crucial for investigation the performance and properties of proposed tensor-based approach. However, since this continuum modeling approach is a mathematical idealization of real traffic dynamics, it has several limitations which will be discussed in subsection 4.2.3.

In current dissertation, the original model proposed by (Jiang et al., 2009 and Long et al., 2017) is adopted and extended. In following subsection, the variables, key definitions and governing equations of original model are explained. Further, since the emphasis in current study is on abnormal traffic patterns, the basic continuum model of traffic dynamics is supplemented by introduction of so-called disruption field. This disruption field emulates real-world disasters and assumed to be a scalar field with variable parameters, such as intensity and localization. Additionally, the model is extended by introducing of probes, individual particles, traveling inside continuum the field, in order to examine the performance of proposed tensor-based approach.

## 4.2. Continuum model of traffic dynamics

### 4.2.1. Original model description

In current subsection the description of original continuum model used in this study is provided. The extension of original model is described in the following subsection. Mathematically, two-dimensional region $\Omega$ with outer boundary $\partial\Omega$ is considered. The travelers are continuously located along $(x, y) \in \Omega$. Following the original model, several variables are introduced. More precisely, the density of travelers $\rho(x, y, t)$ and the travel demand $q(x, y, t)$ at particular location $(x, y) \in \Omega$ inside target region on interest during time interval $t$. The condition exposed onto the density of travelers is $\rho(x, y, t) = 0 \quad \forall (x, y) \in \partial\Omega,$ which means that travelers are not allowed to leave the domain $\Omega$. Further, the velocity and flow vectors are introduced and denoted as the $\mathbf{v}(x, y, t)$ and $\mathbf{F}(x, y, t)$ respectively. The connection between velocity vector, density of travelers and flow vector is as follows

$$\mathbf{F}(x, y, t) = \rho(x, y, t)\mathbf{v}(x, y, t) \tag{4.1}$$

Moreover, the local travel cost $c(x, y, t)$ per unit distance of travel experienced by travelers is introduced and assumed to be inversely proportional to travel speed $u(x, y, t) = \|\mathbf{v}(x, y, t)\|$. Regarding the governing equations, the traffic flow is treated as a compressible fluid with the following conservation law

$$\rho_t(x, y, t) + \nabla \boldsymbol{F}(x, y, t) = q(x, y, t) \quad \forall (x, y) \in \Omega \quad \forall t \in T \tag{4.2}$$

Further, it is assumed that travelers are traveling towards the specific destination inside targeted region of analysis $D \subset \Omega$. In order to describe the decision making process of travelers, following the original model, so-called instantaneous travel cost potential $\varphi(x, y, t)$ is introduced. This cost potential depicts the total travel cost for travelers who depart from location $(x, y)$ at time $t$ to travel towards the destination. As in original model, it is assumed that $\varphi(x, y, t) = 0$ at destination and that this cost potential is related to the local travel cost as $|\nabla\varphi(x, y, t)| = c(x, y, t)$. Moreover,

assuming that travelers try to choose a path that minimizes their travel cost to the destination, this instantaneous travel cost potential is governed by the equation

$$c(x,y,t)\frac{\boldsymbol{F}(x,y,t)}{|\boldsymbol{F}(x,y,t)|}+\nabla\varphi(x,y,t)=0 \tag{4.3}$$

Finally, in order to connect the speed of travelers with their density, it is assumed that the Greenshields's speed-density relationship holds and is defined as follows

$$u(x,y,t)=u_f(x,y,t)\left(1-\frac{\rho(x,y,t)}{\rho_{jam}(x,y,t)}\right) \tag{4.4}$$

Where $u_f(x,y,t)$ and $\rho_{jam}(x,y,t)$ are the free-flow speed and jam density at particular location $(x,y)$ and time interval t respectively. In following subsection, this baseline continuum model is extended in order to incorporate the impact of external disruptions.

### 4.2.2. Extension of original model

An important aspect regarding the continuum model described in previous subsection is connected with the fact that this model is a mathematical idealization. In real-life scenarios it would be too naïve to expect travelers to be able to freely travel in two-dimensional space due to diverse urban design. However, this continuum model could possibly help to track some overall behavioral patterns of motorists. In order to accomplish this and include into consideration the effect of disruption, the utilized basic continuum model is extended by introduction of individual probes (particles traveling inside the continuum field) and modification of the Greenshields's model. This extension is described in current section.

First of all, in order to take into account the impact of external disruptions on traffic dynamics, in current study it is assumed the disruptions exist and leads to the capacity reduction. In particular, it is assumed that the disruption could be characterized as a scalar field with variable intensity parameter $\gamma(x,y,t)\in[0;1)$, which is incorporated into the Greenshields's Model as following

$$u(x,y,t) = u_f(x,y,t)\left(1 - \frac{\rho(x,y,t)}{(1-\gamma(x,y,t))\rho_{jam}(x,y,t)}\right) \tag{4.5}$$

Secondly, regarding the individual probes or particles traveling in continuum field, it is assumed that these particles are uniformly distributed inside the region $\Omega$ and traveling towards the destination $D$, in accordance with the governing equations (4.1) - (4.5). Further, in similar manner as in section 3.3, it is assumed that targeted area is divided into uniform mesh with square mesh cells, whose latitudinal and longitudinal mesh cell indexes are $i$ ($i \in \overline{1,I}$) and $j$($j \in \overline{1,J}$) respectively. Therefore, the total travel distance traveled by individual probe indexed by $k$ inside the mesh cell $(i,j)$ during time interval $t$ could be written as ${}_kTTD_{i,j}^t$, and the total travel time spend by this probe inside this cell at corresponding time interval as a ${}_kTTT_{i,j}^t$. It is further assumed that aforementioned total travel distance and total travel time of individual probe contain an error terms $\varepsilon_k$ and $\delta_k$ respectively. In accordance with this, the average speed inside a particular mesh cell $(i,j)$ during time interval $t$ could be written as follows

$$U_{i,j}^t = \frac{\sum_k({}_kTTD_{i,j}^t + \varepsilon_k)}{\sum_k({}_kTTT_{i,j}^t + \delta_k)} \tag{4.6}$$

In equation (4.6) an important addition is the error terms $\varepsilon_k$ and $\delta_k$, which represent a noise in observations and assumed to follow Gaussian distribution. Without this addition the speed inside particular mesh cell could always be strictly determined, despite the number of probes. In following subsections, the connection between continuum model, its extension and real traffic data is clarified.

### 4.2.3. Connection between continuum model and real traffic data

In current study, the basic continuum model has been adapted and extended in order to emulate the behavioral characteristics of travelers in large urban areas. However, since this model is a mathematical idealization of real-life traffic behavior, it is important to clarify the connection between this continuum model, introduced probes and the real traffic data, which actually can be used to describe traffic dynamics in large urban areas.

The discussion is started with the real traffic data used for traffic dynamics monitoring. It has been shown in the literature review part that in general two different data collection approaches exist: Lagrangian and Eulerian. Moreover, it has been demonstrated that due to the major disadvantage of Eulerian approach in application to traffic dynamics analysis in large transportation networks, namely inability to capture enough information from the arterial roads, the choice of Lagrangian approach for aforementioned purpose seems more reasonable. It also has been shown that the information collected from the probe vehicles, equipped with GPS onboard is typically used under the Lagrangian approach. Further, in this dissertation, it is assumed that the average speed of probe vehicles in particular targeted region and time interval is equal to the average speed of all other vehicles in this region and during same time interval, and following the generalized definitions of traffic state variables, assuming targeted region is divided into uniform mesh with square mesh cells, the average speed of probes is given by equation (3.28) in subsection 3.3.

In other words, by using the equation (3.28) one could calculate the average speed $V_{i,j}^{t}$ inside the particular mesh cell with indexes $(i, j)$ for a given time interval $t$. This indicator could be further used for analysis of traffic conditions. However, there are several practical questions arise. In particular, how to choose the spatiotemporal resolution (mesh cell size and time interval duration)? How this choice affects the accuracy of constructed speed map? And finally, how spatiotemporal resolution is related to the population of probes? By answering to these questions it will be possible to make a concrete recommendations for practitioners regarding suitable choose of parameters for real traffic dynamics monitoring systems.

The continuum model described in subsections 4.2-4.3 is used to answer these questions. More precisely, it could be seen that the calculation of average speed using real probe vehicles (3.28) is similar to calculation the speed using hypothetical probes (4.6) introduced to continuum model. And it also could be noticed that the average speed calculated using these hypothetical probes, using the equation (4.6) is approximated by its continuum limit when the number of probes tends to infinity. Therefore, by using continuum model from the sections 4.2-4.3 it is possible to enhance the numerical simulation, investigate properties of constructed speed map and the performance of proposed abnormal traffic patterns detection approach first, and then switch to the real probe vehicle data. The detailed discussion on these matters are provided in the following subsections.

## 4.3. Numerical experiment

### 4.3.1. Simulation objectives

The simulation has been conducted in current study in order to achieve two main objectives. The first objective is to examine properties and the performance of proposed tensor-based abnormal traffic patterns detection approach. The second objective is related to aforementioned continuum model of traffic dynamics. As it has been highlighted in previous subsection, despite being the mathematical idealization, this continuum model could help to track the overall behavioral characteristics of travelers in large transportation networks. Therefore, examination of the properties of this continuum model and its extension could help to make a practical recommendations on the utilization of real traffic data for patterns analysis in large urban areas.

### 4.3.2. Simulation setup

The simulation setup is as following. A square domain of one unit length with travel demand accumulating inside is considered. The travelers appear in the system and start to travel towards the point destination located in the bottom-left part of the domain, in accordance with the continuum model described in subsection 4.2. The origins of travelers are distributed randomly and uniformly inside the domain for each simulation trial (at points of spatial discretization). It is further assumed that during some simulation trials the disruption exist and located in sub region of simulation

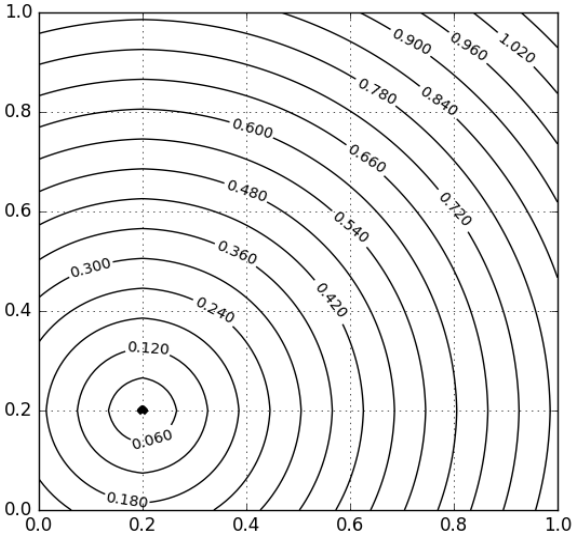


**Figure 4.1** Simulation domain of one square unit length. The destination is located at the point with coordinates (0.2, 0.2). The radial distances from the destination are shown. The travel demand is accumulating inside the simulation domain.

domain with center at the point (0.5, 0.5), and leads to the capacity reduction according to the equation (4.5). The magnitude of disruption (value of gamma in equation (4.5)) is maximum at the point (0.5, 0.5) and decreasing inverse proportional to distance inside the restricted area. The simulation trials when the disruption exist will be further specified. Regarding the solution of original continuum model, the following procedure has been considered in current study. Firstly, the simulation domain in Figure 4.1 was overlaid with the grid with 0.01 spacing. Further, the solution of conservation law (4.2) was obtained with the help of two-dimensional extension of the Lax-Wendroff scheme, which is second-order accurate in both space and time. According to this scheme, at first the values of density of travelers are calculated at each point of discretized domain at half time step and stored. Further, the values of velocities and fluxes at each point of discretized domain at half time step are obtained using the previously stored solution for density. And finally, the values of density are updated (corrected) according to the calculated values at half time step. In order to solve the boundary value Eikonal-type equation (4.3), fast marching method has been utilized. This algorithm is similar to the Dijkstra's algorithm for finding the shortest paths, yet differs in how the values at points of discretized domain are calculated. The detailed description of numerical solutions could be found in (Chopp, 2002; Zwas, 1972).

### 4.3.3. Examination of continuum model behavior

Before switching to the examination of properties and performance of proposed tensor-based anomalous patterns detection approach, it is necessary to examine in what extend the described continuum model corresponds to the real behavior of motorists. In order to meet this objective, the following procedure has been done. According to the extended continuum model, describe in section 4.2.2, the trajectories of 15 probes were tracked for the equal time horizon under the normal and abnormal conditions. These trajectories are depicted with red color in the Figure 4.2. Under the normal conditions it is assumed that the magnitude of disruption (parameter gamma in equation 4.5) is equal to zero. Under the abnormal condition it is assumed that the value of gamma is greater than zero for a square area restricted spatially by $[0.4, 0.6] \times [0.4, 0.6]$. At this point the exact value of parameter gamma is not important, since the general behavior pattern is under investigation.

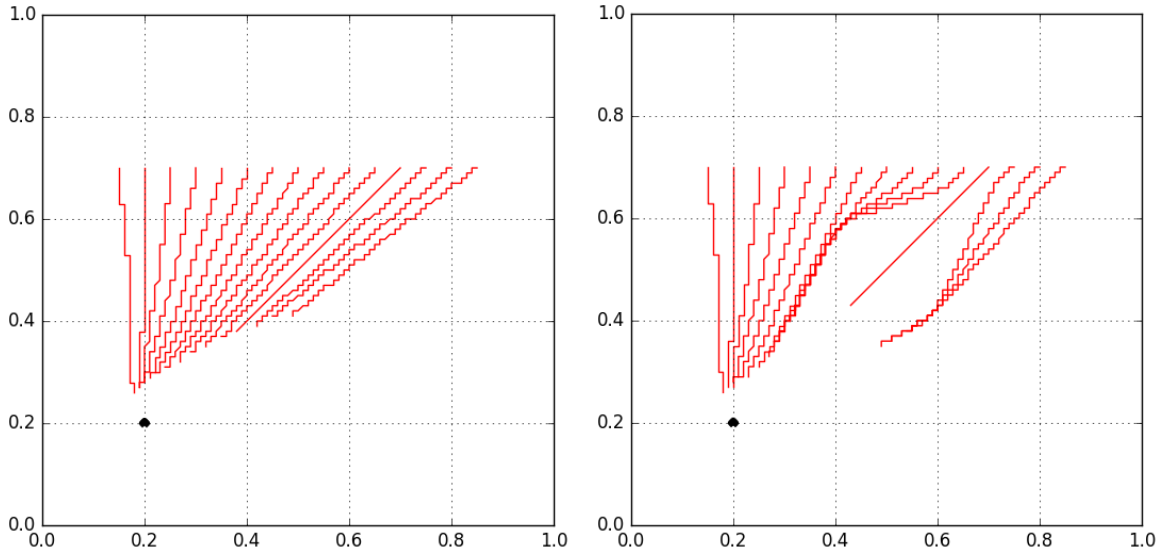


**Figure 4.2** Trajectories of 15 probes moving inside the continuum field under the normal (left) and abnormal (right) conditions. Probes origin is the same for both simulation trials.

As it could be observed from the Figure 4.2, the trajectories of probes follow intuitive assumptions on motorist's behavior. More precisely, the travelers chose the shortest path to the destination under the normal conditions. In a turn, under the abnormal conditions, the travelers try to avoid the disrupted area with capacity reduction. This behavior is in accordance with the real-life scenarios, which makes it reasonable to conclude that in some extend the aforementioned continuum model depicts the real behavioral characteristics of travelers. Therefore, this model could serve as a basis while investigating the performance of proposed tensor-based approach.

### 4.3.4. Examination of the performance of detection

In order to examine the performance of proposed tensor-based abnormal traffic patterns detection approach, the following procedure is considered in current study. First of all, the number of probes used in simulation has been increased and setup to 100 and 1000 consequently. Secondly, for each of these population of probes, the mesh-wise average speed maps have been calculated using the equation (4.6) under variable spatiotemporal resolutions and disruption magnitude. Regarding the parameters of error terms in equation (4.6), $\varepsilon_k$ and $\delta_k$ follow Gaussian distribution with zero mean and the variance estimated using median absolute deviation of total travel distance and total travel time respectively. The median absolute deviation is utilized for estimation, since it is resilient to possible outliers in a dataset. Further, these average speed maps were transformed into a tensor

representation, and tensor robust principal component analysis was applied in order to detect anomalous patterns.

Without loss of generality and for the illustrative purposes, the specific simulation setup is described in details in current subsection. The population of probes is assumed to be equal to 1000, with spatial resolution is setup to 0.2 (square mesh cell size) with 10 time intervals within the simulation horizon. In total seven simulation trials has been conducted. During one of this seven trials, the magnitude of disruption is greater than zero and equal to 0.4 (value of gamma in equation (4.5)). The choice of 7 simulation trials could be thought as observation of traffic patterns during

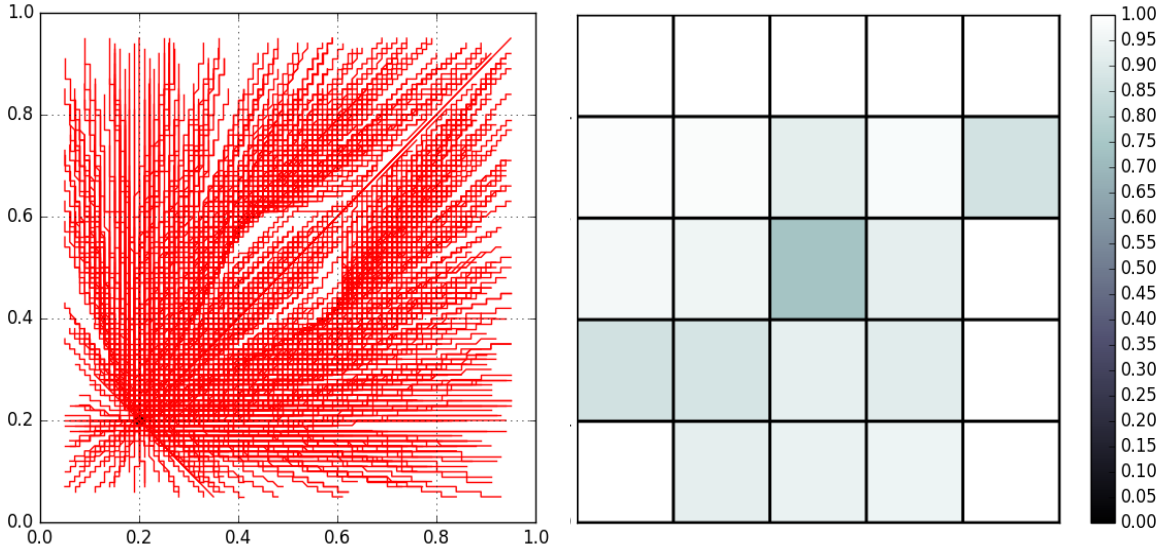


**Figure 4.3** Trajectories of 1000 probes under the abnormal conditions (left) and snapshot of mesh-wise average speed map during corresponding simulation trial (right). Spatial resolution: 0.2 (25 mesh cells). The darker colors corresponds to the lower values of average speed comparing to the maximum values (maximum value: 1.00).

seven consequent days of the week, considering the real-life scenario. The disruption is located in the middle of simulation domain, more precisely in square area restricted spatially by $[0.4, 0.6] \times [0.4, 0.6]$ and leads to the capacity reduction according to the equation 4.5. The trajectories of probes under the disrupted conditions are depicted on the Figure 4.3 (left), and the corresponding snapshot of average speed map is shown on the Figure 4.3 (right). The mesh-wise average speed map has been calculated using the equation 4.6.

From the Figure 4.3 above it could be observed that there are noticeable speed drops in the middle of simulation domain, as well as in the close proximity to destination. The purpose of further

applied tensor robust principal component analysis is to detect these anomalous patterns and inspect them in order to justify if the speed drops are related to abnormal traffic patterns formed due to the disruption or exist under the normal conditions. That's it, the noticeable speed drops could correspond to the abnormal traffic pattern caused by the disruption or could be expected, such as expected low speed values during morning or evening rush hours.

In order to meet this goal, constructed mesh-wise average speed maps during aforementioned seven simulation trials were converted into a tensor-based representation as following. A 3rd order tensor $\boldsymbol{\mathcal{X}} \in \mathbb{R}^{I_1 \times I_2 \times I_3}$ with one spatial dimension ($I_1$) and two temporal dimensions ($I_2$ and $I_3$) has been constructed. The spatial dimension ($I_1$) is of size 25 and corresponds to the total number of mesh cells with chosen spatial resolution. Two temporal dimensions ($I_2$ and $I_3$) are of sizes (10 and 7) and correspond to the number of time intervals within one simulation trial and the number of simulation trials respectively. This data transformation procedure is shown on the Figure 4.4. After transforming average speed maps into a tensor representation, tensor robust principal component analysis, described in subsection 3.2.2, has been applied to decompose constructed traffic data tensor $\boldsymbol{\mathcal{X}} \in \mathbb{R}^{I_1 \times I_2 \times I_3}$ into the low-rank component $\boldsymbol{\mathcal{Y}}$ and a sparse component $\boldsymbol{\mathcal{Z}}$. Once again, the sparse tensor $\boldsymbol{\mathcal{Z}}$ contains the information regarding the anomalous traffic conditions, therefore the

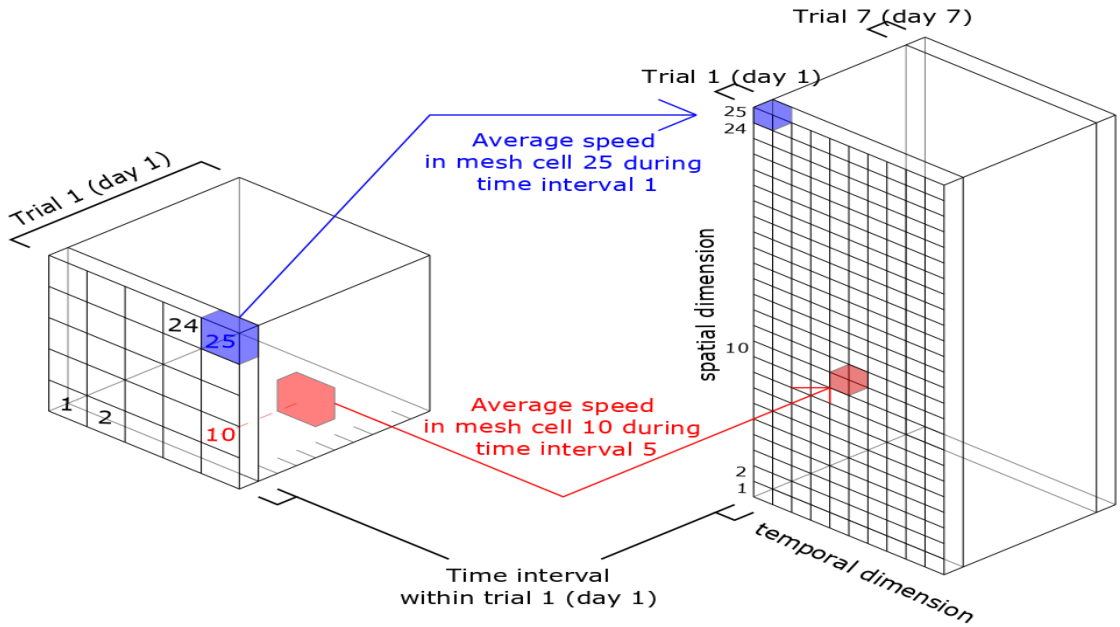


**Figure 4.4** Mesh-wise average speed map during one simulation trial (left) with mesh cell numeration. Constructed tensor (right). Colored arrows depict the transformation process.

entries of this tensor have to be examined.

By slicing tensor $\mathcal{Z}$ trial-wise (total 7 slices), it has been observed that one slice appears significantly different from the others. More precisely, this slice has many negative entries, which correspond to the deviation of average speed from the expected. Other six slices has almost no or much lesser amount of negative entries. This abnormal slice and the normal one for reference are depicted on the Figure 4.5. This abnormal slice corresponds to the simulation trial when the magnitude of the disruption field was setup greater than zero, unlike other six simulation trials. And as one could observe from the Figure 4.5, the abnormal traffic pattern formed due to the presence of the disruption is noticeable and mesh cells affected by this disruption could be correctly identified. At this point it is necessary to clarify the key feature of proposed tensor-based anomalous traffic patterns detection approach once again. Consider traffic speed and one of the most straightforward abnormal traffic patterns detection method, namely threshold-based method, where the speed values below predefined threshold are marked as abnormal. For instance, according to aforementioned threshold-based method, speed drops in the middle of the simulation domain and in vicinity of the destination on Figure 4.3 could be marked as abnormal. However, the speed drops in vicinity of destination were not caused by the existence of disruption, yet due to the traffic compression, which in fact an expected behavior, and in real-life situation could correspond to expected speed drops during morning or evening peak hours at particular region in urban area. On the other hand, the speed drops in the middle of simulation domain are unexpected and caused by the existence of

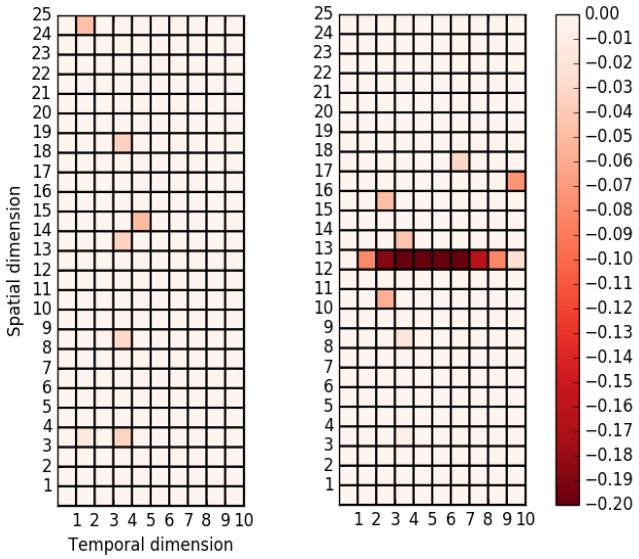


**Figure 4.5** Trial-wise sparse tensor slices. Normal slice (left) and abnormal slice (right). The brighter colors corresponds to the higher values of speed drops (in percentage).

disruption. In contrast to the threshold-based method, proposed tensor-based approach allow not only to detect abnormal patterns, but also to distinguish these two cases, since the expected speed drops are treated as a low-rank patterns, and unexpected speed drops are treated as a sparse components. Therefore, by utilizing proposed tensor-based approach, it is possible to understand if the abnormal traffic pattern was caused by the existence of unexpected disruption, which is one of the key issue raised in subsection 2.4. Additionally, it is worth to mention that the value of regularization parameter lambda in equation (3.15) for current simulation was empirically chosen equal to 0.2. Under the different values of lambda, deviated slightly ($\pm 0.1$) from the empirically chosen value, one still be able to observe the disruption pattern, however less clearly. In general, as it was mentioned beforehand, there is no best value of lambda, and its value should be tuned to each particular data. Additionally, it has been observed that the higher values of magnitude of disruption force traffic pattern to deviate more from the normal conditions, therefore the abnormal pattern is more noticeable.

In order to quantitatively investigate the performance of proposed tensor-based abnormal traffic patterns discovery approach under different spatiotemporal resolutions, the following procedure has been considered. For a given population of probes $N$, spatial resolution $R$ and temporal resolution $T$, the number of negative entries inside each trial-wise tensor slice $S$ (total 7 trials) is calculated and depicted as $P_{R,T}^{S}(N)$. Each of these negative entries corresponds to the speed drop at particular mesh cell and time interval. Further, the modified Z-score (Ahmadi and Sarmad, 2010) has been calculated for each trial within the simulation setup, and used to judge if the tensor slice corresponds to normal or anomalous traffic conditions. The calculation of modified Z-score for each tensor slice is as following

$$Z_S = \frac{0.6745(P_{R,T}^{S}(N) - \bar{P})}{MAD} \tag{4.7}$$

where $\bar{P}$ corresponds to the median and MAD corresponds to median absolute deviation. The reason behind utilization of this statistical indicator is the fact that modified Z-score is a standardized score that measures anomaly strength or how much a particular score differs from the

typical one. This indicator is more robust because it relies on the median for calculating Z-score. The results of calculations of modified Z-scores for different simulation setups are shown in the Table 4.1 for the population of probes 1000 used for the aforementioned simulation setup. Typically, the scores with values greater than three are considered as anomalous.

As one could observe from the Table 4.1, under the high spatiotemporal resolutions (smaller mesh cells and shorter time intervals) the anomalous patterns could be detected (forth row-wise entry) more clearly. On the other hand, when the spatial size of mesh cell is bigger than the size of the disruption or time interval exceed the certain threshold, the abnormal pattern could not be detected. Therefore, by knowing the given number of available probes and several characteristics of the disruption, such as approximate size and the duration, one could chose an appropriate spatiotemporal resolution in order to mine anomalous traffic patterns and analyze traffic dynamics. Moreover, in current subsection the results under the population of probes equal to 1000 were demonstrated, however during the simulation it was also observed that by reducing the population of probes to 100, it became more difficult to detect anomalous pattern due to the higher degree of

**Table 4.1** Modified Z-scores for simulation setups with variable spatiotemporal resolutions. Results are for population of probes: 1000. Spatial resolutions are as a percentage of the simulation domain length. Temporal resolutions are as a percentage of the simulation horizon.

| Tensor slices | Temporal resolution [% of simulation time] | Temporal resolution [% of simulation time] | Temporal resolution [% of simulation time] |
|---|---|---|---|
| | 10% | 20% | 50% |
| | Spatial resolution [% of domain length] | Spatial resolution [% of domain length] | Spatial resolution [% of domain length] |
| | 10% | 10% | 10% |
| | Z-scores | Z-scores | Z-scores |
| 1 | 0.6745 | 0 | 0 |
| 2 | 0 | −0.6745 | −0.6745 |
| 3 | −0.6745 | 1.349 | −0.6745 |
| 4 | 8.7685 | 5.396 | 0.6745 |
| 5 | 2.0235 | −2.698 | 0 |
| 6 | 0 | 0.6745 | −0.6745 |
| 7 | −2.0235 | −0.6745 | 0 |
| Tensor slices | Temporal resolution [% of simulation time] | Temporal resolution [% of simulation time] | Temporal resolution [% of simulation time] |
| | 10% | 20% | 50% |
| | Spatial resolution [% of domain length] | Spatial resolution [% of domain length] | Spatial resolution [% of domain length] |
| | 20% | 20% | 20% |
| | Z-scores | Z-scores | Z-scores |
| 1 | 0 | −0.6745 | 0 |
| 2 | 1.349 | 0 | −0.6745 |
| 3 | −0.6745 | −0.6745 | 0 |
| 4 | 3.3725 | 0.6745 | 0.6745 |
| 5 | −0.6745 | 0 | −0.6745 |
| 6 | 0 | 0.6745 | −0.6745 |
| 7 | 1.349 | 0 | 0 |
| Tensor slices | Temporal resolution [% of simulation time] | Temporal resolution [% of simulation time] | Temporal resolution [% of simulation time] |
| | 10% | 20% | 50% |
| | Spatial resolution [% of domain length] | Spatial resolution [% of domain length] | Spatial resolution [% of domain length] |
| | 25% | 25% | 25% |
| | Z-scores | Z-scores | Z-scores |
| 1 | 0.6745 | 0.6745 | 0 |
| 2 | 0 | 1.349 | −0.6745 |
| 3 | −0.6745 | −0.6745 | −0.6745 |
| 4 | −1.349 | −1.349 | 0.6745 |
| 5 | 0 | 0 | 0 |
| 6 | −1.349 | 0 | 0.6745 |
| 7 | 0.6745 | 0 | 0.6745 |

fluctuations in constructed speed map (since less probes were used for speed map calculations) and existence of missing data (since there were mesh cells with no probes at particular time intervals). The discussion related to the accuracy of speed map is provided in the following subsection. Moreover, need to mention that the magnitude and scale of disruption could affect the results. In particular, it is important to have some a priori knowledge regarding the disruption and chose an appropriate value of regularization parameter lambda while decomposing traffic data tensor into the low-rank and sparse components. Otherwise, the utilized modified Z-score might produce misleading results

### 4.3.5. Examination of accuracy of constructed speed map

In previous subsection the examination of the performance of proposed tensor-based abnormal traffic patterns detection approach with the help of synthetic data has been conducted. Assuming specific spatiotemporal resolution and the population of probes, the average speed maps under normal and abnormal conditions were constructed first, and further transformed into a tensor representation. And finally, with the help of tensor robust principal component analysis the abnormal traffic pattern has been detected. As it has been demonstrated in the literature review part, in particular in section 2.2, the similar flow could be used in real-life situations, where real vehicle data is used for traffic dynamics monitoring. However, there are several important practical questions arises. In particular, since all real-life observations of some phenomena usually contain errors, it is important to understand what level of accuracy one could expect to obtain. More precisely, following the discussion in previous subsection it is important to investigate how accurate the constructed average speed maps actually are.

In order to meet this objective, first of all it is important to clarify what could be considered as an accurate speed map. By examine the equation 4.6, which has been used to calculate the speed maps, it could be seen that the sum of error terms $\varepsilon_k$ and $\delta_k$ is decreasing when the number of probes inside particular mesh cell is increasing, since both of these terms have zero mean and follow Gaussian distribution. Even more, when the number of probes tends to infinity, the aforementioned sum of error terms disappear. This infinite number of probes could be treated as the continuum limit.

That's it, the described continuum model could be thought as a special case when the number of drivers tends to infinity. And since under this condition the errors are vanishing, the speed map calculated using continuum model directly is assumed to be the accurate speed map. Therefore, switching back to the examination of speed map accuracy using finite number of probes, the following procedure is considered. First, mesh-wise average speed map $U_{i,j}^t$ with given spatiotemporal resolution and population of probes is calculated using the equation 4.6. Secondly, with the same spatiotemporal resolution, another speed map $V_{i,j}^t$ is calculated by aggregating the continuum speed (equation 4.4). Further, these two speed maps are compared in terms of root-mean-square error (RMSE) as following

$$RMSE = \sqrt{\frac{1}{T \times I \times J} \sum_{t=1}^{T} \sum_{i=1}^{I} \sum_{j=1}^{J} (U_{i,j}^t - V_{i,j}^t)^2} \tag{4.8}$$

where $I$ and $J$ stands for the latitude and longitude number of mesh cells, and $T$ stands for the total number of time instances within a simulation horizon. Further, the accuracy of each particular speed map is defined as $(1 - RMSE)$. The similar procedure has been conducted for different spatiotemporal resolutions, in particular for temporal resolutions equal to {0.01, 0.05, 0.1, 0.2, 0.5} which are {1%, 5%, 10%, 20%, 50%} of simulation time horizon; and spatial resolutions equal to

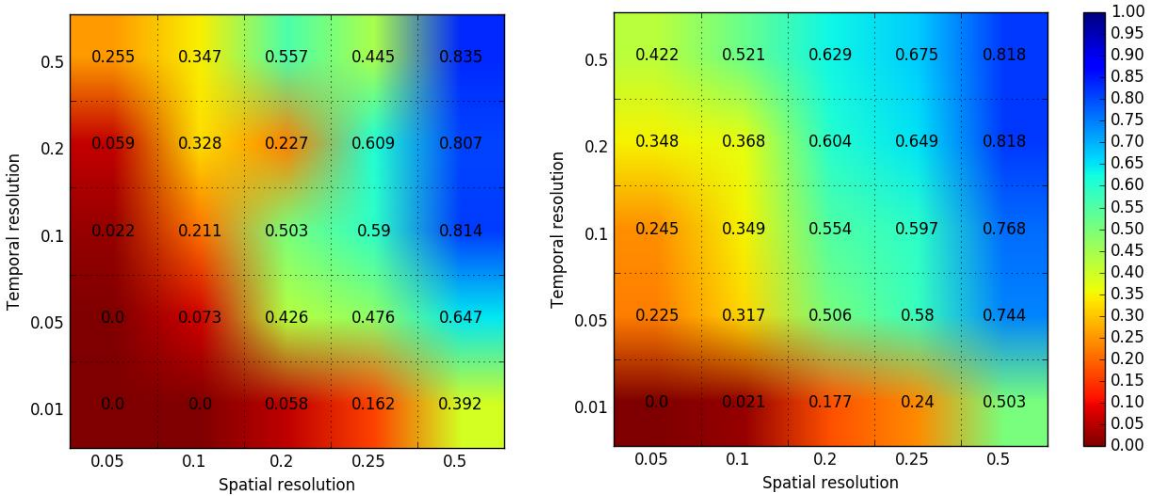


**Figure 4.6** Speed map accuracy (in a heat map form) for different spatiotemporal resolutions and population of probes. Population of probes: 100 (left) and 1000 (right).

{0.05, 0.1, 0.2, 0.25, 0.5} which are the mesh cell sizes.

The results of accuracy calculations are visualized as a heat maps shown on the Figure 4.6 for two different population of probes: 100 (left plot) and 1000 (right plot). The number inside each heat map cell corresponds to the accuracy under certain spatiotemporal resolution, calculated by the subtraction of the value in equation (4.8) from one. From the Figure 4.6 it could be observed that by increasing the population of probes it is possible to achieve the higher accuracy keeping the same spatiotemporal resolution. Moreover, by making the size of mesh cells bigger spatially or by increasing the temporal resolution it is also possible to achieve better accuracy. For illustrative purposes three-dimensional versions of speed map accuracy measurements are provided in Appendix B.

## 4.4. Chapter summary

This chapter is devoted to the validation of proposed tensor-based abnormal traffic patterns detection approach on synthetic data and investigation of its properties. For these purposes the following procedure has been completed. First of all, the continuum modeling approach has been employed in order to model the overall behavioral characteristics of traffic dynamics in large urban areas. The basic continuum model found in the literature has been adopted and extended by introduction of so-called disruption field which emulates real-world disasters, and by introduction of probes, individual particles, traveling inside the continuum field. With the help of continuum modeling approach it is possible to focus on the overall behavior of travelers at the macroscopic level, and to mitigate the problem connected with the presence of large number of parameters and variables in case of conventional models. Moreover, introduction of individual probes allow to make the connection between conceptual continuum model and the real traffic data. By conducting numerical simulation the proposed tensor-based approach has been validated. More precisely, it has been demonstrated that the abnormal traffic patterns occurred due to the presence of external disruption could be correctly identified spatially and temporally. In addition, the performance of detection was investigated under different spatiotemporal resolutions. According to the results, the performance of detection is increasing with the higher spatiotemporal resolutions and decrease vice

versa. Besides investigation of the performance of proposed approach, the investigation of accuracy of constructed speed maps utilized in this chapter has been conducted under different spatiotemporal resolutions. The results demonstrate that unlike the performance of detection, the higher spatiotemporal resolution leads to the less accurate speed maps, and then therefore the appropriate choice of spatiotemporal resolution should be considered.

# 5. Validation on real traffic data

## 5.1. Probe vehicle data

It has been highlighted in literature review section that probe vehicle data is a well-known and valuable source of information regarding vehicle movements. The advantages of utilization of this type of data for analysis of traffic dynamics in large transportation networks were discussed in details in subsection 2.1.3. In particular, probe vehicle data could help to obtain sufficient amount of information from the arterial roads and also this type of data could be collected under the abnormal conditions, such as natural disasters, when fixed-location sensors could not operate due to blackouts or other disruptions (Hara and Kuwahara, 2015). Therefore, probe vehicle data is chosen in this study as a source of information regarding traffic dynamics in order to validate and examine the properties of proposed tensor-based abnormal traffic patterns detection approach.

The real probe vehicle data utilized in this study has been kindly provided by the Fujitsu Traffic & Road Data Service Limited[1]. This raw probe vehicle data is a collection of geo-referenced coordinates, obtained via GPS receivers from the vehicles travelled all across Japan, and corresponding time stamps. For each particular day probe vehicle data consists of several data files obtained from different vehicles. Each data file consists of multiple data records (GPS coordinates and corresponding time stamps), with sampling rate equal to one second.

This raw probe vehicle data has been further aggregated by the assistant professor Takahiko Kusakabe[2] with spatial resolution equal to one square kilometer and temporal resolution equal to five minutes. After the aggregation process the following data is available: total distance traveled by all the probe vehicles inside each particular mesh cell of one square kilometer; total time spend by all these probe vehicles in corresponding mesh cell during every five minutes time interval within a day; total number of probe vehicles, referred further as the number of samples, who was traveling in corresponding mesh cell during each particular five minutes time interval. Without loss of generality, for further analysis the subset of this aggregated data during the year 2014 only and corresponding to the traffic dynamics in greater Tokyo area has been chosen.

[1] Fujitsu Traffic & Road Data Service Limited: http://www.fujitsu.com/jp/group/ftrd/
[2] Center for Spatial Information Science. Dept. of Socio-Cultural Environmental Studies, Graduate School of Frontier Science, The University of Tokyo

### 5.1.1. Data preprocessing

An important step in data analysis of almost any real-life observations is data preprocessing. In general, due to the measurement inaccuracy and other factors, the errors might occur. In this study, in case of probe vehicle data analysis, geo-referenced coordinates obtained via GPS receivers appeared to contain not feasible observations. These observations (outliers) that lies outside the overall pattern of a distribution had to be detected and removed before further analysis. The approach based on the interquartile range (IQR) calculation was implemented in order to detect and exclude these outliers (Shevlyakov et al., 2013). The origin of this method is based on the exploratory data analysis framework proposed by John Tukey in 1977, and known as a Tukey's Outlier Filter, where threshold values (fences) are used to detect outliers, considering the remoteness from the mean value. The algorithm of outlier detection is explained below.

First of all, following the aggregation process described in previous subsection, the targeted region for analysis is divided into a uniform mesh with square mesh cells of one square kilometer. With the respect to this spatial resolution, and taking into account time discretization within a day into 288 equal time intervals (5 minutes time intervals), the average speed $V_{i,j}^{t,d}$ inside the particular mesh cell with indexes $(i,j)$ for a time interval $t$ during day $d$ is calculated. This procedure has been conducted for all the mesh cells, all time intervals and days. Further, the outlier detection algorithm has been performed as follows.

1. For a fixed mesh cell $(i,j)$, the corresponding cell speed profile vector has been calculated:

$$\tilde{P}_{i,j} = \left[V_{i,j}^{1,1}, V_{i,j}^{2,1}, \dots, V_{i,j}^{T,1}, V_{i,j}^{1,2}, \dots, V_{i,j}^{t,d}, \dots, V_{i,j}^{T,D}\right]^T \quad \forall d = \overline{1,D}, \ \forall t = \overline{1,T} \tag{5.1}$$

2. For this cell speed profile vector $\tilde{P}_{i,j}$, the corresponding interquartile range (IQR), lower and upper inner fences were calculated as follow:

$$IQR_{i,j} = Q_{i,j}^3 - Q_{i,j}^1 \tag{5.2}$$

$$LIF_{i,j} = Q_{i,j}^1 - 1.5IQR_{i,j} \tag{5.3}$$

$$UIF_{i,j} = Q^3_{i,j} + 1.5IQR_{i,j} \tag{5.4}$$

where

$Q^1_{i,j}$ : the 25th percentile (the first quartile) of the ordered $\tilde{P}_{i,j}$ vector

$Q^3_{i,j}$ : the 75th percentile (the third quartile) of the ordered $\tilde{P}_{i,j}$ vector

3. The valid average speed values had been defined as values of speed profile, which lie between the lower and upper inner fences. Other values defined as outliers and were removed:

$$V^{t,d}_{i,j} = \begin{cases} valid\ if\ LIF_{i,j} \leq V^{t,d}_{i,j} \leq UIF_{i,j}, \\ outlier, if\ V^{t,d}_{i,j} < LIF_{i,j}\ or\ V^{t,d}_{i,j} > UIF_{i,j.} \end{cases} \tag{5.5}$$

4. The outlier's detection procedure above had been repeated from the first step for all mesh cells.

After conducting the outlier detection procedure above for every consequent month during the year of 2014, it was revealed that the number of non-feasible observations of the speed for each month is almost equal, and the average value (month-wise) of erroneous observations in available data is 0.83%. These non-feasible values of average speed has been detected and removed.

Besides outlier detection, an important step in data preprocessing stage is data filtering. While working with probe vehicle data, the number of samples, in other words the number of probe vehicles available for analysis and used for calculating the average speed, vary according to different temporal intervals and spatial locations. And since the average speed is calculated by the speed of sampled vehicles, the small number of samples leads to volatile estimates. For instance, on the Figure 5.1 (top right) the mesh speed as a function of time within a day for a mesh cell number 53394725 during January 17th (Friday) along with the corresponding number of samples is depicted. The relative position of this cell within greater Tokyo area is depicted on the Figure 5.1 (left). From the Figure 5.1 one could observe that the smaller number of samples probably leads to the higher speed fluctuations. In order to investigate quantitatively the impact of the number of samples into the magnitude of speed value fluctuations, the following procedure has been

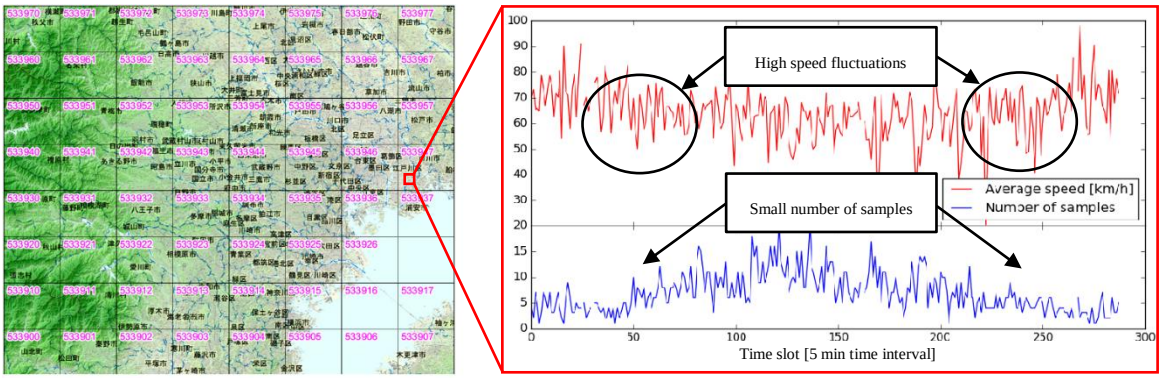


**Figure 5.1** Mesh cell average speed as a function of time within a day (top right) and corresponding number of samples (bottom right). Relative position of mesh cell within the targeted area (left).

considered. The average velocity gap between successive time intervals for a mesh cell $(i,j)$ is introduced and defined as following

$$\Delta_{i,j}^{t,d} = V_{i,j}^{t+1,d} - V_{i,j}^{t,d} \tag{5.6}$$

Whereas before $V_{i,j}^{t,d}$ is a mesh cell average speed during time interval *t* during the day *d*. The typical behavior of velocity gaps as a function of number of samples is shown on the Figure 5.2 below. For illustrative purposes the mesh cell numbered 53392684 during January 16th (Thursday) is chosen since it demonstrate more clear dependency, which in fact similar for the aforementioned mesh cell 53394725. Based on these results, one could conclude that lower number of samples leads to higher degree of fluctuations, and higher number of samples decrease the speed fluctuations. In order to

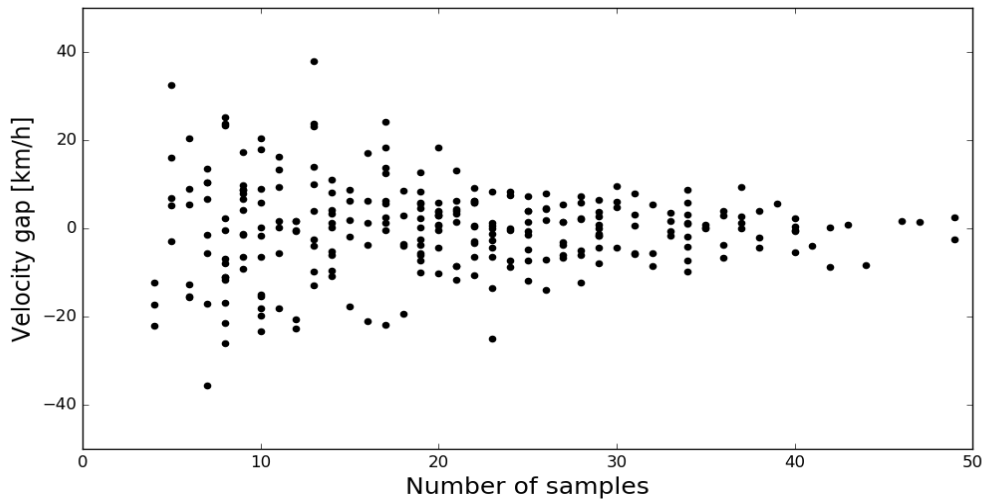


**Figure 5.2** The values of mesh cell velocity gaps as a function of the number of samples for a mesh cell in targeted area.

mitigate these fluctuations, in current study the utilization of filtering technique is proposed. More precisely, proposed utilization of Savitzky–Golay filter (SGF) (Bromba and Ziegler, 1981). In general, SGF is a digital filter that can be applied to a set of data points for the purpose of smoothing the data, that is, to increase the signal-to-noise ratio without distorting the signal. In case of probe vehicle data, filter is applied to a mesh speed profile vector $\tilde{P}_{i,j}$, defined by the eq. (5.1), to obtain filtered profile vector $\hat{P}_{i,j}$. To demonstrate how this filter operates, on the Figure 5.3 the part of a vector $\tilde{P}_{i,j}$ and corresponding part of vector $\hat{P}_{i,j}$ for a mesh cell number 53393676, located in neighboring region with the previously mentioned mesh cell 53394725, during January 16th (Thursday) is depicted.

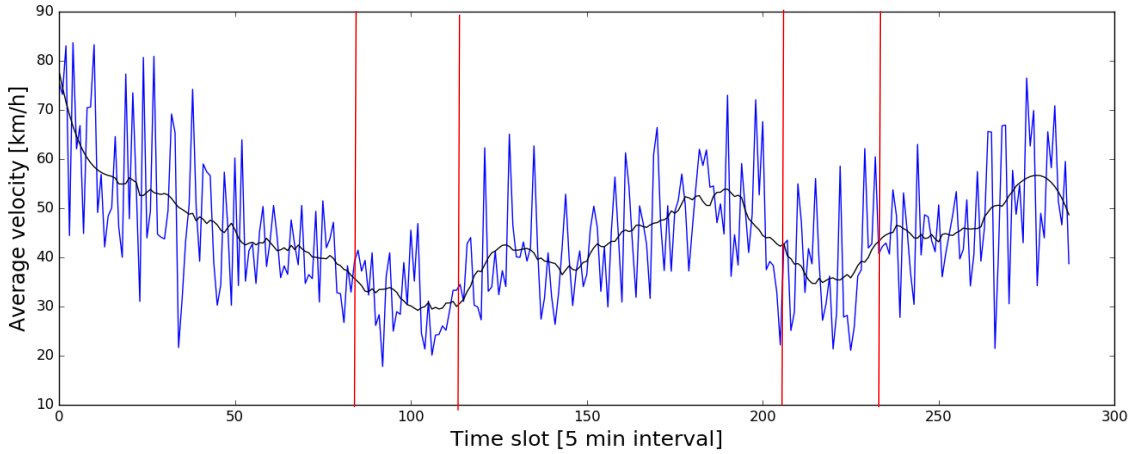


**Figure 5.3** Mesh cell average speed evolution process in time within a day for a mesh cell in targeted area. Blue plot: mesh average speed obtained from the raw probe vehicle data. Black plot: average speed after SGF procedure. With red colors depicted time intervals: 7:00am-9:00am and 17:00pm-19:00pm.

First of all, from the Figure 5.3 one could observe that the day-wise speed profile follows the intuitive expectations. In particular, the average speed is higher during early morning, daytime and late night time periods due to the less congested traffic conditions. Moreover, the decrease in speed during morning and evening peak hours also noticeable. Additionally, from this Figure 5.3 one could observe that the values of speed obtained from the raw data have a high degree of fluctuations due to the limited number of samples, and the proposed utilization of SGF filtering technique allows to smooth the speed profile, as well as to eradicate these high frequency fluctuations. In addition, proposed SGF filtering method also helps to mitigate the issue connected with the existence of missing data by linear interpolating the regions with missing data at first. However, need to mention

that application of filtering technique to the data has several disadvantages. In particular, the evolution of speed profile that exhibit abrupt departures from their typical trends, such as sharp waves or steps, tend to be oversmoothed by the SGF filtering, which possibly can lead to the loss of information regarding some abnormal event. Moreover, the performance of this filtering technique depends on the choice of parameters of the filter, such as polynomial order and window length. In addition, the interpolation of the regions with missing data should be considered carefully if order to avoid not realistic speed values.

### 5.1.2. Visual data examination

In order to examine in what extend utilized probe vehicle data could represent the real traffic conditions, the visualization has been conducted. First of all, the average speed maps for the whole targeted area, depicted in the Figure 5.4, during two consequent days: February 2nd (Sunday) and February 3rd (Monday) of the year 2014 are calculated. The calculation is done assuming spatial resolution equal to one square kilometer and temporal aggregation corresponds to the morning hours: 7:00am – 9:00 am. The results are shown on the Figure 5.5.

The following observation could done from the Figure 5.5. First of all, one could observe that in constructed average speed maps the topological objects, such as Tokyo bay area and highways could be identified. Secondly, it also could be observed that the average speed during morning hours


**Figure 5.4** Targeted region for analysis of 80 sq. km. inside the greater Tokyo area.

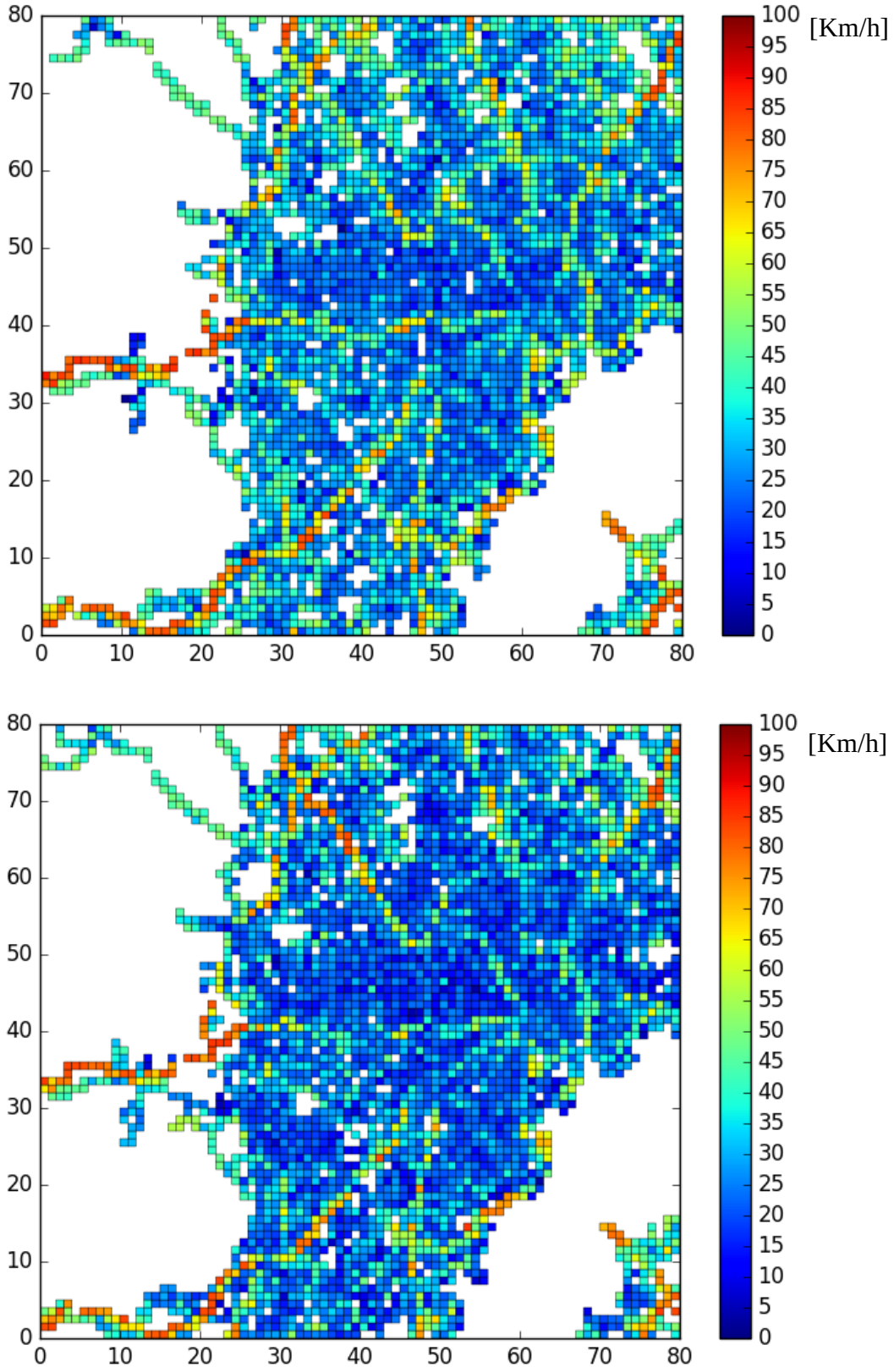


**Figure 5.5** Mesh-wise average speed for targeted region of 80 sq. km inside Tokyo area. Spatial resolution: 1 sq. km. temporal dimension correspond to the morning hours: 7:00 am – 9:00 am during Feb 2nd (Sunday; upper plot) and Feb 3rd (Monday; bottom plot). Mesh cells numeration (longitude and latitude cell numbers) are depicted.

On February 2nd (Sunday) is on average higher than the average speed on Monday (3rd of February). More precisely, the mesh-wise average speed during morning hours on Sunday is equal to 34.1 km/h and the corresponding mesh-wise average speed during morning hours on Monday is equal to 30.5 km/h, which gives the 11.8% difference in average speed comparing aforementioned weekend and weekday. This is intuitively expected observation, since traffic conditions tend to be busier during weekdays. Additionally, by comparing the mesh-wise average speed during daytime: 13:00-15:00 on Monday (3rd of February), which is equal to 33.0 km/h and depicted on the Figure 5.6, one could notice the increase in average speed by the 8.1%. This is also an expected results since the traffic during daytime is less busy comparing to the one during morning hours.

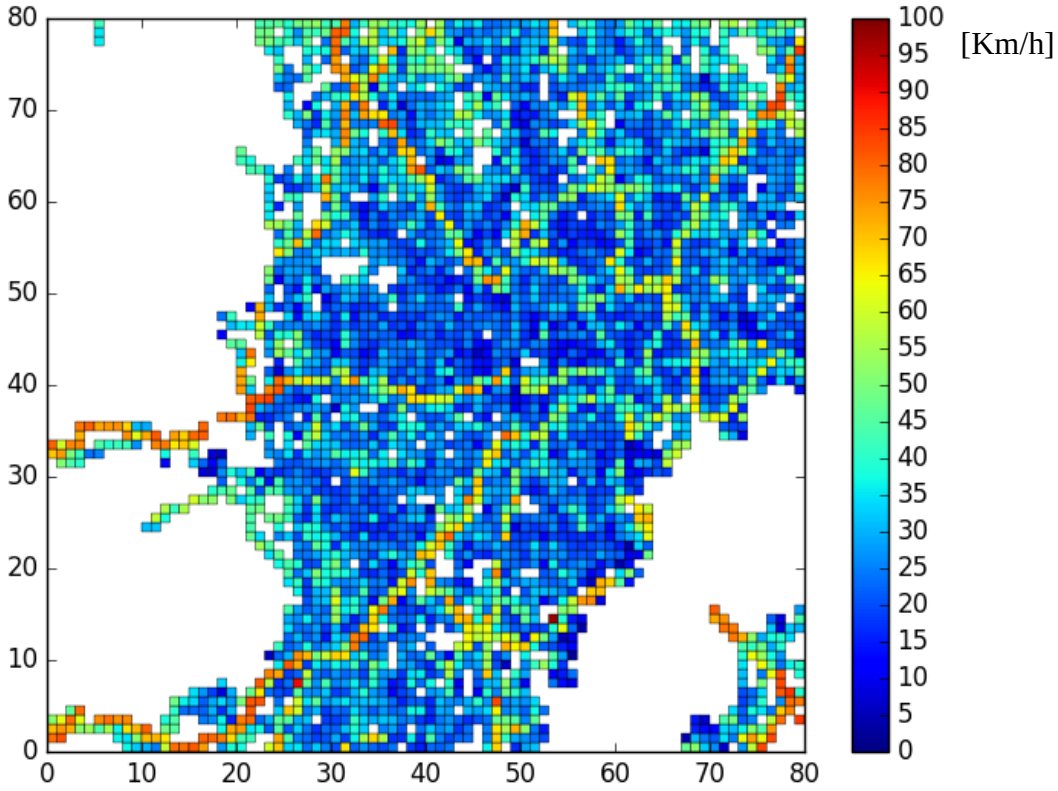


**Figure 5.6** Mesh-wise average speed for targeted region of 80 sq. km inside Tokyo area. Spatial resolution: 1 sq. km. temporal dimension correspond to the daytime hours: 13:00 pm – 15:00 pm during Feb 3rd (Monday). Mesh cells numeration (longitude and latitude cell numbers) are depicted.

Based on aforementioned observations, at this point, it seems reasonable to further investigate properties of traffic flow, since aggregated probe vehicle data appeared to justify the intuitive expectations regarding traffic conditions. However, before switching to the investigation of abnormal traffic patterns it is necessary to take a closer look at the spatiotemporal dependencies.

## 5.2. Examination of spatiotemporal dependencies

Besides visual examination of constructed speed maps, provided in previous subsection, it is desirable to formally investigate spatiotemporal dependencies before switching to the abnormal traffic patterns detection. For this purpose, the following procedure is considered in this study.

Firstly, the metric to measure the distance between spatially adjusted mesh cells is introduced as following. Assume mesh cells A and B. If these cells have common edge, the distance between them is assumed to be equal to zero. If cells A and B does not have common edges, but there is exist another cell C, which have common edges with A and B, it is assumed that the distance between them is equal to one. Using this metric, several triplets (three neighboring mesh cells) in different regions inside Tokyo area are chosen. For example, assume that the mesh cell with index $(i, j)$ is chosen. Thus, two neighboring cells with indexes: $(i + 1, j)$ and $(i + 2, j)$ with distances (describe above) equals to zero and one, relative to cell $(i, j)$. Here, the choice of $(i + 1, j)$ or $(i - 1, j)$ or $(i, j + 1)$ or $(i, j - 1)$ is equivalent, since the spatial homogeneity is assumed. Further, for each of those mesh cells from the triplet the daily mesh average speed profile vectors are constructed in similar manner as in the equation 5.1: $\tilde{P}^d_{i,j}; \tilde{P}^d_{i+1,j}; \tilde{P}^d_{i+2,j}$. These profile vectors contain the information regarding average speed evolution inside particular mesh cell within a day *d*. Further, following the data preprocessing stage described in subsection 5.2.2, filtered speed profile vectors are obtained: $\hat{P}^d_{i,j}; \hat{P}^d_{i+1,j}; \hat{P}^d_{i+2,j}$. Besides the distance metric, the following metric is introduced to compare the speed evolution processes in different mesh cells during the day within a triplet. More precisely, for the chosen mesh cell with indexes $(i, j)$ this metrics is calculated as following

$$ {}_0SIM^d_{i,j} = \sqrt{\frac{1}{T}\sum_{t=0}^{T-1}(\hat{P}^d_{i,j} - \hat{P}^d_{i+1,j})^2} \tag{5.7} $$

$$ {}_1SIM^d_{i,j} = \sqrt{\frac{1}{T}\sum_{t=0}^{T-1}(\hat{P}^d_{i,j} - \hat{P}^d_{i+2,j})^2} \tag{5.8} $$

In order to examine spatiotemporal dependencies using constructed metrics, the following triplets are further chosen. In total ten triplets, depicted in the Figure 5.7 are chosen for analysis and grouped

by their local features. More precisely, group 1 triplets (number 7,8,9) are the highway dominant regions, remoted from the central Tokyo area. Group 2 triplets (number 1,3,4,5,10) are the arterial roads dominant regions, located closer to central Tokyo area. Group 3 triplets (number 2,6) are remoted more from the central Tokyo area, however located closer than the ones in group 1. All these triplets and their relative positions inside the targeted region are shown on the Figure 5.7. The metrics defined by the equations 5.7 and 5.8 show how similar are the processes of evolution of average speed in a neighboring mesh cells within a triplet. These metrics are calculated and the results are demonstrated in the Table 5.1 below.

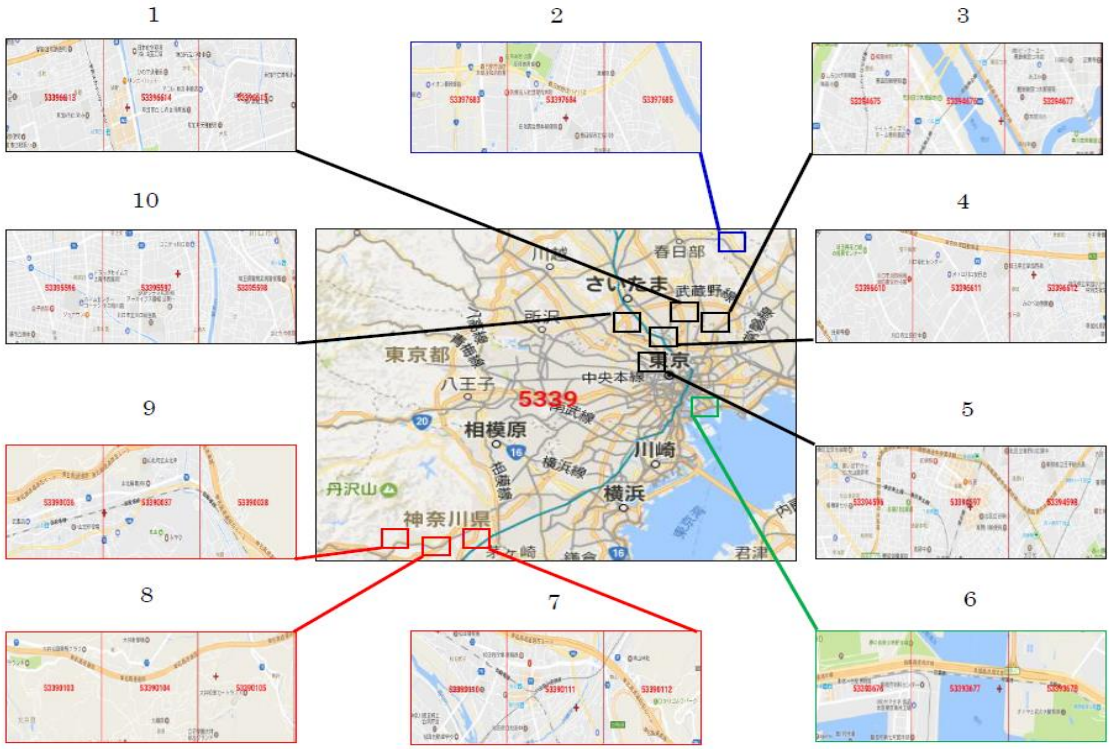


**Figure 5.7** Ten triplets chosen for analysis in different regions. They are grouped by, according to the relative features similarities. Group 1: triplets 7, 8, 9; Group 2: triplets 1, 3, 4, 5, 10; Group 3: triplets 2, 6.

From the results in Table 5.1 the following observations could be made. For a group 1 triplets (highway dominant regions), the values of ${}_0SIM^d_{i,j}$ are always lower than the values of ${}_1SIM^d_{i,j}$. This means that the closer mesh cells spatially, the more similar evolution processes of average speed inside them. Moreover, the values of ${}_0SIM^d_{i,j}$ and ${}_1SIM^d_{i,j}$ for this group 1 are in general smaller, comparing to other groups. This means that in triplets from this group 1, the behavior of

**Table 5.1** Similarity measurements of speed profiles for spatially adjusted mesh cells within different triplets.

| Triplet number | 1 | 2 | 3 | 4 | 5 | 6 | 7 | 8 | 9 | 10 |
|---|---|---|---|---|---|---|---|---|---|---|
| Group number | 2 | 3 | 2 | 2 | 2 | 3 | 1 | 1 | 1 | 2 |
| ${}_0SIM_{i,j}^d$ | 14.99 | 39.08 | 14.50 | 5.71 | 10.58 | 9.82 | 6.51 | 4.48 | 2.61 | 5.22 |
| ${}_1SIM_{i,j}^d$ | 10.77 | 41.66 | 15.61 | 7.01 | 11.78 | 9.38 | 8.95 | 5.04 | 6.48 | 9.69 |

mesh average speed as a function of time, are similar between the cells inside the corresponding triplets. This aspect could be clearly seen from the figures below (Figure 5.9; Figure 5.10; Figure 5.11). These figures show the evolution of mesh average speed as a function of time for 3 triplets from different groups (Figure 5.9: triplet from group 1; Figure 5.10: triplet from group 2; Figure 5.11: triplet from group 3. On all these figures, red plot corresponds to mesh cell with index $(i, j)$, blue plot corresponds to mesh cell with index $(i + 1, j)$, green plot corresponds to mesh cell with index $(i + 2, j)$, and black plot corresponds to the average speed inside the whole mesh, calculated as the total travel distance of all probe vehicles divided by the total time spend of these vehicles in corresponding 5 minutes time intervals. On these figures, only one triplet from each group is shown, more precisely triples number one, two and eight. One could observe from these figures that inside the triplet from the first group (highway dominant regions), the behavior of average speed values as a function of time in neighboring cells are more similar, comparing to the same behavior in other groups. This makes ${}_0SIM_{i,j}^d$ and ${}_1SIM_{i,j}^d$ lower, in general, for the first group. As for the arterial roads dominant regions (triplets from the second group), the values of ${}_0SIM_{i,j}^d$ are also less than the values of ${}_1SIM_{i,j}^d$. In other words, for the triplets from this group the evolution of speed profiles in closer mesh cells is more similar, comparing the evolution of speed profiles in spatially more remoted cells. As for the triplets from the third group, it could be noticed that the values of ${}_0SIM_{i,j}^d$ are also less or near equal to the values of ${}_1SIM_{i,j}^d$. However, in this group the behavior of 2nd triplet is very different, which gives large values of ${}_0SIM_{i,j}^d$ and ${}_1SIM_{i,j}^d$. This could be explained by the fact that in the left-most cell inside this triplet, the highway junction exist, and this probably is the reason why the average speed in this cell is always lower, comparing to other cells inside the triplet.

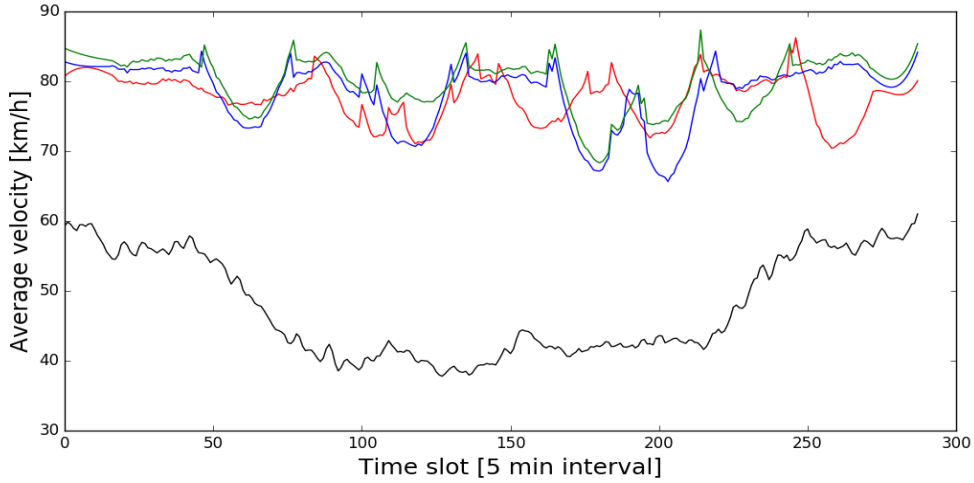


**Figure 5.9** Mesh cells average speed profiles for triplet 8 (group 1). Red plot: cell *(i,j)*. Blue plot: cell *(i+1,j)*. Green plot: cell *(i+2,j)*. Black plot: whole area of 80 sq. km. average speed.

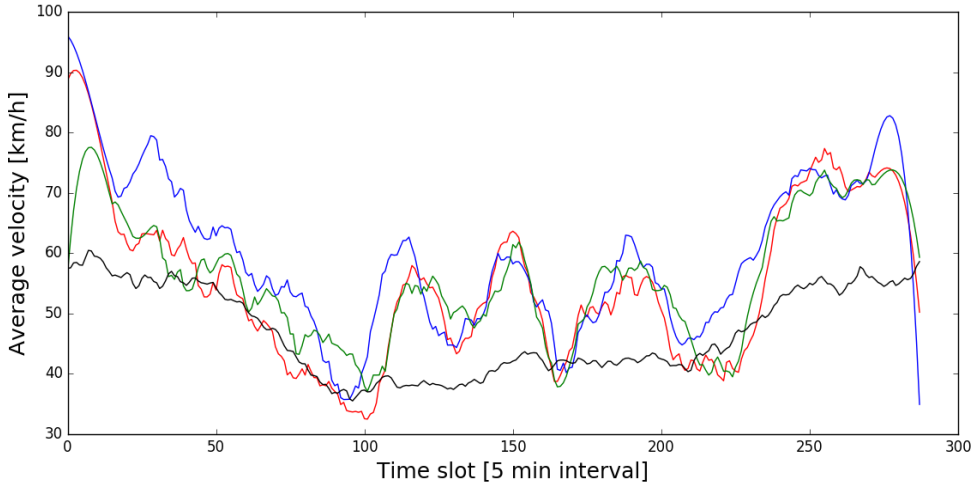


**Figure 5.10** Mesh cells average speed profiles for triplet 1 (group 2). Red plot: cell *(i,j)*. Blue plot: cell *(i+1,j)*. Green plot: cell *(i+2,j)*. Black plot: whole area of 80 sq. km. average speed.

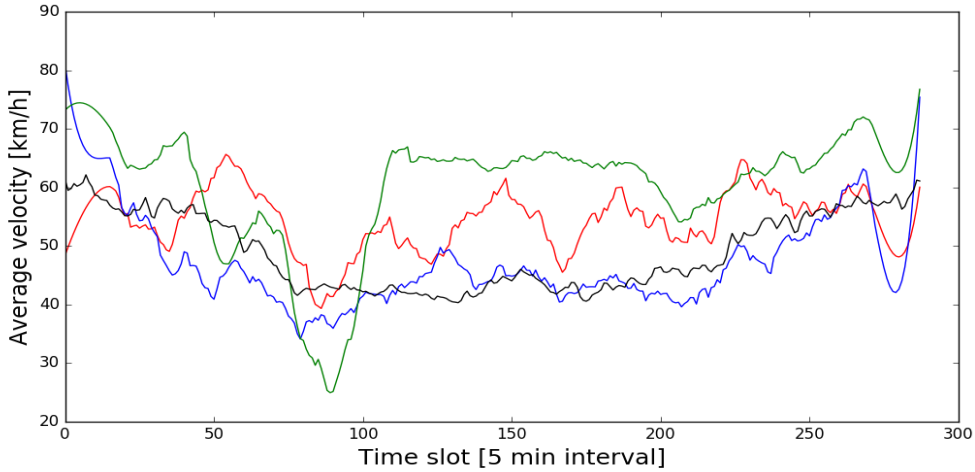


**Figure 5.11** Mesh cells average speed profiles for triplet 2 (group 3). Red plot: cell *(i,j)*. Blue plot: cell *(i+1,j)*. Green plot: cell *(i+2,j)*. Black plot: whole area of 80 sq. km. average speed.

Additionally, the behavior of two triplets from the highway dominant and arterial road dominant regions during ordinary and non-ordinary days (January 5th (Sunday) and January 6th (Monday)) were also compared. Without loss of generality, triplet number 8 (highway dominant region) and 10 (arterial roads dominant region) were chosen. In similar manner as above, the values of ${}_0SIM_{i,j}^d$ and ${}_1SIM_{i,j}^d$ are calculated and results are shown of the Figure 5.12. Based on the results from the Figure 5.12, the following observations could be made. In highway dominant region, the values of ${}_0SIM_{i,j}^d$ and ${}_1SIM_{i,j}^d$ are smaller during non-ordinary day, and higher during ordinary day. On the other hand, in case of arterial dominant region, the situation is opposite. Moreover, the value of ${}_1SIM_{i,j}^d$, comparing to the value of ${}_0SIM_{i,j}^d$ is higher for arterial road dominant region, therefore

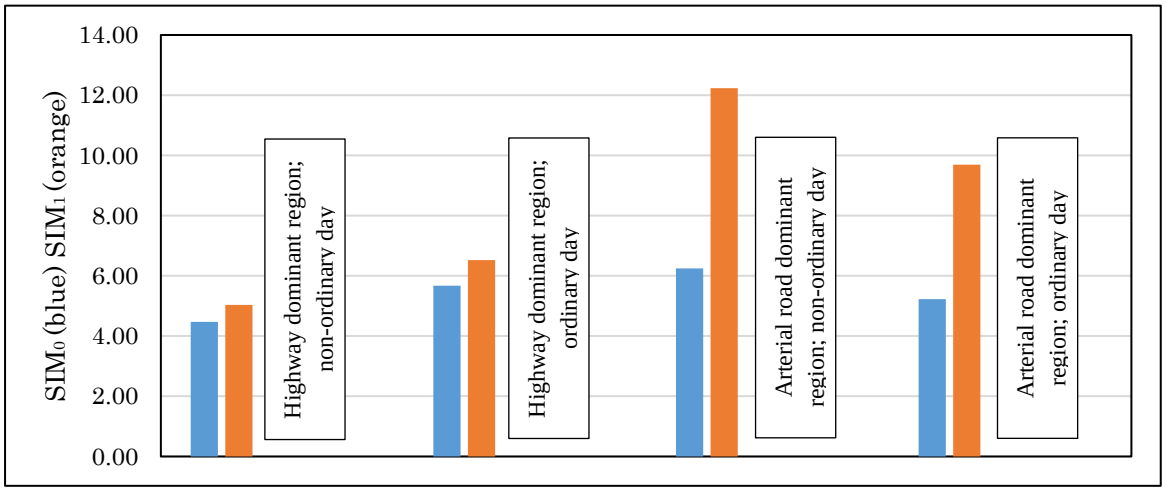


**Figure 5.12** Similarity of speed profiles for spatially adjusted mesh cells in highway and arterial road dominant triplets. Blue plot: neighboring mesh cells. Orange plot: mesh cells with distance equal to one cell

there is less similarity between left-most and right-most cells in this triplet, comparing to the ones in highway dominant region. Therefore, in case of highway dominant regions there is a higher degree of spatiotemporal similarity of speed profiles in neighboring mesh cells, comparing to the ones in arterial roads dominant regions. Moreover, this degree of similarity is higher during ordinary days and lower during non-ordinary days.

Summarizing the discussion in current subsection, the following observations has been made. First of all, the results demonstrated that in general similarity between evolutions processes of mesh cells average speed are affected by the spatial proximity. The closer two mesh cells spatially, the more similar the average speed profiles of these two cells. Moreover, local features, such as

existence of highways or high degree of arterial roads also affect this similarity. Additionally, it was demonstrated that temporal characteristics, such as ordinary or non-ordinary days affect the average speed evolution processes. Moreover, as it has been demonstrated in previous subsection that with the help of available probe vehicle data it is also possible to grasp the temporal characteristics of traffic dynamics. These results lead to the conclusion that utilized probe vehicle data could be used in order to capture spatiotemporal dependencies inside targeted urban region. However, since the emphasis in current dissertation is on anomalous traffic patterns formed due to the presence of disruptions, it is necessary to additionally investigate if the impact of external disruption could also be grasp from the available probe vehicle data. The following subsection is devoted to this matter, as well as to investigating the performance of proposed tensor-based abnormal traffic patterns detection approach.

## 5.3. Anomalous traffic pattern discovery

In previous section it has been demonstrated that spatiotemporal features of traffic dynamics in large urban transportation networks could be captured with the help of probe vehicle data. Therefore, in current dissertation this data is used in order to examine the validity and properties of proposed tensor-based abnormal traffic patterns discovery approach. This section is devoted to this matter.

### 5.3.1. Abnormal event specification

Without loss of generality, in current study it is assumed that abnormal climate conditions could be a potential reason for anomalous traffic conditions. More precisely, a heavy snowfall observed in Tokyo area during February of the year 2014 is considered. In the Table 5.1 below, the snow depth in centimeters and a corresponding date and time (during morning peak hours) are partially shown. This data is obtained from the Japan Meteorological Agency.

In order to be used for further analysis, a subset of data has been extracted from the one year data. More precisely, the data during non-ordinary days (weekends and national holidays) during January and February of the year 2014 are excluded from the analysis first. This exclusion and choosing months during winter period has been done in order to assure that the traffic dynamics

exhibit similar pattern. Moreover, the specific time intervals during morning peak hours only are considered. After this exclusion, the further analysis is conducted for the 38 ordinary days during January and February (January: 6, 7, 8, 9, 10, 14, 15, 16, 17, 20, 21, 22, 23, 24, 27, 28, 29, 30, 31; February: 3, 4, 5, 6, 7, 10, 12, 13, 14, 17, 18, 19, 20, 21, 24, 25, 26, 27, 28).

**Table 5.2** Hourly snow depth in Tokyo area during morning peak hours from 7th till 15th of February. Weekends are marked with red color. Data according to Japan Meteorological Agency.

| MM/DD/YY Hrs. | Snow depth [cm] | MM/DD/YY Hrs. | Snow depth [cm] | MM/DD/YY Hrs. | Snow depth [cm] | MM/DD/YY Hrs. | Snow depth [cm] |
|---|---|---|---|---|---|---|---|
| 2/7/14 7:00 | 0 | 2/10/14 7:00 | 8 | 2/13/14 7:00 | 0 | 2/16/14 7:00 | 9 |
| 2/7/14 8:00 | 0 | 2/10/14 8:00 | 8 | 2/13/14 8:00 | 0 | 2/16/14 8:00 | 9 |
| 2/7/14 9:00 | 0 | 2/10/14 9:00 | 8 | 2/13/14 9:00 | 0 | 2/16/14 9:00 | 9 |
| 2/8/14 7:00 | 1 | 2/11/14 7:00 | 4 | 2/14/14 7:00 | 0 | 2/17/14 7:00 | 4 |
| 2/8/14 8:00 | 2 | 2/11/14 8:00 | 3 | 2/14/14 8:00 | 0 | 2/17/14 8:00 | 4 |
| 2/8/14 9:00 | 3 | 2/11/14 9:00 | 3 | 2/14/14 9:00 | 0 | 2/17/14 9:00 | 4 |
| 2/9/14 7:00 | 23 | 2/12/14 7:00 | 1 | 2/15/14 7:00 | 22 | 2/18/14 7:00 | 0 |
| 2/9/14 8:00 | 22 | 2/12/14 8:00 | 0 | 2/15/14 8:00 | 21 | 2/18/14 8:00 | 0 |
| 2/9/14 9:00 | 22 | 2/12/14 9:00 | 0 | 2/15/14 9:00 | 20 | 2/18/14 9:00 | 0 |

### 5.3.2. Targeted region specification

Without loss of generality, the following region of 20 sq. km. inside central Tokyo area (marked with red color on Figure 5.13) has been chosen for further analysis. This particular choice was made

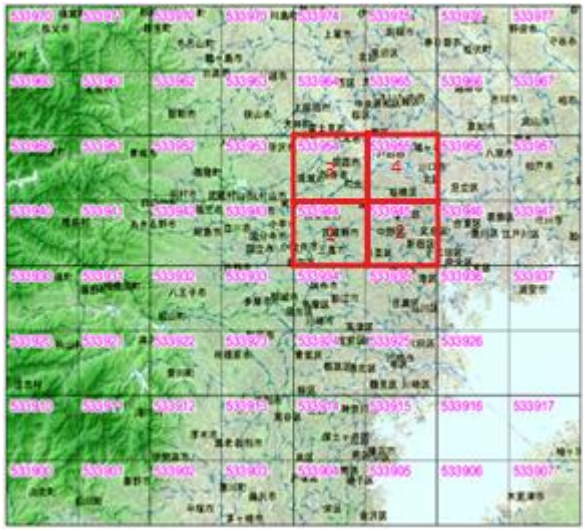

**Figure 5.13** Targeted region for analysis of 20 sq. km. (marked with red color) inside central Tokyo area.

for mainly two reasons. The first one is the intension to keep the sufficient population of probe vehicles during the whole time span. The second reason is the intention to include as much arterial roads into analysis as possible in order to keep spatial homogeneity. In following subsection the remarks on data aggregation and choice of spatiotemporal resolutions has been made.

### 5.3.3. Anomalous traffic pattern mining

In order to investigate the impact of aforementioned snowfall onto the traffic conditions and validate proposed tensor-based anomalous traffic patterns detection approach, the following procedure has been considered. Firstly, following the style in chapter four, targeted region of 20 sq. km. from the previous subsection was discretized with empirically chosen spatiotemporal resolution of 10 sq. km. (total 4 mesh cells, numeration according to the Figure 5.13) and 9 time interval equal to 20 minutes during morning hours from 6:00 am till 9:00 am. The discussion related to the choice of different spatiotemporal resolutions and its impact is provided in the following subsection. Further, after raw data preprocessing stages described in subsection 5.2.2, mesh-wise average speed maps have been calculated using the equation 3.28. These speed maps were transformed into a tenor-based representation in similar manner as in subsection 3.3. The resulting tensor is of shape $\boldsymbol{\mathcal{X}} \in \mathbb{R}^{4\times9\times38}$, where 4 corresponds to four 10 square kilometers mesh cells inside targeted region; 9 corresponds to nine 20 minutes time intervals during morning hours; and 38 corresponds to the thirty eight ordinary days during January and February. Following the procedure described in subsection 3.2.2, this tensor is decomposed into the low-rank $\boldsymbol{\mathcal{Y}}$ and a sparse $\boldsymbol{\mathcal{Z}}$ components, each of the size as original tensor $\boldsymbol{\mathcal{X}}$. As before, tensor $\boldsymbol{\mathcal{Z}}$ contains the information regarding the deviation of traffic conditions from the expected ones. Further, this tensor $\boldsymbol{\mathcal{Z}}$ is sliced day-wise, forming 38 matrices of size $\boldsymbol{Z}_{:,:,n} \in \mathbb{R}^{4\times9}$ each. For each of those matrices, the number of negative entries is calculated and shown (partially) in Table 5.3 as a fraction to the total number of matrix elements.

According to the Table 5.3, two tensor slices $\boldsymbol{Z}_{:,:,25}$ and $\boldsymbol{Z}_{:,:,29}$ have the number of negative elements that are significantly higher than the others (depicted with red color). The meaning of each of these negative value is the speed drop, which is noticeable and higher than expected. Those two slices $\boldsymbol{Z}_{:,:,25}$ and $\boldsymbol{Z}_{:,:,29}$ are shown on the Figure 5.14 below.

**Table 5.3** Fraction of day-wise slices with negative entries; corresponding slice number and the date during February.

| Slice number | Date | Negative fraction of $Z_{:,:,n}$ | Slice number | Date | Negative fraction of $Z_{:,:,n}$ | Slice number | Date | Negative fraction of $Z_{:,:,n}$ |
|---|---|---|---|---|---|---|---|---|
| 20 | 2/3/14 | 0 | 27 | 2/13/14 | 0 | 34 | 2/24/14 | 0 |
| 21 | 2/4/14 | 3 | 28 | 2/14/14 | 0 | 35 | 2/25/14 | 8 |
| 22 | 2/5/14 | 6 | 29 | 2/17/14 | 25 | 36 | 2/26/14 | 0 |
| 23 | 2/6/14 | 6 | 30 | 2/18/14 | 0 | 37 | 2/27/14 | 0 |
| 24 | 2/7/14 | 0 | 31 | 2/19/14 | 0 | 38 | 2/28/14 | 3 |
| 25 | 2/10/14 | 19 | 32 | 2/20/14 | 0 | | | |
| 26 | 2/12/14 | 0 | 33 | 2/21/14 | 6 | | | |

According to the Figure 5.14, in both cases of $\boldsymbol{Z}_{:,:,25}$ and $\boldsymbol{Z}_{:,:,29}$, the leftmost column has the highest number of negative entries, therefore, has the higher degree of deviation from the expected traffic conditions. These values in leftmost columns $\boldsymbol{Z}_{1,:,25}$ and $\boldsymbol{Z}_{1,:,29}$ corresponds to the traffic conditions

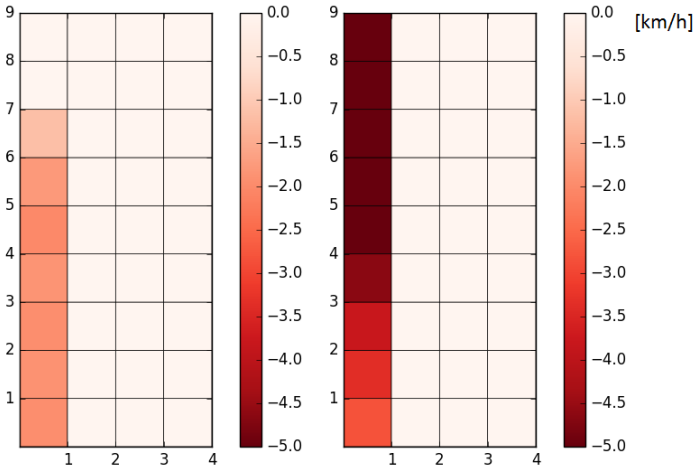


**Figure 5.14** Tensor slices $\boldsymbol{Z}_{:,:,25}$ (left) and $\boldsymbol{Z}_{:,:,29}$ (right). Vertical axis corresponds to the 20 minutes time intervals during morning hours. Horizontal axis corresponds to different mesh cells (numeration according Figure 5.13). Brighter colors depict higher values of speed drop in [km/h].

during morning hours on 10th and 17th of February in a mesh cell number 1 (numeration according to the Figure 5.13). These anomalous traffic patterns are further compared with the ground truth values of average speed, calculated for each mesh cell inside the targeted area (mesh cells with numbers: 533944, 533945, 533954, and 533955, which correspond to numbers 1, 2, 3, and 4 on the Figure 5.13), shown in Appendix C. The results of comparison demonstrate that by utilizing proposed tensor-based approach it became possible to correctly identify not only the days when the traffic conditions were affected by the snowfall, but also the region which was affected the most

(cell number 533944). Therefore, proposed tensor-based anomalous traffic patterns discovery approach shows the promising results, and the validity of problem formulation as a low-rank modeling problem appears reasonable. Moreover, by comparison with the threshold-based anomaly detection method, where the abnormal speed values could be detected statistically by utilizing the three sigma rule, where speed values which deviate from the mean more than $\pm 3\sigma$ are marked as abnormal, the following observation has been done. In particular, the following speed range was setup for the mesh cell numbered 533944 as normal: $22.13 \pm 3 * 2.99$ [km/h], which allow to detect abnormal speed value of 11.63 [km/h] during 17$^{th}$ of February. This value was also detected by utilizing the proposed approach. However, the abnormal speed value of 17.22 [km/h] during 10$^{th}$ of February was not be able to detect despite being detected by proposed method. Additionally, by utilizing the statistical method, the speed value of 33.59 [km/h] during January 6$^{th}$ in the mesh cell 533955 was marked as abnormal, however according to the proposed approach this value is expected and should be treated as a part of the low-rank structure. In addition, during the examination of proposed approach on synthetic data it was shown that the performance of detection could vary depending on different spatiotemporal resolutions. This issue is investigated in the following subsection.

Additionally, it is necessary to discuss the situations when the abnormal traffic patterns caused by the heavy snowfall are treated as a normal or expected pattern and vice versa. In particular, under the empirically chosen value of regularization parameter lambda in equation (3.15) equal to 0.2, the abnormal patterns have been correctly identified. By varying the value of regularization parameter the following observations has been made. For the value lambda equal to 0.1, the anomalous patterns still could be correctly identified, however less clearly comparing to empirically chosen value. For the value of lambda equal to 0.3 the abnormal patterns could be correctly identified only partially, in case of the tensor slice $\boldsymbol{Z}_{:,:,29}$, and tensor slice $\boldsymbol{Z}_{:,:,25}$ contains zero values. For the values of lambda ranging from the value 0.4 till the value 1.0 with step of 0.1, the proposed methodology mistakenly identified abnormal patterns as the expected ones, so therefore treated them as a part of a low-rank structure. These results demonstrate once again that proposed methodology is target depended and a priori knowledge regarding the disruption is desirable to obtain reliable results.

### 5.3.4. Impact of variable spatiotemporal resolutions

As it has been mentioned in previous subsection, it is necessary to investigate the impact of different spatiotemporal resolutions onto the performance of detection of proposed tensor-based abnormal traffic patterns detection approach, since according to the simulation results (subsection 4.3.4) the performance could vary greatly under the different resolutions. More precisely, in subsections 4.3.4 and 4.3.5 it was demonstrated that by choosing lower spatiotemporal resolution (bigger mesh cells and longer time intervals) it is possible to keep more accurate speed map, however the performance of detection is decreasing. On the other hand, the choice of higher spatiotemporal resolution (smaller mesh cells and shorter time intervals) results in a less accurate speed map, however the performance of detection in this case is increasing. In order to investigate the validity of these results the following procedure is considered in this dissertation. In total 9 sets of experiments has been conducted for 3 different spatial resolutions and 3 different temporal resolution. The results are shown below and grouped by the different spatial resolution.

**(1) Spatial resolution: 5 sq. km., temporal resolution: 5 min, 20 min, 60 min.**

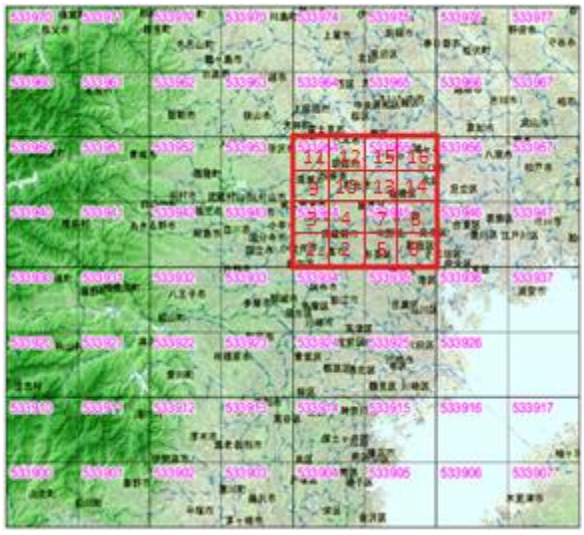

**Figure 5.15** Targeted region for analysis of 20 sq. km. inside central Tokyo area, and its discretization into 16 mesh cells of 5 sq. km. with mesh cells numeration.

Following the similar style as in previous subsection, the targeted region of 20 sq. km. depicted in the Figure 5.13 is considered. This region is discretized into 16 mesh cells of 5 sq. km. each

(numeration is according to the Figure 5.15). The mesh-wise average speed maps during morning hours (6:00 am – 9:00 am) are calculated under different temporal resolutions (5, 20 and 60 minutes) and transformed into a tensor-based representation, resulting in tensors with shapes $\boldsymbol{\mathcal{X}}_1 \in \mathbb{R}^{16\times36\times38}$ and $\boldsymbol{\mathcal{X}}_2 \in \mathbb{R}^{16\times9\times38}$ and $\boldsymbol{\mathcal{X}}_3 \in \mathbb{R}^{16\times3\times38}$ accordingly. After decomposing these three tensors into low-rank and sparse components, the entries of later ones $\boldsymbol{\mathcal{Z}}_1$ and $\boldsymbol{\mathcal{Z}}_2$ and $\boldsymbol{\mathcal{Z}}_3$ are analyzed. By slicing these tensors day-wise and calculating the number of negative entries, in similar manner as in previous subsection, two slices in each tensor, which correspond to be the same as the ones detected in subsection 5.3.3 showed different behavior (larger number of negative entries). These slices are shown on the Figure 5.16 (spatial resolution: 5 sq. km.; temporal resolution: 5 mins), Figure 5.17 (spatial resolution: 5 sq. km.; temporal resolution: 20 mins) and Figure 5.18 (spatial resolution: 5 sq. km.; temporal resolution: 60 mins).

From these Figures 5.16-5.18 one could observe significant speed drops in the left part of speed maps under different temporal resolutions. These observations are similar to the results from the previous subsection, where significant speed drops due to the heavy snowfall were also detected inside the leftmost mesh cell numbered 533944. In case of the Figure 5.17, first four columns are the sub regions of the mesh cell number 1 in the Figure 5.14. Therefore it is reasonable to conclude that the speed drops caused by the heavy snowfall could also be detected with the higher spatiotemporal resolution. However, by observing the Figure 5.16 and Figure 5.17 it is possible to get more detailed information regarding the speed profiles, since the smaller mesh cells are under examination. These results are in accordance with the observations made during the simulation, where higher spatiotemporal resolutions allowed to detect anomalous pattern more clearly. Moreover, by comparison the magnitude of speed drops in figures above it become clear that by utilizing higher spatiotemporal resolution it is possible to detect the abnormal traffic pattern more sharply and with higher precision.

Additionally, it was demonstrated in subsection 5.1.1 that number of samples, in other words number of probe vehicles used for speed map calculations, affects the results. Therefore it is necessary to make a comment regarding number of samples during the days when heavy snowfall occurred. The number of samples during these days (tensor slice $\boldsymbol{\mathcal{Z}}_{:,:,25}$, and tensor slice $\boldsymbol{\mathcal{Z}}_{:,:,29}$) were 6.8% and 3.6% lower comparing to the average number of samples for targeted region in Fig.5.13.

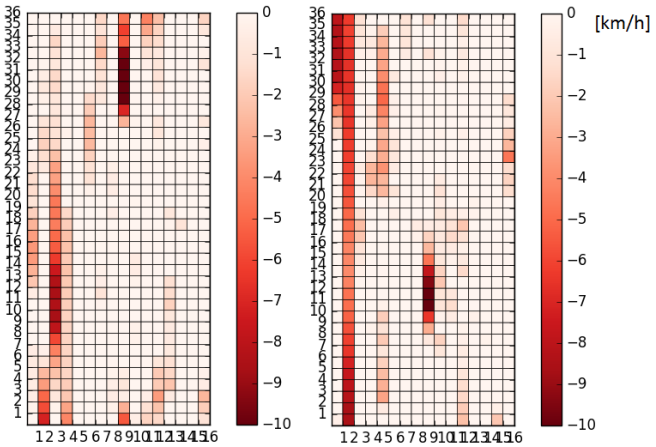


**Figure 5.16** Tensor slices $\boldsymbol{Z}_{:,:,25}$ (left) and $\boldsymbol{Z}_{:,:,29}$ (right). Vertical axis corresponds to the 5 minutes time intervals during morning hours. Horizontal axis corresponds to different mesh cells (numeration according Figure 5.15). Brighter colors depict higher values of speed drop in [km/h].

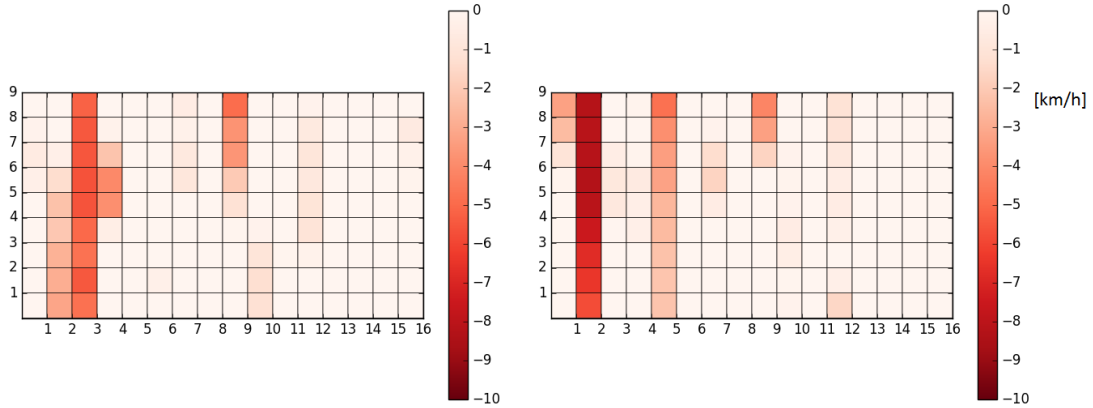


**Figure 5.17** Tensor slices $\boldsymbol{Z}_{:,:,25}$ (left) and $\boldsymbol{Z}_{:,:,29}$ (right). Vertical axis corresponds to the 20 minutes time intervals during morning hours. Horizontal axis corresponds to different mesh cells (numeration according Figure 5.15). Brighter colors depict higher values of speed drop in [km/h].

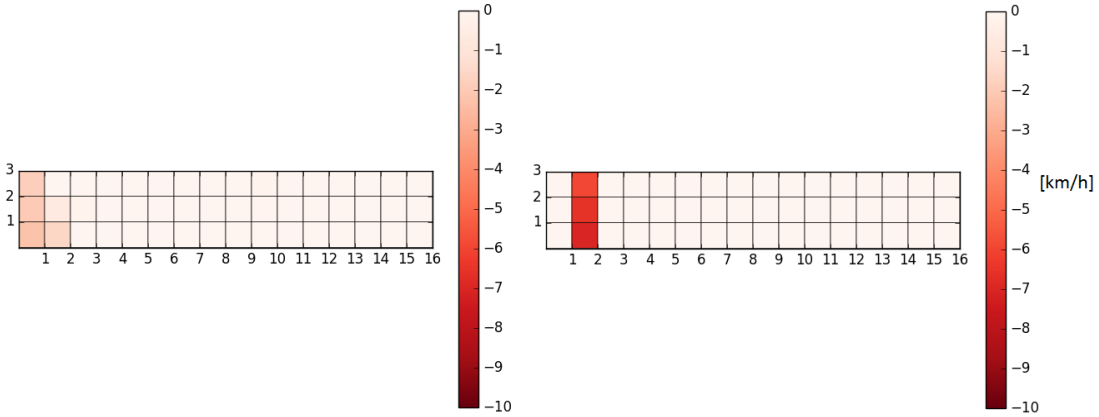


**Figure 5.18** Tensor slices $\boldsymbol{Z}_{:,:,25}$ (left) and $\boldsymbol{Z}_{:,:,29}$ (right). Vertical axis corresponds to the 60 minutes time intervals during morning hours. Horizontal axis corresponds to different mesh cells (numeration according Figure 5.15). Brighter colors depict higher values of speed drop in [km/h].

**(2) Spatial resolution: 10 sq. km., temporal resolution: 5 min, 20 min, 60 min.**

In current experimental setup, the targeted region of 20 sq. km. depicted in the Figure 5.13 is discretized into 4 mesh cells of 10 sq. km. each (numeration is according to the Figure 5.13). The mesh-wise average speed maps during morning hours (6:00 am – 9:00 am) are calculated under different temporal resolutions (5, 20 and 60 minutes) and transformed into a tensor-based representation, resulting in tensors with shapes $\boldsymbol{\mathcal{X}}_1 \in \mathbb{R}^{4\times36\times38}$ and $\boldsymbol{\mathcal{X}}_2 \in \mathbb{R}^{4\times9\times38}$ and $\boldsymbol{\mathcal{X}}_3 \in \mathbb{R}^{4\times3\times38}$ accordingly. After decomposing these three tensors into low-rank and sparse components, the entries of later ones $\boldsymbol{\mathcal{Z}}_1$ and $\boldsymbol{\mathcal{Z}}_2$ and$\boldsymbol{\mathcal{Z}}_3$ are analyzed. By slicing these tensors day-wise and calculating the number of negative entries, in similar manner as in previous subsection, two slices in each tensor, which correspond to be the same as the ones detected in subsection 5.3.3 demonstrate different behavior (larger number of negative entries). These slices are shown on the Figure 5.19 (spatial resolution: 10 sq. km.; temporal resolution: 5 mins), Figure 5.20 (spatial resolution: 10 sq. km.; temporal resolution: 20 mins) and Figure 5.21 (spatial resolution: 10 sq. km.; temporal resolution: 60 mins).

From these Figures 5.19-5.21 the following observations could be made. Again, similar to the previous experimental setup, the leftmost part of tensor slices contain the higher number of negative entries, therefore the anomalous patterns formed due to the heavy snowfall could be detected. However, in case of the spatial resolution of 10 sq. km. it could be observed that the sharpness of detected abnormalities is decreasing, since more coarse resolution is used. Moreover, due to this coarse spatial resolution, with longer temporal intervals, the detection of performance is decreasing. This could be clearly observed from the Figure 5.21 (left), where the proposed tensor-based approach failed to detect anomaly under the spatial resolution of 10 sq. km. and temporal resolution of 60 mins. This observation is also in accordance with the simulation results, where it has been demonstrated that the lower spatiotemporal resolution (larger mesh cells and longer time intervals) leads to the decrease in performance of proposed tensor-based anomalous traffic patterns detection approach.

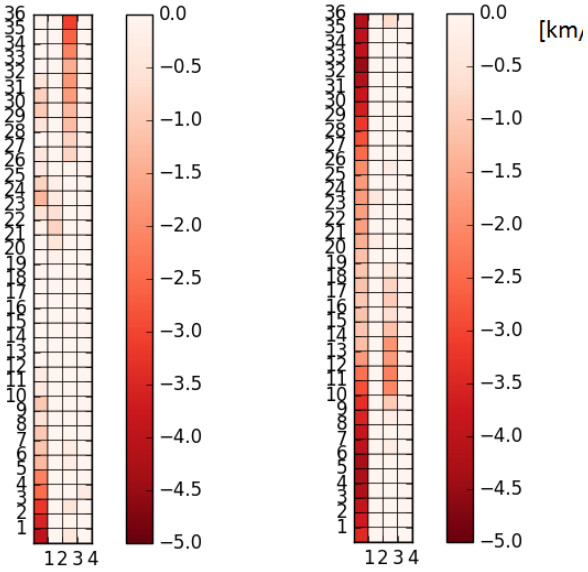


**Figure 5.19** Tensor slices $\boldsymbol{Z}_{:,:,25}$ (left) and $\boldsymbol{Z}_{:,:,29}$ (right). Vertical axis corresponds to the 5 minutes time intervals during morning hours. Horizontal axis corresponds to different mesh cells (numeration according Figure 5.15). Brighter colors depict higher values of speed drop in [km/h].

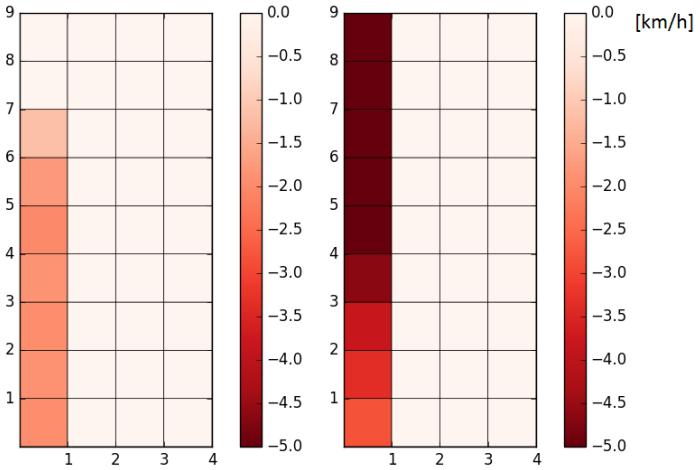


**Figure 5.20** Tensor slices $\boldsymbol{Z}_{:,:,25}$ (left) and $\boldsymbol{Z}_{:,:,29}$ (right). Vertical axis corresponds to the 20 minutes time intervals during morning hours. Horizontal axis corresponds to different mesh cells (numeration according Figure 5.13). Brighter colors depict higher values of speed drop in [km/h].

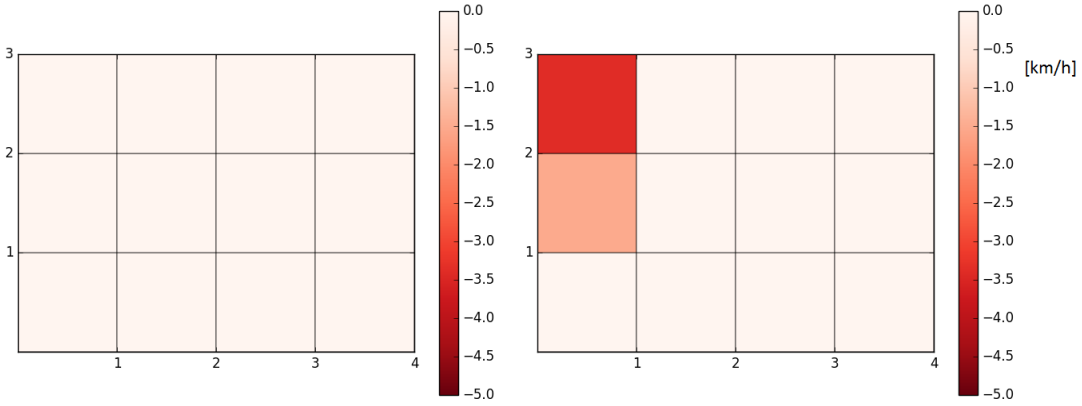


**Figure 5.21** Tensor slices $\boldsymbol{Z}_{:,:,25}$ (left) and $\boldsymbol{Z}_{:,:,29}$ (right). Vertical axis corresponds to the 60 minutes time intervals during morning hours. Horizontal axis corresponds to different mesh cells (numeration according Figure 5.15). Brighter colors depict higher values of speed drop in [km/h].

**(3) Spatial resolution: 20 sq. km., temporal resolution: 5 min, 20 min, 60 min.**

By making the spatial resolution even coarser and following the same procedure as in previous two experimental setups, it was observed that the proposed tensor-based approach failed to detect any anomalous patterns. The results of day-wise tensor slices for the days when there were anomalous patterns are shown of the Figures 5.22-5.24.

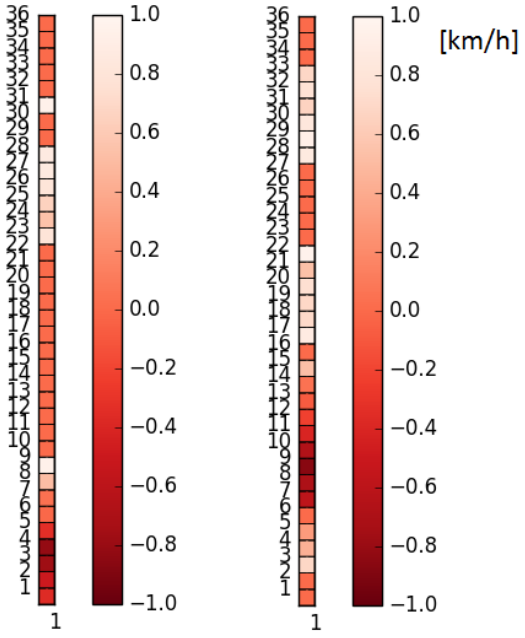


**Figure 5.22** Tensor slices $\boldsymbol{Z}_{:,:,25}$ (left) and $\boldsymbol{Z}_{:,:,29}$ (right). Vertical axis corresponds to the 5 minutes time intervals during morning hours. Horizontal axis corresponds to different mesh cells (numeration according Figure 5.13). Brighter colors depict higher values of speed drop in [km/h].

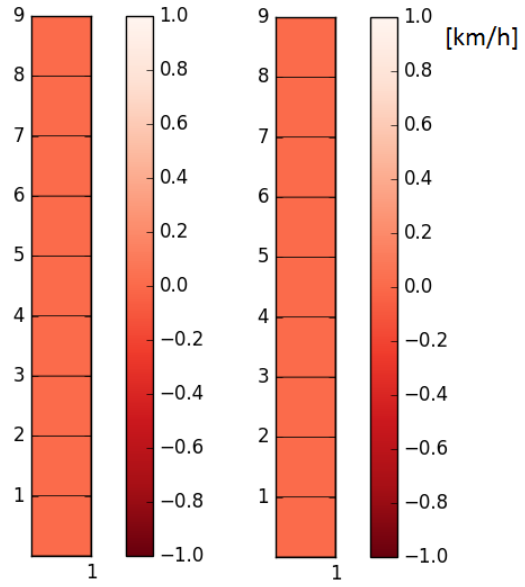


**Figure 5.23** Tensor slices $\boldsymbol{Z}_{:,:,25}$ (left) and $\boldsymbol{Z}_{:,:,29}$ (right). Vertical axis corresponds to the 20 minutes time intervals during morning hours. Horizontal axis corresponds to different mesh cells (numeration according Figure 5.13). Brighter colors depict higher values of speed drop in [km/h].

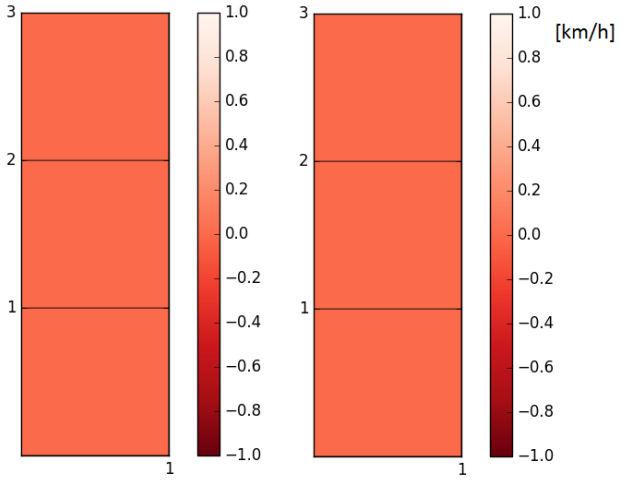


**Figure 5.24** Tensor slices $\boldsymbol{Z}_{:,:,25}$ (left) and $\boldsymbol{Z}_{:,:,29}$ (right). Vertical axis corresponds to the 60 minutes time intervals during morning hours. Horizontal axis corresponds to different mesh cells (numeration according Figure 5.13). Brighter colors depict higher values of speed drop in [km/h].

It is worth to mention that the day-wise slices are identical and equal to zero despite different choices of regularization parameter lambda in equation 3.15. This means that prosed approach failed to detect any anomalous traffic patterns under this particular spatiotemporal resolution. These results are also in accordance with the results from the simulation part, where it was demonstrated that lower spatiotemporal resolution decrease the detection performance.

## 5.4. Chapter summary

This section is devoted to the verification of proposed tensor-based abnormal traffic patterns detection approach on real traffic data. For this purposes, probe vehicle data obtained from the vehicles travelled all across Japan has been utilized. The raw data, which is a collection of geo-referenced coordinates and corresponding time stamps, has been aggregated first with spatial resolution equal to one square kilometer and temporal resolution equal to five minutes. Further, without loss of generality, for further analysis the subset of this aggregated data during the year 2014 only and corresponding to the traffic dynamics in greater Tokyo area has been chosen. Further, this aggregated data has been preprocessed, since geo-referenced coordinates obtained via GPS receivers appeared to contain not feasible observations. The preprocessing stage includes outlier's detection and data filtering. After preprocessing stage, the visual data examination and the examination of spatiotemporal dependencies has been conducted.

Further, without loss of generality, in current study it is assumed that abnormal climate conditions could be a potential reason for anomalous traffic conditions. More precisely, a heavy snowfall occurred in Tokyo area during February 2014 is considered. After applying proposed

tensor-based approach, the following results has been obtained. First of all, it was demonstrated that simulation findings are in accordance with the results observed by utilizing the real large-scale traffic data. More precisely, the performance of detection of proposed tensor-based abnormal traffic patterns detection approach is increasing with higher spatiotemporal resolutions and decrease otherwise. This was demonstrated by analyzing the impact of heavy snowfall on traffic dynamics in Tokyo area in a year of 2014. By choosing different spatiotemporal resolutions, it was investigated under which conditions the anomalous patterns could be detected. Therefore, it is reasonable to conclude that proposed extended continuum model could grasp general behavioral characteristics of traffic dynamics in large urban transportation networks and could be used in order to investigate the performance and properties of tensor-based abnormal traffic patterns detection approach. Moreover, the results from this subsection suggest the reasonable choice of parameters for traffic engineers on choice of parameters for traffic monitoring systems. In particular, by knowing the available population of probe vehicles and approximate parameters of the disruption, one could use aforementioned research findings to choose appropriate spatiotemporal resolutions. For example, in case of available and utilized probe vehicle data it was revealed that the anomalous traffic patterns formed due to the heavy snowfall could be detected by utilizing the spatial resolution of 5 sq. km. with temporal resolutions: 5 mins, 20 mins, 60mins; and by utilizing spatial resolution of 10 sq. km. with temporal resolutions: 5 mins, 20 mins. On the other hand, by utilizing the coarser resolutions of 10 sq. km. with temporal resolution of 60 mins the proposed approach failed to detect any abnormality. Additionally, by utilizing spatial resolution of 20 sq. km., despite the choice of temporal resolution, the abnormal patterns are failed to be detected. In other words, the proposed tensor based abnormal traffic patterns detection approach is target-specific and tuning of parameters should be done a priori.

# 6. Conclusions

## 6.1. Achievements

This dissertation is devoted to the problem of detection and description of abnormal traffic patterns in large transportation networks formed due to the presence of unexpected disruptions, such as natural or manmade disasters. This analysis of behavior of transportation systems not only under the normal, but also under abnormal conditions is essential in order to provide better management of urban transportation and keep an efficient and stable operations of transportation systems.

In current dissertation the aforementioned problem of abnormal traffic patterns detection and description in large urban transportation networks is addressed, and the following research framework is considered. First of all, the clarification of research needs and objectives is provided in the first chapter. In second chapter the review of previous studies related to the dissertation is provided. More precisely, the discussion starts with the description of most commonly used traffic data collection methods. Advantages and disadvantages of each particular method in application to the traffic dynamics analysis are described. The discussion continues with the description of abnormal traffic patterns discovery techniques. Most commonly used approaches are described and explained, and the discussion on the utilization of traffic data in the process of anomalous traffic patterns detection is provided. It was emphasized that the majority of previous studies focuses only on the problem of detection of anomalous patterns, without necessary consideration of the reasons behind these abnormalities. Therefore, in current study the problem of detection of abnormal patterns is considered along with the problem of understanding the reasons behind those anomalies. In chapter three the emphasis on the complexity of traffic dynamics in large transportation networks has been made. And the tensor-based traffic data representation is put forward in order to take into account complex spatiotemporal nature of traffic dynamics in those networks. Additionally, in order to detect anomalous traffic patterns formed due to the presence of aforementioned unexpected disruption, the novel approach, based on tensor robust principal component analysis has been proposed, explained in details and theoretically proved. As mentioned above, this approach allow not only to detect anomalous patterns, but also to clarify if these anomalies were caused by the external disruptions. In chapter four, the comprehensive examination of the performance and

properties of proposed abnormal traffic patterns detection approach with the help of synthetic data has been conducted. More precisely, in current dissertation in order to model behavioral characteristics of traffic dynamics in large transportation networks, the continuum modeling approach has been employed. It was mentioned, that even if this continuum modeling approach is a mathematical idealization of real traffic dynamics, it could help to grasp overall behavioral characteristics of traffic dynamics. The original model has been employed and extended by introduction of so-called disruption field for the purpose of modeling the impact of real-world natural or manmade disasters. Moreover, the model has been extended by introduction of so-called probes, individual particles, traveling inside the continuum field, in order to emulate the behavior of individual motorists and examine the performance of proposed tensor-based approach. With the help of extended model, the properties of proposed tensor-based anomalies traffic patterns detection approach were examined. Chapter five starts with the description of real large-scale traffic data and the discussions on how this data could be utilized for the purpose of traffic dynamics monitoring. The necessary remarks on traffic data collection, aggregation and preprocessing are provided. Additionally, the available probe vehicle data, sampled from the vehicles traveled in Tokyo area, has been aggregated and analyzed, following the procedures in this chapter five. Further, the proposed abnormal traffic patterns detection approach has been applied to aforementioned probe vehicle data in order to mine abnormal traffic patterns formed due to the severe weather conditions. The results demonstrate the validity and applicability of proposed tensor-based approach in order to mine abnormal traffic patterns in large transportation networks. Moreover, it was demonstrated that extended continuum model could be used to grasp behavioral characteristics of motorists in large urban areas, and could be used in order to examine properties and performance of proposed tensor-based approach. The results of examination of real probe vehicle data are in accordance with the results obtained from the numerical experiment, where it was demonstrated that the performance of abnormality detection is increasing with higher spatiotemporal resolutions and decreasing otherwise. Therefore, the results of the study possess not only the theoretical interest, but also the practical interest for the practitioners who are in charge of analysis of traffic dynamics in large urban transportation networks.

## 6.2. Future research directions

Based on the research findings described in current dissertation, the following possible future extensions of the study could be considered.

- Modeling traffic dynamics as a higher order tensor

In this dissertation the tensor-based traffic data representation has been put forward in order to preserve complex spatiotemporal nature of traffic dynamics in large and complex transportation networks. And throughout the dissertation the 3rd order tensor has been utilized in order to represent traffic conditions in those networks. However, it is desirable to investigate if additional information regarding traffic dynamics could be included into this tensor representation for the purpose of describing traffic dynamics more accurately. This could be done by increasing the number of dimensions of the traffic data tensor. Need to mention that this extension will probably leads in increasing of computation cost, yet by following this procedure an additional meaningful insights could be mined from the available traffic data.

- Validation of methodology considering different disruption type

Without loss of generality, in current study it has been assumed that abnormal climate conditions could be a potential reason for anomalous traffic conditions. More precisely, a heavy snowfall observed in Tokyo area was under analysis. However, in order to conduct more comprehensive examination of proposed tensor-based abnormal traffic patterns detection approach it is desirable to investigate the impact of other natural and manmade disasters.

- Incorporation of traffic data fusion approaches

In this dissertation it has been highlighted that probe vehicle data is a well-known and valuable source of information regarding vehicle movements. Moreover it has been demonstrated that this

type of data is more appropriate for analysis of traffic dynamics in large urban transportation networks. Therefore probe vehicle data was utilized in current study and the performance of proposed tensor-based approach has been investigated with its help. However, nowadays the sensing techniques are becoming more and more advanced. And therefore it is desirable to investigate how probe vehicle data could be fused with the data obtained from the other sources in order to assure more accurate traffic data representation.

# Appendix A

In this appendix the advantages and disadvantages of commercially available sensor technologies are depicted, and the comparison of characteristics is provided. The data is from the Traffic Control Systems Handbook (Gordon et al., 2005), modified.

**Figure A1**. Comparison of commercially available sensor technologies. According to:

Traffic Control Systems Handbook (Gordon et al., 2005), modified.

| Technology | Advantages | Disadvantages |
|---|---|---|
| Inductive Loop | Flexible design to satisfy large variety of applications.<br>Mature, well-understood technology.<br>Provides basic traffic parameters (e.g., volume, presence, occupancy, speed, headway, and gap).<br>Insensitive to inclement weather such as rain, fog, and snow.<br>Common standard for obtaining accurate occupancy measurements.<br>High frequency excitation models provide classification data. | Installation requires pavement cut.<br>Improper installation decreases pavement life.<br>Installation and maintenance require lane closure.<br>Wire loops subject to stresses of traffic and temperature.<br>Multiple detectors usually required to monitor a location. |
| Magnetic | Can be used where loops are not feasible (e.g., bridge decks).<br>Some models are installed under roadway without need for pavement cuts. However, boring under roadway is required.<br>Insensitive to inclement weather such as snow, rain, and fog.<br>Less susceptible than loops to stresses of traffic. | Installation requires pavement cut or tunneling under roadway.<br>Cannot detect stopped vehicles unless special sensor layouts and signal processing software are used. |
| Microwave Radar | Typically insensitive to inclement weather at the relatively short ranges encountered in traffic management applications.<br>Direct measurement of speed.<br>Multiple lane operation available. | CW Doppler sensors may not detect stopped vehicles.<br>Some models have problem when used in large steel structures. (i.e. steel bridges)<br>Overhead conductors within beam cone can cause problems. |
| Active Infrared (Laser radar) | Transmits multiple beams for accurate measurement of vehicle position, speed, and class.<br>Multiple lane operation available. | Operation may be affected by fog when visibility is low or in case of blowing snow is present.<br>Installation and maintenance, including periodic lens cleaning, require lane closure. |
| Passive Infrared | Multizone passive sensors measure speed. | Passive sensor may have reduced vehicle sensitivity in heavy rain, snow & dense fog.<br>Some models not recommended for presence detection. |
| Video Image Processor | Monitors multiple lanes and multiple detection zones/lane.<br>Easy to add and modify detection zones.<br>Rich array of data available.<br>Provides wide-area detection when information gathered at one camera location can be linked to another.<br>Generally cost-effective when many detection zones within the camera field-of-view or specialized data are required. | Installation and maintenance, including periodic lens cleaning, require lane closure when camera is mounted over roadway (lane closure may not be required when camera is mounted at side of roadway)<br>Performance affected by inclement weather such as fog, rain, and snow; vehicle shadows; vehicle projection into adjacent lanes; occlusion; day-to-night transition; vehicle / road contrast; and water, salt grime, icicles, and cobwebs on camera lens.<br>Movement from other structures (i.e. span wires or overhead conductor) within field of view can cause problems. |

# Appendix B

Visualization of speed map accuracy under variable spatiotemporal resolutions and population of probes, corresponding to the subsection 4.3.5.

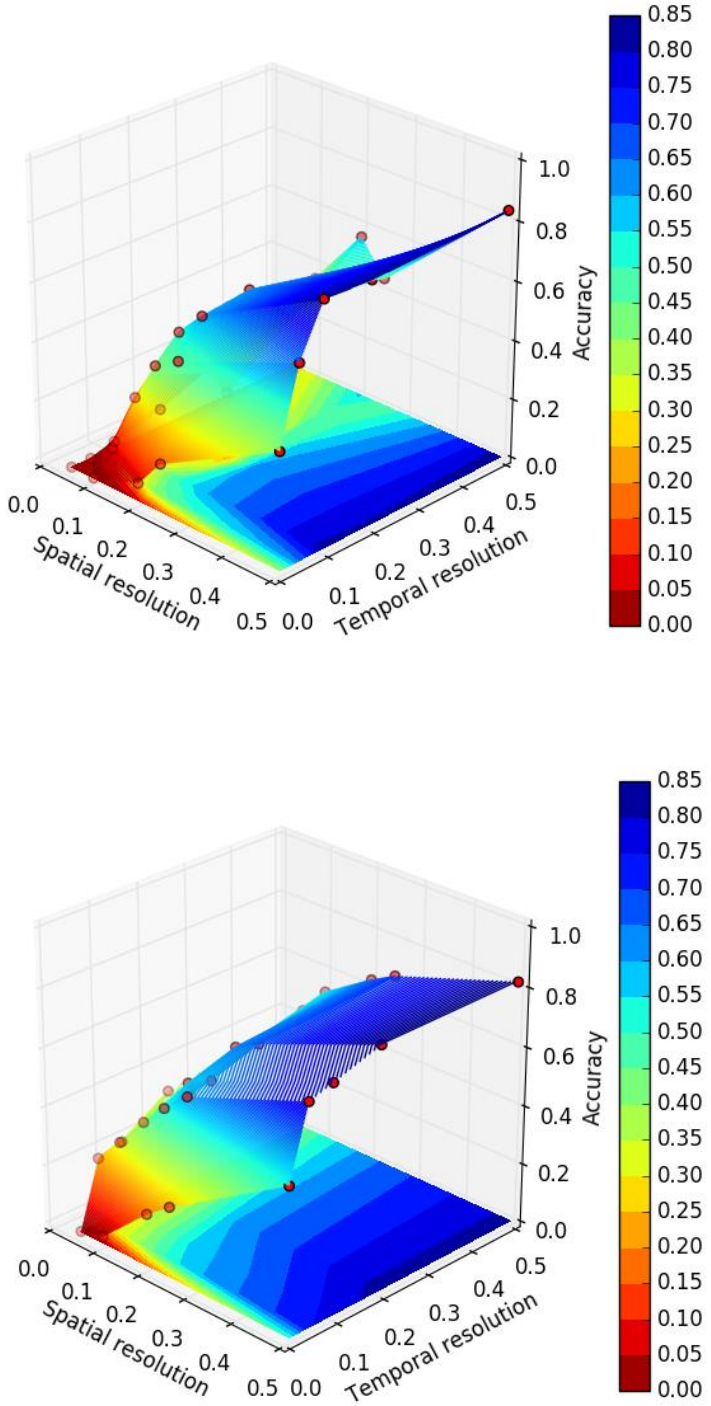


**Figure B1** Visualization of speed map accuracy during simulation under different spatiotemporal resolutions and population of probes. Probes population: 100 (upper plot); probes population: 1000 (below). Colder colors corresponds to higher accuracy.

# Appendix C

Mesh-wise average speed values (in km/h) calculated for a 20 sq. km. region inside central Tokyo area, discretized into four 10 sq. km. sub regions. The specification of the region is provided in subsection 5.4.3, in particular on the Figure 5.2. With the red colors depicted the anomalous speed values detected with the help of proposed tensor-based abnormal traffic patterns detection approach.

| 533944 | | 533945 | | 533954 | | 533955 | | Corresponding date | |
|---|---|---|---|---|---|---|---|---|---|
| January | February | January | February | January | February | January | February | January | February |
| 29.96 | 21.92 | 30.95 | 25.67 | 36.71 | 27.20 | 33.59 | 24.35 | 1/6 | 2/3 |
| 26.29 | 22.01 | 29.89 | 24.69 | 34.14 | 23.49 | 30.69 | 23.48 | 1/7 | 2/4 |
| 25.23 | 25.82 | 28.69 | 26.37 | 32.51 | 25.39 | 28.60 | 29.74 | 1/8 | 2/5 |
| 23.47 | 24.59 | 27.84 | 26.01 | 33.12 | 26.47 | 27.69 | 27.95 | 1/9 | 2/6 |
| 20.88 | 22.45 | 28.20 | 24.37 | 30.67 | 23.76 | 25.50 | 23.40 | 1/10 | 2/7 |
| 22.17 | 17.22 | 29.01 | 24.70 | 31.51 | 22.88 | 25.26 | 25.79 | 1/14 | 2/10 |
| 25.10 | 23.36 | 26.99 | 25.27 | 30.74 | 23.92 | 27.41 | 23.22 | 1/15 | 2/12 |
| 22.27 | 22.54 | 26.99 | 24.78 | 29.27 | 23.30 | 25.68 | 24.64 | 1/16 | 2/13 |
| 21.15 | 27.98 | 25.99 | 25.06 | 32.89 | 26.65 | 25.52 | 26.14 | 1/17 | 2/14 |
| 23.48 | 11.63 | 26.24 | 23.04 | 24.69 | 21.74 | 26.74 | 24.10 | 1/20 | 2/17 |
| 19.47 | 20.93 | 27.05 | 23.86 | 34.57 | 21.73 | 27.61 | 23.90 | 1/21 | 2/18 |
| 23.52 | 19.91 | 27.25 | 24.80 | 29.68 | 22.23 | 24.92 | 24.81 | 1/22 | 2/19 |
| 21.10 | 22.66 | 25.61 | 23.98 | 30.18 | 22.91 | 26.45 | 24.39 | 1/23 | 2/20 |
| 22.60 | 21.50 | 25.98 | 24.04 | 31.06 | 22.22 | 24.81 | 23.19 | 1/24 | 2/21 |
| 20.55 | 21.88 | 25.33 | 24.22 | 29.14 | 23.12 | 25.45 | 22.70 | 1/27 | 2/24 |
| 19.21 | 21.21 | 25.39 | 23.80 | 31.94 | 23.58 | 26.05 | 20.15 | 1/28 | 2/25 |
| 21.59 | 20.36 | 25.73 | 23.76 | 27.96 | 24.33 | 27.17 | 22.47 | 1/29 | 2/26 |
| 22.32 | 20.79 | 27.47 | 22.71 | 31.69 | 23.40 | 26.26 | 21.17 | 1/30 | 2/27 |
| 21.05 | 20.58 | 26.17 | 23.74 | 28.34 | 25.08 | 26.30 | 22.93 | 1/31 | 2/28 |

## References


Abuelela M., Olariu S., Weigle M. C.: Notice: An architecture for the notification of traffic incidents, *Proceedings of IEEE Vehicular Technology*, pp. 3001-3005, 2008.

Ahmadi M., Sarmad M.: Detecting outliers in normal data using modified Z-Scores., *Journal of Statistical Sciences*, Vol. 3, pp. 119-139, 2010.

Ahmed S. A., Hussain T. M., Saadawi T. N.: Active and passive infrared sensors for vehicular traffic control, *Proceedings of IEEE Vehicular Technology Conference*, Vol. 2, pp. 1393-1397, 1994.

Ahmed M.S., Cook A.R.: Analysis of freeway traffic time-series data using Box Jenkins techniques, *Transportation Research Record, No. 722, TRB, National Research Council*, pp. 1-9, 1977.

Andrienko G., Andrienko N., Hurter C., Rinzivillo S., Wrobel. S.: From Movement Tracks through Events to Places: Extracting and Characterizing Significant Places from Mobility Data, *Proceedings of IEE VAST*, pp. 161-170, 2011.

Asakura Y., Kusakabe T., Nguyen L. X., Ushiki T.: Incident detection methods using probe vehicles with on-board GPS equipment, *Transportation Research Part C: Emerging Technologies*, Vol. 81, pp. 330-341, 2017.

Bauza R., Gozalvez J.: Traffic congestion detection in large-scale scenarios using vehicle-to-vehicle communications, *Journal of Network and Computer Applications*, Vol. 36, pp. 1295-1307, 2013.

Bolton R., Hand D.: Unsupervised profiling methods for fraud detection, *Proceedings of the Conference on Credit Scoring and Credit Control VII*, 1999.

Bronstein A., Das J., Duro M., Friedrich R., Kleyner G., Mueller M., Singhal S., Cohen I.: Bayesian networks for detecting anomalies in Internet-based services, *Proceedings of the International Symposium on Integrated Network Management*, 2001.

Brotherton T., Johnson T.: Anomaly detection for advanced military aircraft using neural networks, *Proceedings of the IEEE Aerospace Conference*, 2001.

Bhaskar A., Tsubota T., Kieu L. M., Chung, E.: Urban traffic state estimation: Fusing point and zone based data, *Transportation Research Part C: Emerging Technologies*, Vol. 48, pp. 120-142, 2014.

Cai J. F., Candes E. J., Shen Z.: A singular value thresholding algorithm for matrix completion, SIAMJ. On Optimization, Vol. 20 (4), pp. 1956-1982, 2008.

Candes E. J., Li X., Ma Y., Wright J.: Robust Principal Component Analysis? *Journal of the ACM*, Vol. 58 (3), pp. 1-37, 2011.

Chandola V., Eilertson E., Ertoz L., Simon G., Kumar V.: Data mining for cyber security, *Data Warehousing and Data Mining Techniques for Computer Security*, A. Singhal, Ed. Springer, 2006.

Chandola V., Banerjee A., Kumar V.: Anomaly detection: a survey, *ACM Computing Surveys*, Vol. 41, pp. 1-58, 2009.

Chawla S., Zheng Y., Hu J.: Inferring the root cause in road traffic anomalies, *International Conference on Data Mining (ICDM)*, 2012.

Chen X., He Z., Wang J.: Spatial-temporal traffic speed patterns discovery and incomplete data recovery via SVD-combined tensor decomposition. *Transportation Research Part C: Emerging Technologies*, Vol. 86, pp. 59-77, 2018.

Chen C.-H., Chang, G.-L.: A dynamic real-time incident detection system for urban arterials-system architecture and preliminary results, *Proceedings of the Pacific Rim Transtech Conference*, Vol. 1, Seattle, WA, pp. 98-104, 1993.

Chi E. C., Kolda T. G.: Making Tensor Factorizations Robust to Non-Gaussian Noise, *Tech. Rep. No. SAND2011-1877, Sandia National Laboratories*, 2011.

Chopp D. L.: Some improvements of the fast marching method, *SIAM Journal on Scientific Computing*, Vol. 23(1), pp. 230-244, 2002.

De Fabritiis C., Ragona R., Valenti G.: Traffic estimation and prediction based on real time floating car data, *Intelligent Transportation Systems, ITSC 11th International IEEE Conference*, 2008.

Desforges M., Jacob P., Cooper J.: Applications of probability density estimation to the detection of abnormal conditions in engineering, *Proceedings of the Institute of the Mechanical Engineers*, Vol. 212, pp. 687-703, 1998.

Dudek C.L., Messer C.J., Nuckles N.B.: Incident detection on urban freeway, *Transportation Research Record, No. 495, TRB, National Research Council*, pp. 12-24. 1974.

Edie L. C.: Discussion of traffic stream measurements and definitions, in Almond, J. ed. *Proceedings of the 2nd International Symposium on the Theory of Traffic Flow*, pp. 139–154, 1963.

Eskin E.: Anomaly detection over noisy data using learned probability distributions, *Proceedings of the 17th International Conference on Machine Learning*, pp. 255-262, 2000.

Eskin E., Arnold A., Prerau M., Portnoy L., Stolfo S.: A geometric framework for unsupervised anomaly detection, *Proceedings of the Conference on Applications of Data Mining in Computer Security*, pp. 78-100, 2002.

Fanaee-T H., Gama J.: Event detection from traffic tensors: A hybrid model, *Neurocomputing*, Vol. 203, pp. 22-33, 2016.

Fanaee-T H., Gama J.: Tensor-based anomaly detection: An interdisciplinary survey, *Knowledge-Based Systems*, Vol. 98, pp. 130-147, 2016.

Ghosh S., Reilly D. L.: Credit card fraud detection with a neural-network, *Proceedings of the 27th Annual Hawaii International Conference on System Science*, Vol. 3, 1994.

Goulart J. H. de M., Kibangou A. Y., Favier G.: Traffic data imputation via tensor completion based on soft thresholding of Tucker core, *Transportation Research Part C: Emerging Technologies*, Vol. 85, pp. 348-362, 2017.

Gordon R. L., Tighe W. et al.: Traffic control systems handbook, *U.S. Department of Transportation, Federal Highway Administration*, 2005.

Guhnemann A., Schafer R. P., Thiessenhusen K. U., Wagner P.: Monitoring traffic and emissions by floating car data, *working paper of the Institute of Transport Studies*, Vol. 4, 2004.

Han Y., Moutarde F.: Analysis of large-scale traffic dynamics in an urban transportation network using non-negative tensor factorization. *International Journal of Intelligent Transportation Systems Research*, Vol. 14, pp. 36-49, 2016.

Hara Y., Kuwahara M.: Traffic monitoring immediately after a major natural disaster as revealed by probe data - a case in Ishinomaki after the Great East Japan Earthquake, *Transportation Research Part A: Policy and Practice*, Vol. 75, pp. 1–15, 2015.

Hale E. T., Yin W., Zhang Y.: Fixed-point continuation for $l_1$-minimization: Methodology and convergence, *SIAM Journal on Optim*, Vol. 19, pp. 1107-1130, 2008.

Herring R. J.: Real-time traffic modeling and estimation with streaming probe data using machine learning, *UC Berkeley: Industrial Engineering & Operations Research*, 2010.

Horiguchi R., Iijima M., Hanabusa H.: Traffic Information Provision Suitable for TV Broadcasting Based on Macroscopic Fundamental Diagram from Floating Car Data, *13th International IEEE Annual Conference on Intelligent Transportation Systems*, 2010.

Hofleitner A., Herring R., Abbeel P., Bayen A.: Learning the dynamics of arterial traffic from probe data using a dynamic Bayesian network, *IEEE Transactions on Intelligent Transportation Systems*, Vol. 13, pp. 1679-1693, 2012.

Huachun T., Bin C., Jianshuai F., Guangdong F., Yujin Z.: Tensor Recovery via Multi-linear Augmented Lagrange Multiplier Method, Sixth International Conference on Image and Graphics, pp. 141-146, 2011.

Jiang Y., Xiong T., Wong S. C., Shu C. W. Zhang M., Zhang P., Lam W.H.K.: A reactive dynamic continuum user equilibrium model for bi-directional pedestrian flows, *Acta Mathematica Scientia*, Vol. 29, pp. 1541-1555, 2009.

Jeon S., Kwon E., Jung I.: Traffic measurement on multiple drive lanes with wireless ultrasonic sensors. *Sensors (Basel)*, Vol. 14, pp. 22891-906, 2014.

Kerner B., Demir C., Herrtwich R., Klenov S., Rehborn H., Aleksic M., et al.: Traffic state detection with floating car data in road networks, *Proceedings IEEE Intelligent Transportation Systems*, 2005.

Kolda T. G., Bader B. W.: Tensor decompositions and applications, *Society for Industrial and Applied Mathematics Rev*, Vol. 51 (3), pp. 455-500, 2009.

Koonce P., Rodegerdts L., Lee K., Quayle S., Beaird S., Braud C., et al.: Traffic signal timing manual, *NCHRP Report*, 2008.

Khan S.I., Ritchie S.G.: Statistical and neural classifiers to detect traffic operational problems on urban arterials, *Transportation Research Part C*, Vol. 6, No. 3, pp. 291-314, 1998.

Lakhina A., Crovella M., Diot. C.: Diagnosing network-wide traffic anomalies, *Proceedings of the ACM SIGCOMM*, pp. 219-230, 2004.

Long J., Szeto W. Y., Du J., Wong R.C.P.: A dynamic taxi traffic assignment model: A two-level continuum transportation system approach. *Transportation Research Part B: Methodological*, Vol. 100, pp. 222-254. 2017.

Li L., Li Y., Li Z.: Efficient missing data imputing for traffic flow by considering temporal and spatial dependence, *Transportation Research Part C: Emerging Technologies*, Vol. 34, pp. 108-120, 2013.

Liu Y., Zheng Y., Chawla S., Yuan J., Xing X.: Discovering spatio-temporal causal interactions in traffic data streams, *Proceedings of the 17th ACM SIGKDD international conference on knowledge discovery and data mining*, pp. 1010-1018, 2011.

Lin J., Keogh E., Fu A., Herle H. V.: Approximations to magic: Finding unusual medical time series, *Proceedings of the 18th IEEE Symposium on Computer-Based Medical Systems*, IEEE Computer Society, pp. 329-334, 2005.

Levin M., Krause G.M.: Incident detection: a Bayesian approach, *Transportation Research Record, No. 682, TRB, National Research Council*, pp. 52-58, 1978.

Lykov S., Seo T., Asakura Y.: Analysis of spatiotemporal dependencies in two-dimensional traffic flow in large-scale urban area with probe vehicle data, *Journal of the Eastern Asia Society for Transportation Studies*, Vol. 12, pp. 1676-1696, 2017.

Ma J., Perkins S.: Time-series novelty detection using one-class support vector machines, *Proceedings of the International Joint Conference on Neural Networks*, Vol. 3, pp. 1741-1745, 2003.

Meta S., Cinsdikici M.: Vehicle-Classification Algorithm Based on Component Analysis for Single-Loop Inductive Detector, *Vehicular Technology*, *IEEE Transactions*, Vol. 59, pp. 2795-2805, 2010.

Oudat E., Mousa M., Claudel C.: Vehicle Detection and Classification Using Passive Infrared Sensing, *IEEE International Conference on Mobile Ad Hoc and Sensor Systems*, pp. 443-444, 2015.

Odin T., Addison D.: Novelty detection using neural network technology, *Proceedings of the COMADEN Conference*, 2000.

Pang L. X., Chawla S., Liu W., Zheng Y.: On mining anomalous patterns in road traffic streams, *International Conference on Advanced Data Mining and Applications*, 2011.

Parkany A. E.: A complete review of incident detection algorithms & their deployment: What works and what doesn't, *New England Transportation Consortium., United States., & University of Massachusetts at Amherst*, 2005.

Ran B., Tan H., Wu Y., Jin P. J.: Tensor based missing traffic data completion with spatial-temporal correlation, *Physica A: Statistical Mechanics and its Applications*, Vol. 446, pp. 54-63, 2016.

Ratsch G., Mika S., Scholkopf B., Muller K. R.: Constructing boosting algorithms from SVMS: An

application to one-class classification, *IEEE Trans. Patt. Anal. Mach. Intel.*, Vol. 24, pp.1184-1199, 2002.

Rahmani M., Jenelius E., Koutsopoulos H. N.: Non-parametric estimation of route travel time distributions from low-frequency floating car data, *Transportation Research Part C: Emerging Technologies*, Vol. 58, pp. 343-362, 2015.

Rempe F., Huber G., Bogenberger K.: Spatio-Temporal Congestion Patterns in Urban Traffic Networks, *Transportation Research Procedia*, Vol. 15, pp. 513-524, 2016.

Signoretto M., De Lathauwer L., Suykens, J. A. K.: Nuclear Norms for Tensors and Their Use for Convex Multilinear Estimation, *Technical report, ESAT-SISTA*, K. U. Leuven, Belgium, 2010.

Sossoe K.S., Lebacque J.P., Mokrani A., Haj-Salem, H.: Traffic flow within a two-dimensional continuum anisotropic network. *Transportation Research Procedia*, Vol 10, pp. 217-225, 2015.

Seo T., Kusakabe T.: Probe vehicle-based traffic state estimation method with spacing information and conservation law, *Transportation Research Part C: Emerging Technologies*, Vol. 59, pp. 391-403, 2015.

Seo T., Kusakabe T., Asakura Y.: Estimation of flow and density using probe vehicles with spacing measurement equipment, *Transportation Research Part C: Emerging Technologies*, Vol. 53, pp. 134-150, 2015.

Setcheil C., Dagless E. L.: Vision-based road-traffic monitoring sensor, *Vision, Image & Signal Proc.*, 2001.

Stefano C., Sansone C., Vento M.: To reject or not to reject: that is the question: An answer in the case of neural classifiers, *IEEE Trans. Syst. Manag. Cyber*. Vol. 30, pp. 84-94, 2000.

Sheu J.: A sequential detection approach to real-time freeway incident detection and characterization, *European Journal of Operation Research*, Vol. 157, no. 2, pp. 471-485, 2004.

Sheu J.-B., Ritchie, S.G.: A new methodology for incident detection and characterization on surface streets, *Transportation Research Part C*, Vol. 6, No. 3, pp. 315-335, 1998.

Shevlyakov G., Andrea K., Choudur L., Smirnov P., Ulanov A., Vassilieva N.: Robust versions of the Tukey boxplot with their application to detection of outliers, *IEEE International Conference on Acoustics, Speech and Signal Processing*, pp. 6506-6510, 2013.

Tan H., Feng J., Feng G., Wang W., Zhang Y.-J.: Traffic volume data outlier recovery via tensor model, *Math. Probl. Eng.*, 2013

Tan H., Feng G., Feng J., Wang W., Zhang Y.-J., Li F.: A tensor-based method for missing traffic data completion, *Transportation Research Part C: Emerging Technologies*, Vol. 28, pp. 15-27, 2013.

Tabibiazar A., Basir O.: Kernel-based modeling and optimization for density estimation in transportation systems using floating car data, *Intelligent Transportation Systems (ITSC)*, 2011.

Tseng B. L., Lin C. Y., Smith J. R.: Real-time video surveillance for traffic monitoring using virtual line analysis, *Proceedings. IEEE International Conference on Multimedia and Expo*, Vol. 2, pp. 541-544, 2002.

Treiber M., Kesting A.: Trajectory and Floating-Car Data. Traffic Flow Dynamics. Data, Models and Simulation, *Springer-Verlag Berlin Heidelberg*, pp. 7-12, 2013.

Thajchayapong S., Barria J. A.: Anomaly detection using microscopic traffic variables on freeway segments, *Proceedings of Transportation Research Board*, 2010.

Wang J., Gao F., Cui P., Li C., Xiong Z.: Discovering urban spatio-temporal structure from time-evolving traffic networks, *Web Technologies and Applications, Springer*, pp. 93-104, 2014.

Williams G., Baxter R., He H., Hawkins S., Gu L.: A comparative study of RNN for outlier detection in data mining, *Proceedings of the IEEE International Conference on Data Mining, IEEE Computer Society*, 709, 2002.

Willsky A.S., Chow E.Y., Gershwin S.B., Greene C.S., Houpt, P., Kurkjian, A.L.: Dynamic model-based techniques for the detection of incidents on freeways, *IEEE Transactions on Automatic Control*, Vol. 25, No. 3, pp. 347-360, 1980.

Wong W. K., Moore A., Cooper G., Wagner M.: Bayesian network anomaly pattern detection for disease outbreaks, *Proceedings of the 20th International Conference on Machine Learning*, pp. 808-815, 2003.

Zameni M., He M., Moshtaghi M., Ghafoori Z., Leckie C., Bezdek J. C., Ramamohanarao K.: Urban sensing for anomalous event detection: Distinguishing between legitimate traffic changes and abnormal traffic variability, *European Conference on Machine Learning and Principles and Practice of Knowledge Discovery in Databases (ECML PKDD)*, 2018.

Zhang J., Cao J., Mao B.: Application of deep learning and unmanned aerial vehicle technology in traffic flow monitoring, *International Conference on Machine Learning and Cybernetics (ICMLC)*, pp. 189-194, 2017.

Zhao Y., Qin Q., Li J., Xie C., Chen R.: Highway map matching algorithm based on floating car data, *IEEE International Geoscience and Remote Sensing Symposium*, pp. 5982-5985, 2012.

Zwas G.: On two step Lax-Wendroff methods in several dimensions, *Numer. Math.*, Vol. 20, 1972.